

Confocal Laser Scanning Microscopy of Nanoparticles
Applied to Immunosorbent Assays

Homanaz Ghafari

School of Sciences and Technology

Nottingham Trent University

Supervisor:

Dr. Quentin S. Hanley

Thesis submitted for the Degree of Doctor of Philosophy (PhD)

at Nottingham Trent University

2011

کارمانیت شناسایی "راز" گل سرخ

کارماناید این است

که در "افزون" گل سرخ شناور باشیم

کارماناید این است

که میان "گل نیلوفر" و "قرن" پی آواز حقیقت بدویم!

سہراب سہری

It is not our job to investigate the "secret" of the beauty of a red rose,

Maybe our job is,

Overwhelming in the "charm" of its beauty,

Maybe our job is,

Looking for the rhythm of truth anywhere, anytime.

Sohrab Sepehri (1928 -1980)

Abstract

The aim of this project was to demonstrate and develop a confocal readout method for fluorescent immunosorbent assays and investigate its potential advantages in comparison to traditional immunoassays. The key point of a confocal immunosorbent assay is the ability to detect the thin layer of immunoassay in the presence of unbound fluorescent reagents without washing the overlayer. Heterogeneous and homogeneous sandwich immunoassays of human IgG model were demonstrated successfully followed by the use of an empirical decomposition method for quantitative separation of the signals of the thin fluorescent assay layer from the overlayer. The detection limits for the homogeneous and heterogeneous formats of the model were 2.2 and 5.5 ng/ml, respectively. The application of confocal microscopy in kinetic analysis of the antigen-antibody reaction of the human IgG model was studied for homogeneous and heterogeneous formats and two fluorescent labels antibodies (FITC and QDs). The association rates of binding of FITC and QD605 conjugated antibodies to human IgG on prepared surfaces were 5.7×10^4 and 2.6×10^4 ($M^{-1}s^{-1}$) respectively. Confocal detection immunosorbent assay enables the detection of more than one assay along the z-axis. By replacing standard substrates with multiple 30 μm layers of substrates, a high density array of immunosorbent assays was created within a stratified medium. Stacks of up to five modified thin mica substrates of model immunoassays were detected by confocal microscopy. When applied to model assays consisting of human and mouse IgGs on different layers, the z-axis multiplexing of immunosorbent assays was demonstrated. The arrays of multiplexed immunosorbent assays were extended to 3D format by using microcontact printing and the assay density was increased twice by detecting the stack of two substrates which each contained two IgGs assays.

Acknowledgments

I would like to express my gratitude to my supervisor, Dr. Quentin Hanley for his encouragement and guidance throughout my Ph.D. I am great indebted to Dr. Haida Lee, my second supervisor, who gave special attention and support to my work.

I would like to thank my lovely friends in Iran, Mehrak Javadi Paydar, Mandana Yazdanshenas and Banafsheh Ramezani, who their devoted energy from far away, supporting and encouraging me during these four years.

Most of all, I would like to thank my family for their constant support and encouragement throughout my PhD. This thesis is dedicated to my parents, who have so much enjoyed seeing their daughter get the title "Doctor".

The financial support of the European Union Sixth Framework Programme as part of the FLUOROMAG consortium (under Contract No. 037465) is gratefully appreciated.

Content:

Abstract	I
Acknowledgments	II
List of Figures	VII
List of Tables	X
List of Abbreviations	XI
Chapter 1: Aims & objectives	1
1.1 Background	2
1.2 Thesis objectives	7
1.3 Thesis outline	8
Chapter 2: Background	10
2.1 Confocal microscopy	11
2.1.1 History	11
2.1.2 Principle of confocal microscopy	11
2.1.3 Advantages	12
2.1.4 Disadvantages	13
2.1.5 Resolution	14
2.1.5.1 Lateral resolution	14
2.1.5.2 Axial resolution	15
2.1.6 Parameters effecting confocal imaging	15
2.1.6.1 Numerical aperture (NA)	15
2.1.6.2 Pinhole size	16
2.1.7 Major components of CLSM	16
2.1.8 Types of confocal microscopy	17
2.1.8.1 Stage scanning confocal microscope	17
2.1.8.2 Beam scanning confocal microscope	17
2.1.8.3 Spinning disk confocal microscope (SDCM) or Nipkow disk microscope	18
2.1.8.4 Line scanning confocal microscopy (LSM)	18
2.1.8.5 Programmable Array Microscopes (PAM)	19
2.1.9 Other optical sectioning techniques	20
2.1.9.1 Deconvolution (Computational optical sectioning microscopy or COMS)	20
2.1.9.2 Nonlinear optical techniques	20
2.1.9.2.1 Two-photon and multi-photon excitation microscopy	21
2.1.9.2.2 Second harmonic generation (SHG) imaging microscopy (SHIM)	22
2.1.9.2.3 Third harmonic imaging (THG) microscopy	23
2.1.9.3 Structured illumination microscopy (SIM)	24
2.1.9.4 4Pi and I ³ M microscopy	24
2.1.9.5 Stimulated emission depletion microscopy (STED)	25
2.2 Immunoassay	25
2.2.1 History of immunoassays	25
2.2.2 Classification of immunoassays	26
2.2.2.1 Limited or excess reagent format	27
2.2.2.1.1 Limited or competitive assays	27
2.2.2.1.2 Reagent excess assays or non-competitive assays	28
2.2.2.1.3 Ambient analyte assays	29
2.2.2.2 Homogeneous and heterogeneous assay	30
2.2.2.2.1 Homogeneous assays	30
2.2.2.2.2 Heterogeneous assays	31

Chapter 3: Confocal detection of planar immunosorbent assay	33
3.1 Introduction	34
3.1.1 Optical sectioning immunoassay detection methods	34
3.1.1.1 Fluorometric micro-volume assay technology (FMAT)	34
3.1.1.2 Two-photon excitation fluoreometry (TPX):	36
3.1.1.3 Confocal readout of microarray format immunoassays	36
3.1.1.4 Confocal detection of planar immunosorbent assay	37
3.1.2 Hepatitis C	37
3.1.2.1 Diagnosis of HCV infection	38
3.1.2.1.1 Serological tests	38
3.1.2.1.1.1 Anti-HCV screening tests	38
3.1.2.1.1.2 Anti-HCV supplementary or confirmatory tests	39
3.1.2.1.1.3 HCV core antigen test	39
3.1.2.1.2 Nucleic acid techniques (NAT)	39
3.1.2.1.3 Genotyping tests	40
3.2 Theory of confocally detection of planar immunoassays	40
3.3 Materials and methods	43
3.3.1 The model assay systems	43
3.3.2 Reagents	43
3.3.3 Instrumentation	44
3.3.3.1 CLSM	44
3.3.3.2 PAM	44
3.3.4 Preparation of confocal immunosorbent assay	45
3.3.4.1 Heterogeneous format of human IgG model	45
3.3.4.2 Homogeneous format of human IgG model	45
3.3.4.3 HCV core assay	45
3.3.4.3.1 Indirect assay	46
3.3.4.3.2 Sandwich assay	46
3.3.5 Analysis	47
3.3.5.1 Image analysis of CLSM	47
3.3.5.2 Detection limit	47
3.3.5.3 Adsorption of proteins to a solid phase	48
3.4 Results	49
3.4.1 Quality assessment of parameters affecting the confocal axial response	49
3.4.1.1 Numerical aperture	49
3.4.1.2 Pinhole size	50
3.4.2. Heterogeneous Confocal Sandwich Assay	52
3.4.2.1 Response of film and overlayer	52
3.4.2.2 Decomposition of the signals with Cauchy-Lorentz distribution function	53
3.4.2.3 Step size optimization	54
3.4.2.4 Heterogeneous confocal sandwich assay optimization	55
3.4.2.5 Heterogeneous confocal planar immunoassay detection limit	56
3.4.3 Homogeneous confocally detected planar immunoassay	58
3.4.4 Hepatitis C core immunoassay	59
3.4.4.1 Sandwich format assay	59
3.4.4.2 Indirect format assay	60
3.4.5 Immunoassay detection with PAM	61
3.4.5.1 Decomposition of signals	61
3.4.5.2 Dose response measurements	62
3.5 Discussion:	64
Chapter 4: Kinetic analysis of antigen-antibody interactions with CLSM	69
4.1 Introduction	70
4.1.1 Antigen-antibody interaction	70
4.1.2 Kinetics of antigen-antibody interaction and rate limitations	72
4.1.3 Affinity	76

4.1.4 Thermodynamic of antigen-antibody interaction	77
4.1.5 Methods for kinetic and equilibrium analysis	78
4.1.5.1 Immunosorbent assays	78
4.1.5.2 Fluorescence	79
4.1.5.2.1 Fluorescence polarization	79
4.1.5.2.2 Fluorescence correlation spectroscopy (FCS)	80
4.1.5.2.3 Fluorescence resonance energy transfer (FRET)	81
4.1.5.3 Optical techniques	81
4.1.5.3.1 Reflectometric techniques	82
Reflectometry:	82
Ellipsometry:	82
Reflectometric interference spectroscopy (RIFS):	83
4.1.5.3.2 Evanescent wave techniques	83
Surface Plasmon resonance (SPR):	85
Waveguides:	88
4.1.5.4 Magnetorelaxometry	89
4.1.5.5 Optical sectioning methods	90
Two photon excitation microscopy:	90
CLSM:	90
4.2 Theory	91
4.2.1 Heterogeneous format	91
4.2.2 Homogeneous format	96
4.3 Materials and methods	97
4.3.1 Reagents	97
4.3.2 Instruments	98
4.3.3 Preparation of sandwich FLISA for kinetic measurements	98
4.3.4 Homogenous versus heterogeneous format assays	99
4.3.5 Data analysis	99
4.4 Results	100
4.4.1 Association rate constant analysis	100
4.4.1.1 Heterogeneous FLISA with FITC conjugated secondary antibody	100
4.4.1.2 Heterogeneous FLISA with QD565 conjugated secondary antibody	103
4.3.2 Diffusion or reaction limited	106
4.3.2.1 FITC conjugated secondary antibody	106
4.3.2.2 QD565 conjugated secondary antibody	108
4.3.3 Heterogeneous versus homogenous assay formats	110
4.4 Discussion and conclusion	112
Chapter 5: Z-axis multiplexing immunosorbent assays with CLSM	119
5.1 Introduction	120
5.1.1 Volume measurements in CLSM	120
5.1.2 Confocal detection of stratified media	121
5.1.3 Multiplexing assays	122
5.1.4 Mica as substrate	122
5.2 Theory	123
5.2.1 Measuring the thickness of a single substrate with CLSM	123
5.2.2 Measuring z-position within a stack of substrates	125
5.3 Materials and Methods	127
5.3.1 Instrumentation	127
5.3.2 Reagents	127
5.3.3 Substrates	127
5.3.4 Modification of substrates	128
5.3.5 Labelling with carboxyl terminated quantum dots	128
5.3.6 Preparation of sandwich immunoassay on mica	129
5.4 Results	129

5.4.1 Modification of substrates	129
5.4.2 Measurement of substrate thickness and refractive index	130
5.4.2.1 One layer of substrate:	130
5.4.2.2 Stack of the substrates	131
5.4.3 Immunoassays on mica	133
5.4.3.1 Dose response of IgG immunoassay on mica layers	133
5.4.3.2 Sandwich immunoassays on multilayer of mica	134
5.4.3.3 Multiplexed sandwich immunoassays on mica layers	135
5.5 Discussion and Conclusion	136
Chapter 6: 3D z-axis multiplexing immunosorbent assay with CLSM	139
6.1 Introduction	140
6.1.1 Microfabrication technology	140
6.1.2 Soft lithography	142
6.1.3 Microcontact printing technique	143
6.1.3.1 PDMS stamp	144
6.1.3.2 Protein patterning with μ CP	146
6.1.3.3 Multiprotein patterning with μ CP	148
6.1.3.2 Substrates for μ CP of proteins	149
6.2 Material and methods	150
6.2.1 Reagents	150
6.2.2 Instrumentation	150
6.2.3 Substrate	150
6.2.4 Preparation of PDMS stamp	151
6.2.5 Mica modification	153
6.2.6 Printing carboxyl terminated quantum dots on modified surface	153
6.2.7 Microcontact printing of human IgG immunoassay on mica	153
6.2.8 Microcontact printing of multiprotein immunoassays on mica	154
6.2.9 Image analysis	155
6.3 Results and discussion	155
6.3.1 Microcontact printing of carboxyl terminated quantum dots	155
6.3.2 Microcontact printing of an indirect human IgG immunoassay	156
6.3.2. Dose response of microarrays of human IgG immunoassays	158
6.3.3 Stacked of human IgG immunoassays microarrays	159
6.3.4 Microcontact printing of multiprotein immunoassays	160
6.3.5 Stacked of microarrays of multiprotein immunoassays	162
6.4 Conclusion	163
Chapter 7: Conclusions & future work	165
7.1 Conclusion	166
7.2 Future work	169
7.3 Publications arising from this work	172
7.3.1 Papers	172
7.3.2 Patent	172
7.3.3 Conference Presentations	172
Appendix: Optical model of planar confocal immosorbent assay	173
References	<i>Error! Bookmark not defined.</i>

List of Figures

Figure 2-1: The principle of a confocal microscope.....	12
Figure 2-2: A competitive assay for detection of antigen.....	27
Figure 2-3: Non-competitive or sandwich assay.....	28
Figure 3-1: HCV genome.....	38
Figure 3-2: Schematic diagram of a confocal sandwich immunoassay.....	41
Figure 3-3: The FLISA indirect design for detection of HCV core antibody.....	46
Figure 3-4: The FLISA sandwich design for detection of HCV core antigen.....	47
Figure 3-5: The axial response from a thin immunoassay film for a variety of objectives.....	50
Figure 3-6: The axial response from a thin immunoassay film for a variety of pinhole sizes.....	51
Figure 3-7: Variation of the FWHM of the axial response as a function of pinhole size.....	51
Figure 3-8: The axial response of confocal sandwich immunoassay has three zones.....	52
Figure 3-9: Decomposition the signal of confocal immunoassay to the thin film and overlayer.....	54
Figure 3-10: Variation in SNR as step size increases over a fixed z axis scan range.....	55
Figure 3-11: Optimization of the model assay system for wide dynamic range.....	56
Figure 3-12: Calibration curves of low concentrations of antigen in heterogeneous format.....	57
Figure 3-13: Calibration curves of low concentrations of antigen in homogeneous format.....	59
Figure 3-14: Dose response curve of HCV core antigen detected in sandwich assay.....	60
Figure 3-15: Dose response curve of anti-HCV core antibody detected in indirect assay.....	60
Figure 3-16: The axial response of sandwich immunoassay with PAM.....	61
Figure 3-17: Decomposition the signal of the PAM immunoassay.....	62
Figure 3-18: Dose response curve of human IgG FLISA assay detected with PAM.....	63
Figure 4-1: Schematic representation of a human IgG molecule.....	71
Figure 4-2: Generation of the evanescent wave at an interface.....	84
Figure 4-3: Schematic diagram of a prism-based SPR biosensor.....	86
Figure 4-4: Schematic illustration of diffusion-limited binding of labelled antibodies in solution with immobilized antigen on a solid surface in heterogeneous format assay.....	92
Figure 4-5: Schematic illustration of diffusion-limited binding of labelled antibodies in solution with immobilized antigen on a solid surface in a homogeneous format assay.....	97
Figure 4-6: Binding curves of different concentrations of anti-human IgG-FITC to immobilized human IgG.....	100
Figure 4-7: Binding curves of different concentrations of anti-human IgG-FITC to immobilized human IgG fitted to double exponential.....	102
Figure 4-8: Concentration dependence of k_{obs1} values derived from double exponential curve fitting of human IgG binding to of anti-human IgG-FITC.....	103
Figure 4-9: Binding curves of different concentrations of anti-human IgG-QD565 to immobilized human IgG.....	104
Figure 4-10: Binding curves of different concentrations of anti-human IgG-QD565 to immobilized human IgG fitted to double exponential.....	105

Figure 4-11: Concentration dependence of k_{obs} values derived from fitting parameters for the reaction of human IgG binding to of QD565 anti-human IgG.....	106
Figure 4-12: Theoretical values of bound anti-human IgG-FITC on the surface of the chamber slide calculated from the diffusion-limited amount of bound antibody.....	107
Figure 4-13: Quantitative description of the amount of bound anti-human IgG-FITC antibody at the surface.....	107
Figure 4-14: Theoretical values of bound anti-human IgG-QD565 on the surface of the chamber slide calculated from the diffusion-limited amount of bound antibody.....	109
Figure 4-15: Quantitative description of the amount of bound anti-human IgG-FITC antibody at the surface.....	110
Figure 4-16: Binding curves of different concentrations of anti-human IgG-QD565 to immobilized human IgG on the surface in heterogeneous and homogeneous format assay.....	111
Figure 5-1: Ray traces for light focusing on the front (ray 1) and rear (ray 2) surface of a substrate assuming ($n_1 < n_2$).....	124
Figure 5-2: Rays traces for light interacting with a layered system consisting of uniform substrates separated by a variable fluid layer assuming $n_1 < n_3$ and $n_3 < n_2$	126
Figure 5-3: Mica modification with APTES.....	128
Figure 5-4: The axial response of modified (■) and non-modified (□) mica labelled with QDs.....	130
Figure 5-5: Axial response of substrates labelled on both sides with carboxyl quantum dots on glass (■) and mica (□).....	131
Figure 5-6: Axial response of the stack of two, three and four mica layers labelled with carboxyl quantum dots by CLSM.....	132
Figure 5-7: Dose response curve of human IgG on the first (■) and second (●) layers of a stacked mica system.....	134
Figure 5-8: Axial response of the stack of five mica layers containing human IgG immunoassays by CLSM.....	135
Figure 5-9: Multiplexed confocal immunosorbent assays arrayed along the z-axis.....	136
Figure 6-1: PDMS chemical structure before and after crosslinking.....	145
Figure 6-2: Schematic representation of fabrication and application of a PDMS stamp in μ CP of proteins.....	148
Figure 6-3: The casting station used for PDMS stamp fabrication.....	151
Figure 6-4: The different patterned stamp masters used for μ CP.....	152
Figure 6-5: A prepared PDMS membrane on a polycarbonate stamp holder.....	152
Figure 6-6: Schematic of μ CP of two-protein arrays on mica surface.....	154
Figure 6-7: Fluorescence image of QDs 565 patterned on a modified mica surface by μ CP accompanied by the intensity profile.....	156
Figure 6-8: Fluorescence image of human IgG QDs 605 patterned on a modified mica surface by μ CP accompanied by the intensity profile.....	157
Figure 6-9: Confocal fluorescent images of different concentrations of human IgG in μ CP of human IgG immunoassays.....	158

Figure 6-10: Dose response curve of printed human IgG immunoassay with μ CP.....	159
Figure 6-11: The 3D view and z-axis response of stack of two mica layers containing QDs human IgG immunoassays.....	159
Figure 6-12: The 3D view and z-axis response of stack of three mica layers containing QDs human IgG immunoassays.....	160
Figure 6-13: Fluorescent images of sequentially stamped multiprotein QDs immunoassays.....	161
Figure 6-14: The Fourier spectra of confocal images of sequentially stamped multiprotein QD immunoassays.....	162
Figure 6-15: Different 3D views of stacking two mica substrates with multiprotein immunoassays on each.....	162

List of Tables

Table 1-1: Comparison of methodologies used in separation-free detection.....	5
Table 3-1: Variation of the FWHM of the axial response.....	49
Table 4-2: Best-fit kinetic parameters of the binding of human IgG and anti-human IgG-FITC in heterogeneous format assay.....	101
Table 4-3: Best-fit kinetic parameters of the binding of human IgG and anti-human IgG-QD565 in heterogeneous format assay.....	105
Table 4-4: Best-fit kinetic parameters of the binding of human IgG and anti-human IgG-QD565 in homogeneous and heterogeneous format assays.....	111
Table 5-1: Measurement the thickness of glass and mica substrates with CLSM.....	130
Table 5-2: Measurements of layered of mica and glass substrates with micrometer and CLSM.....	131

List of Abbreviations

AFM	Atomic force microscopy
CLSM	Confocal laser scanning microscopy
CoMS	Computational optical sectioning microscopy
DMD	Digital micromirror device
EIA	Enzyme immunoassay
ELISA	Enzyme-linked immunosorbent assay
FITC	fluorescein 5-isothiocyanate
FLISA	Fluorescence-linked immunosorbent assay
FMAT	Fluorescent microvolume assay technology
FWHM	Full width at half maximum
HCV	Hepatitis C virus
IA	Immunoassay
LCos	Liquid-crystalon-silicon
NA	Numerical aperture
PAM	Programmable array microscopy
PDMS	Polydimethylsiloxane
PMMA	Poly(methyl methacrylate)
PMT	photomultiplier tube
QD	Quantum dot
RIA	Radioimmunoassay
RIfS	Reflectometric interference spectroscopy
S/N	signal to noise ratio
SAM	Self-assembled monolayer
SHG	Second harmonic generation
SHIM	Second harmonic imaging microscopy
SIM	Structured illumination microscopy
SLM	Spatial light modulators
SPR	surface plasmon resonance
SSHG	Surface second harmonic generation
STED	Stimulated emission depletion microscopy
THG	Third harmonic generation
TPM	Two-photon excitation microscopy
TPX	Two-photon excitation microparticle fluorometry
VCC	Volumetric capillary cytometry
μCP	Microcontact printing

Chapter 1

Aims & objectives

This chapter introduces the objective of my thesis: the development of confocal readout method for immunosorbent assay and the consequential advantages. Section 1.1 looks at the main advantage of confocally readout method: “separation free” and the current state of non-separation readout methods in the literature. In section 1.2 a synopsis of the project is given, establishing the novelty of using confocal readout method and proposed implementation of this method. Section 1.4 summarises the details of the subsequent chapters in this thesis, highlighting the development of the project towards its goals.

1.1 Background

Bioaffinity assay methods are commonly used for quantitative analysis of various biologically active molecules. Immunoassay is a very popular bioaffinity assay method for clinical, pharmaceutical, biochemical and environmental samples, based on the high specific recognition between antigens by antibodies. Antibodies are considered to be well-suited recognition elements for bioassays and can be produced against nearly all analytes.¹ The other common bioaffinity assays are used for measuring the interaction between a ligand with its receptor (ligand-receptor binding assay) and cell-based assays also have important role in diagnosis of disease and drug discovery.² The major criteria in developing and improving immunoassay technique are performance, simplicity, sensitivity, automation, speed, miniaturization, capable of multiplexing, stability of reporters, safety and cost. It is hard to achieve all of the aforementioned characteristics together.

Non-radioactive assay formats are preferable because of reducing health risks and environmental pollution as well as cost. Also, the inherent limitation of radioactive assays for miniaturization avoids using radioactive isotopes in high-throughput screening technology (HTS) method.³ The alternative labels to radioactive are enzymes, fluorescent and chemiluminescent. Compared to radioactive labels, fluorescent labels are more sensitive, inexpensive, have easier detection method and rapid read times, and capable of multiplexing.² However, fluorescent dyes have their own drawbacks such as quenching, photobleaching and interference from autofluorescence background. The long lifetime lanthanides can overcome the problem of interfering fluorescent background signals and improve the sensitivity and precision of detection.

Bioaffinity assays can be classified according to the need for separation of bound from free unbound labelled fraction before measurement into homogenous (separation free) and heterogeneous (requires separation) formats. A homogeneous assay is also called mix-and-read or mix-and-measure assays that show the simplicity of this format. There is an argument for the term homogeneous to be restricted to assays where the antibody-antigen reaction takes place in solution without using any kind of solid surface materials (beads or microtiter plates). However, there is no general agreement on this point. There are several reports of using the term of homogeneous for the assays where one component of the assay is immobilized on a solid surface (bead or planar solid surface) and the signal is centred on or around it, so there is no need to do physical separation of free and bound fraction.² This type of assay has also been called by other terms in the literature such as semi-homogeneous assay,⁴ separation-free or non-separation assay,⁵ and no-wash heterogeneous assay.⁶ There is a wide range of homogeneous format assays in the literature. These vary from simple assays within a single liquid phase followed by different detection schemes such as turbidimetric,⁷ colorimetric,⁸⁻¹⁰ fluorometric,^{11, 12} and luminescent¹³ to biphasic assays in which reagents partition between a liquid and a solid phase. Examples of the latter include beads,¹⁴⁻¹⁷ colloidal gold and latex particles,^{18, 19} membranes,^{20, 21} and cells.²²⁻²⁴

Separation-free or non-separation assay methods are highly desirable for miniaturization and HTS. Most current *in vitro* drug discovery assays rely on separation-free technologies.²⁵ Separation is time-consuming, difficult to automate and therefore slow in HTS. Separation procedure may affect the equilibrium in saturation analysis, reducing assay sensitivity and precision. Low affinity binding reagents are potentially influenced by separation methods and needs careful control of separation conditions.^{26, 27}

Among non-separation methods, the one that can detect both small and large analyte molecules is highly desirable. Non-separation methods provide this in both non-competitive (sandwich) for macromolecules and competitive formats for small molecules.²⁸ Sandwich format immunoassays are the routine format in clinical laboratories for quantification of large numbers of protein markers for its enhanced sensitivity compared to competitive format.²⁹ Most existing sandwich assays are heterogeneous and need several washing and incubation steps. The requirement for discrete separation and washing steps has hampered the efforts to adapt sandwich format assay in homogeneous or separation-free techniques.³⁰ Therefore, a sandwich format assay in non-separation would be attractive in assay development.

Over the past years, several different separation-free technologies have been developed for detection of immunoassays. An overview of these technologies, regarding to advantages and disadvantages of them, is given in Table 1-1. Most of them are fluorescent based platform which can be easily adapted to HTS, miniaturization, and mix-and-read assays. The main drawback of the current detection technologies is the need of labelling and/or immobilization of at least one of the reactants on the surface. Some of the techniques which are more relevant to the subject of this study such as FMAT, TPX, magnetorelaxometry and SPR will be discussed more later in this thesis. Confocal detection immunoassay method is a separation-free method with possible potential to be adapted to HTS and the ability to be used in multiplexing and miniaturized assays.

Table 2-1: Comparison of methodologies used in separation-free detection. (Continued on next page)

Technology	Principle	Advantages	Disadvantages	Ref.
Scintillation proximity assay (SPA)	Energy transfer of radioactive decay in close proximity	Ease of automation HTS	Radioactive label Expensive Need reagent immobilization Time consuming Lower sensitivity compared to heterogeneous radioactive assay	31-33
Fluorescence resonance energy transfer (FRET)	Energy transfer between two fluorescent molecules in close proximity	Non radioactive labelled No immobilization	Dual labelling (donor and acceptor) Background fluorescence interference	34, 35
Time-resolved FRET (TR-FRET)	Energy transfer between long excited state lifetime donor and fluorescent acceptor	Low interfering autofluorescence background Sensitive	Dual labelling Limited choice of donor/acceptor pairs Labelling can affect affinity	6, 2525
BRET	Energy transfer between a bioluminescent donor and fluorescent acceptor	Cheaper and simpler instrumentation HTS More sensitive than FRET No background signal Multiplexing	Dual labelling Interfering by matrix components Highly purified reagents required	36
FP	Light polarization	One labelling step No immobilization Ease of automation Miniaturization	Lack of precision at low concentrations Limited to small molecules (<5 kDa) Limited to competitive assay	6, 12
FMAT	Single cell or bead based fluorescent measurement	Multiplexing Miniaturization	Expensive instrument Requires immobilization	16, 24
Amplified luminescence proximity homogeneous assay (AlphaScreen™)	Energy transfer between singlet oxygen on donor bead and fluorophores on acceptor bead	Probe interaction over longer distance (200 nm) HTS	Donor and acceptor beads labelling Requires immobilization	37

Table 1-1: Comparison of methodologies used in separation-free detection. (Continued from previous page)

Technology	Principle	Advantages	Disadvantages	Ref.
Flow cytometry-based immunoassay (FCI)	Single cell measurement	Multiplexing HTS Minimal background	Requires immobilization of one compartment and labelling the other	38, 39
Fluorescence correlation spectroscopy (FCS)	Diffusion mediated intensity fluctuations	HTS Minimal background Real-time kinetics No immobilization	Complex instrumentation Requires labelling Requires water soluble, photostable and quantum yield label Sensitive to noise	40, 41
Surface plasmon resonance (SPR)	Refractive index	No labelling Binding reaction monitoring	Requires immobilization Low sensitivity	42, 43
Total internal reflection fluorescence (TIRF)	Refractive index	Real-time kinetics Sensitive	Requires immobilization Requires labelling	44, 45
Magnetic relaxation immunoassay (MARIA)	Measurement of magnetic relaxation times of magnetic nanoparticles	Real-time kinetics <i>In-vivo</i> applications	Requires labelling	46, 47
Two-photon excitation assay (TPX)	Two-photon excitation microscopy	Real-time kinetics Multiplexing Sensitive	Requires immobilization Requires labelling	48, 49
Cloned enzyme donor immunoassay (CEDIA)	Enzyme formation	No immobilization Sensitive	Limited to competitive assay Limited to small molecules	9, 50
Nonseparation electrochemical enzyme immunoassay (NEEIA)	Electrochemical detection of enzyme immunoassay on gold coating nylon membrane	Adoptable to both competitive and sandwich format assays Multiplexing	Immobilisation on gold surface Large volume of sample/reagent nM detection limit	28, 30

1.2 Thesis objectives

The overall objective of this thesis was to develop a method allowing non separation detection of fluorescent linked immunosorbent assays (FLISA) by using confocal laser scanning microscopy (CLSM). To achieve the objective, a FLISA model of human sandwich immunoglobulin (IgG) assay was selected and detection was carried out in both homogenous and heterogeneous formats. In this thesis, the term homogeneous refers to a biphasic assay that does not require separation of free reagents via wash steps and is prepared by mixing antigen and reporter antibody after preparing the solid surface with a first antibody. In heterogeneous format, there was a washing step after adding each reagent.

The unique optical sectioning capability of CLSM presents more advantages than traditional immunoassay methods and the novel aspects of this are the topics of this thesis as below:

1. To demonstrate and optimize a planar confocal immunosorbent assay in homogeneous and heterogeneous formats using a model of human IgG assay. The dose response curve and detection limits of both formats are studied and compared.
2. To study the feasibility of the application of CLSM for analysing the kinetics of antigen-antibody reaction on the model assay and quantitative measurements of the binding parameters.
3. To develop the confocal readout along z-axis and propose a novel multiplexing detection method in a stratified medium.

4. To extend the two dimensional (2D) confocal immunosorbent assay to three dimensional (3D) by microcontact printing immunoassay and detection the stack of them in z-axis.

1.3 Thesis outline

This section provides an overview of the research presented over the following six chapters.

Chapter 2 gives background for the main issues in my thesis, consisting of confocal microscopy and immunoassay. Section 2.1 is an overview of the principles of confocal microscopy including advantages, disadvantages and different types of it. The various types of optical sectioning techniques are described, with emphasis on techniques feasible to the project's objectives. The immunoassay section introduces important definitions relevant to its classification.

Chapter 3 describes the theoretical and experimental section of the main goal of my thesis: the confocal read-out of FLISA. At first, the current state of confocal readout method in the literature is reviewed. Then a confocal readout method based on CLSM for a FLISA model of human IgG is presented and optimized in homogeneous and heterogeneous formats. An empirical method based on distribution function is used to decomposition of the fluorescent signal of unbound labelled reagent in solution above the thin layer of antigen-antibody complex. HCV FLISA was also studied by CLSM to study its practicality for a real disease.

Chapter 4 reports the implementation of CLSM detection method for analysing the kinetics of antigen-antibody reaction. This chapter starts with a review of the methods

for kinetic analysis and the theory of the kinetic of antigen-antibody reaction. Then the experimental section for measuring the kinetic parameters of the human IgG model assay is presented and the results discuss.

Chapter 5 describes the idea of multiplexing of immunoassays along z-axis by CLSM. By replacing standard substrates with multiple thin layers of glass or mica, a high density array of immunosorbent assays is created within a stratified medium. Theoretical treatment of focal anomaly caused by refractive index mismatch is studied theoretically and experimentally.

Chapter 6 expands the subject of chapter 5 to a microarray format by microcontact printing of immunoassay on modified mica surfaces.

Chapter 7 gives an overall review of the technique developed in this thesis and concludes the thesis by summarizing the main findings and routes for further work are presented.

Chapter 2

Background

This Chapter presents a general overview of the main issues related to the thesis: confocal microscopy and immunoassay. In section 1 a brief description of confocal microscopy and other sectioning methods is presented with focus on the methods suitable for the goal of this thesis “immunoassay readout”. Section 2 is about immunoassay technology. The overview includes the history, classification and the principles of antigen-antibody reactions. In classification of immunoassays, the focus is on homogeneous/heterogeneous assay formats since its definition is important in content of this thesis.

2.1 Confocal microscopy

Confocal microscopy is a well-known optical sectioning technique used to image thick specimens at high axial resolution and contrast without physically sectioning the sample and perform three-dimensional imaging. It provides optical sectioning in both reflection and fluorescence modes and has found applications in metrology and life science.⁵¹

2.1.1 History

Confocal microscopy was invented in 1955 by Marvin Minsky⁵² and the concept was patented in 1957. The key elements of Minsky's design were using pinhole apertures and point-by point illumination of the specimen. The first mechanically scanned confocal microscope which used laser illumination was designed and built in the early 1970s by Davidovits and Egger for biological research.⁵³ Advances in computers, lasers, and digital imaging software allowed its further development and became commercially available in the late 1980s.⁵⁴

2.1.2 Principle of confocal microscopy

In conventional (widefield) light microscopy, the entire depth or volume of a specimen is uniformly and simultaneously illuminated and the emission light is collected. This causes out-of-focus blur from above and below of the specimen plane of focus that reduces contrast and resolution. In confocal microscopy, most out-of-focus light is eliminated by combination of using small apertures (pinholes) for both illumination and detection at an image plane of the objective and point by point illumination of the specimen. The excitation light is focused on a small point of a specimen and the emitted light from the object plane passes through the pinhole and

enters the detector. Only the fluorophores that are in locations conjugate to both the illumination and detection pinholes are detected. The schematic of confocal microscopy principle is shown in Figure 2-1.

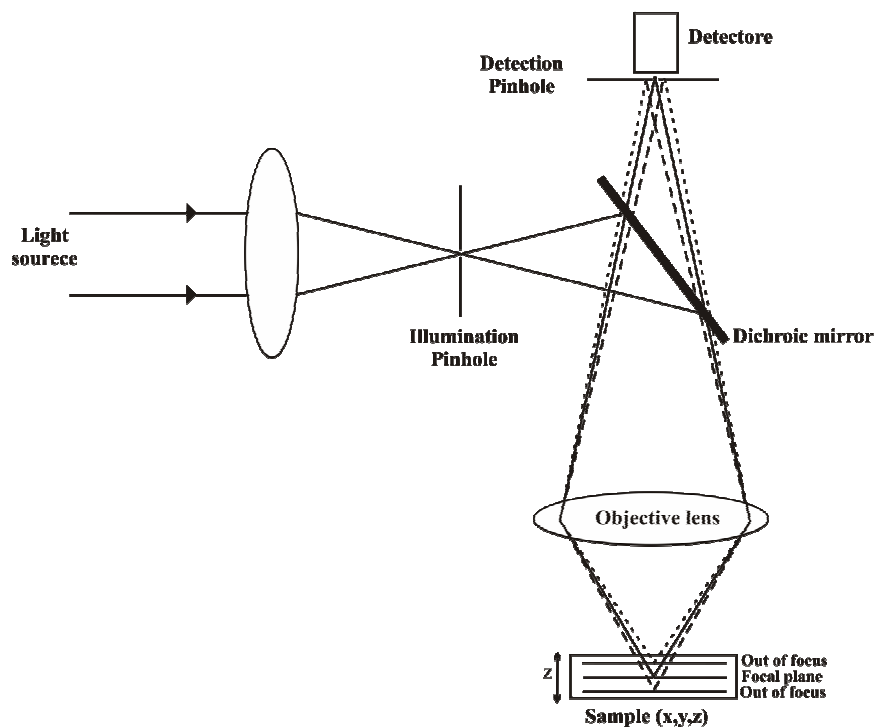


Figure 2-1: The principle of a confocal microscope. Excitation light passes through an illumination pinhole, reflects off a dichroic mirror, and is focused on a sample by an objective lens. The longer wavelength emissions from the sample pass through the dichroic mirror. Only light from the focal plane can pass through the detection pinhole and is detected by a detector. Out of focus light from above (dotted lines) and below (dashed lines) is blocked by the detection pinhole.⁵⁵

2.1.3 Advantages

Confocal microscopy offers several advantages over conventional light and electron microscopy. The main advantage of confocal microscopy is its optical sectioning ability in imaging 3D samples. A stack of optical sections is easily combined to reveal a 3D image of a transparent object.⁵⁶ The axial and lateral resolution of a confocal microscope is better than a conventional microscope. It non-invasively sections both

live cells and fixed samples providing an advantage over electron microscopy. Typical axial resolution (0.5-1.5 μm) allows collection of data from a thin slice rather than the entire thickness of the specimen. The ability to restrict the image to a small portion is a major advantage of a confocal microscope.

The elimination of out-of-focus light results in improvement of contrast, resolution and signal-to-noise ratio (SNR) in imaging thick specimens. The ability of scanning in different planes (xy , xz and yz planes) is mentioned as an advantage of the confocal imaging technique.⁵¹

2.1.4 Disadvantages

The main disadvantage of point-scanning confocal microscopy is the slow speed of image formation due to raster scanning of the sample by point-by-point illumination and detection. The temporal resolution of confocal microscopy is behind most biological dynamic processes in cells, tissues and model organisms. The frame rate of raster scanning is about 1 s per frame.⁵⁷ Some confocal systems such as direct-view confocal scanner increase the scanning speed to video-rate ($\sim\text{ms}$) by using microlenses.⁵⁸ The ideal imaging system for analysing dynamic process should have an acquisition frame rate in the range of tens to hundreds frames per second to record events taking place at milliseconds.⁵⁹

The increased risk of photobleaching of the fluorophore in focal planes above and below the plane being observed can be problematic as focusing on one plane can produce photobleaching in all planes, including those that have not yet been observed.⁶⁰ Photobleaching limits the total number of available fluorescent photons for detection. It is also limits the number of images that can be recorded for 3D imaging due to photobleaching occurring throughout the specimen in recording each 2D image.⁶¹

Confocal microscopy is not suitable for imaging very thick specimens due to scattering and aberration problems of deep imaging.⁶² The resulting image is severely blurred and has a very low signal-to-noise ratio (SNR).

2.1.5 Resolution

Resolution is the ability to resolve two point objects from each and is defined as the minimum distance between two objects such as they are distinguishable in the image of an optical system.⁵¹ Spatial resolution (both lateral and axial) of an optical system depends on characterization of the system such as type of microscope, numerical aperture (NA), refractive index of embedding medium, coverglass thickness, emission wavelength and depth of observation below the coverglass.^{51, 63} In confocal microscopy, pinhole size is another important factor in determining resolution.

2.1.5.1 Lateral resolution

The lateral resolution is defined as the radius of the first dark ring around the central disk of the Airy diffraction image of an infinite small object point. This is the Rayleigh criterion and is approximately equal to the width of the point spread function (PSF) in focal plane. The PSF may be measured by collecting a z-series extending 6-8 μm axially above and below the given sample.⁶¹ According to the Rayleigh criteria, the lateral resolution of a light microscope is given by:⁶¹

$$r_{Airy} \approx 0.61 \frac{\lambda}{NA} \quad (2-1)$$

where λ is the wavelength of the light and NA is the numerical aperture of the lens. The lateral resolution of a confocal microscope can be determined by measuring the size of small particles or by measuring distances between two particles or lines. The lateral point resolution (Δx) of a confocal microscope is:⁶⁴

$$\Delta x \approx \frac{1.22}{\sqrt{2}} \frac{\lambda}{NA} \quad (2-2)$$

Equation 2-2 describes the distance (Δx) of two point objects in terms of the excitation wavelength (λ) and the numerical aperture (NA) of the objective.

2.1.5.2. Axial resolution

Axial (z-axis) resolution is measured along the optical axis of the microscope and is defined as the minimum distance that the diffraction images of two points can approach each other along the z-axis. The distance from the centre of a 3D diffraction pattern to the first axial minimum is given by:⁶¹

$$z_{\min} \approx \frac{2\lambda n}{NA^2} \quad (2-3)$$

Where n is the refractive index of the object medium. An estimate for axial resolution of a point object in confocal fluorescent microscopy is:⁶⁴

$$\Delta z_{fl} \approx 1.5n \frac{\lambda}{NA^2} \quad (2-4)$$

The factor 1.5 is an example when a FITC fluorophore is illuminated at 488 nm and detected at about 520 nm. The factor depends on the ratio of excitation and emission wavelengths.⁶⁴

An alternative criterion for comparing the axial resolution of different systems is the full width at half-maximum (FWHM) of the plot of intensity profile in the x- and z-direction.

2.1.6 Parameters effecting confocal imaging

2.1.6.1 Numerical aperture (NA)

NA is a measure of the light gathering and resolving power of the lens and defined as the product of the sine of half angle of the cone of light (α) and the refractive index of

the material between lens and sample. In confocal microscopy, the resolution depends on the NA and with higher NA the thinner optical slice can be scanned. Higher NA may not be practical in some instances due to the short working distance. The best selection of the NA depends on the nature of sample and the refractive index of the immersion medium.⁵¹

2.1.6.2 Pinhole size

The pinhole prevents light originating from the out-of-focus plane to reach the detector. The size of pinhole is an important factor in resolution of confocal microscopy. The diameter of the pinhole is usually adjusted to the size of Airy disk in which it is proportional to the total magnification between object and pinhole plane. If the pinhole size is made very small (<0.1 Airy unit), the lateral resolution improves by $\sim 40\%$ but the signal level reduces by 95%. There is an optimum pinhole size that is large enough to allow the signal to be detected with adequate signal-to-noise (S/N), and small enough to reject the noise from the background.⁶¹

2.1.7 Major components of CLSM

The basic components of a CLSM consist of: microscope, objective lens, laser, scan head, photodetector and computer software. Confocal microscopes use either a laser or a mercury (or xenon) arc lamp (spinning disk confocal microscopy) as a light source. A laser beam has unique properties that make it an ideal light source for confocal microscopy. These properties are: high brightness, highly collimated and low beam divergence, high degree of spatial coherence, low noise, high degree of monochromaticity and the ability to be focused into a very small spot.^{51, 61} There are different types of laser varied in power, emission wavelength, gas content, cooling system and operational life time in commercial confocal systems. Detectors for

confocal microscopy have been mostly photomultiplier tubes (PMT). PMTs are excellent detectors due to high photon efficiency, high spatial and temporal resolutions and low-noise.⁶⁵

2.1.8 Types of confocal microscopy

All confocal techniques are based on the same fundamental scanning concept. There are several types of confocal microscopy based on the method of scanning: stage scanning, beam scanning, spinning disk, line scanning and programmable array microscopy.

2.1.8.1 Stage scanning confocal microscope

In this type of confocal microscope, the sample stage is moving and the beam is stationary. It has the advantage of scanning a larger field of view of the microscope. Also, due to the stationary optical arrangement and single beam scanning, the axial illumination is constant that presents the advantage of minimizing optical aberration to produce an even optical response across the scanned field. The speed of scanning is slow and can be improved by scanning a smaller pixel field. This type of confocal microscope is useful for slowly changing living samples, fixed samples and biochips or microarray analysing.⁵¹

2.1.8.2 Beam scanning confocal microscope

The beam scanning type of confocal microscope uses scanning mirrors to scan a beam across a stationary sample. The single beam laser confocal microscope (CLSM) is the most commonly employed confocal microscopy in biology. It has a higher resolution and faster scan rate than the stage scanning type. Two main types of CLSM are slow scan and video rate confocal microscope that differ in capture and image store times.⁵¹

2.1.8.3 Spinning disk confocal microscope (SDCM) or Nipkow disk microscope

The third type of confocal microscopy uses a spinning Nipkow disk and stationary light source and stage. In SDCM, a sample is illuminated by many separate spots simultaneously through an array of $\sim 20,000$ pinholes on a disk which rotates rapidly.⁶⁶ The emission light passes back through the same disk of pinhole array or another disk and is projected onto a sensitive CCD camera as detector. This type of confocal microscopy is used widely to image a variety of dynamic process of cells and tissues due to the high speed of scanning compared to CLSM.⁶²

Unlike CLSM that uses a single beam to illuminate the specimen, spinning disk confocal microscopes do scanning with thousands of light spots simultaneously. So, laser light sources with coherent property are not well-suited for this type of microscope. Mercury or xenon arc lamps that have broad spectrum, noncoherent light and are used in spinning disk confocal microscopy to excite fluorophores ranging from UV to red regions of the spectrum. Also, a video camera or cooled CCD camera is needed to generate sufficient signals and improve signal-to-noise ratio.⁵¹

A disadvantage of Nipkow disk microscope is that only a small fraction of the illuminating light passes through the pinholes to the specimen. This leads to weak signal and poor imaging in fluorescent imaging mode. Recent developments in SDCM to equipping it with microlenses raise the illumination transmittance and present a highly sensitive 3D imaging system in real time.

2.1.8.4 Line scanning confocal microscopy (LSM)

In LSM, galvanometer scanners are used to scan the line across the sample and then the signals are detected in parallel using a slit aperture.⁶¹ The major benefit of this system is increasing the rate of data collection and frame rate. LSM is categorized as a

high-speed confocal imaging microscopy for observing the fast biological processes in cells and tissues with 3D resolution.

2.1.8.5 Programmable Array Microscopes (PAM)

The PAM is an optical sectioning method based on programmable spatial light modulators (SLM) in the image plane of a widefield microscope to create spatial distributions in light beam to generate patterns of illumination and conjugate/nonconjugate detection of emitted light to generate optically sectioned images in real time.^{67, 68} The “conjugate” image corresponds to the focus-plane confocal data generated by a CLSM, whereas the “nonconjugate” image corresponds to the out-of-focus light rejected by the CLSM pinhole. A PAM provides much more temporally efficient excitation than CLSMs to 50% coverage of the sample compared with single point scanning systems.⁶⁹ To generate the final image, the conjugate and non-conjugate images are subtracted. Image registration, scaling, background subtraction, filtering, and other image processing operations are performed in real time (processing and display requires 10 ms per image).⁶⁹ The theory of operation of the PAM for fluorescence image formation has been described previously in detail.⁷⁰

The family of PAMs include optical sectioning systems operating in fluorescence,⁷¹ and reflection⁷² as well as spectroscopic imaging systems.^{73, 74} Two generations of PAM has been developed until now. First generation of the PAM used digital micromirror device (DMD) for optical sectioning⁶⁸ or transmissive liquid crystals SLMs for spectroscopic imaging.⁷⁵ It suffered from some limitations and needed two cameras for imaging conjugate and non-conjugate images.⁶⁹ Second generation of the PAM based on a ferroelectric liquid-crystalon-silicon (LCoS) microdisplay and an emCCD camera enables real-time sectioned imaging.⁷⁶ The second generation of the PAM has several advantages compared to other types of

confocal microscopy. The major advantages are: (i) simple with no moving parts unlike the rotating disc microscope allows software to control the parameters of illumination or detection patterns easily (ii) high speed optical sectioning due to a illumination duty cycle for each pixel of up to 50%; (iii) high detection sensitivity due to using emCCD camera; (iv) compatibility with variety of modalities and other imaging modes; (v) efficient and sensitive optical sectioning due to simultaneous detection and processing of both conjugate and non-conjugate light; and (vi) minimal photobleaching.⁶⁹

2.1.9 Other optical sectioning techniques

2.1.9.1 Deconvolution (Computational optical sectioning microscopy or COMS)

In this technique, a wide-field microscope is used to collect 2D images of different planes through a specimen. Then a computational method derived from the process of image formation and recording is used to remove out-of-focus light from each optical slice. Different mathematical models have been used in COMS such as nearest neighbours, frequency-based and constrain deconvolution.⁶²

2.1.9.2 Nonlinear optical techniques

A number of nonlinear optical techniques have been introduced to laser scanning microscopy over the past decades. Advances in ultrashort pulse laser technology made it possible for these techniques to open a new field in microscopy. The common characteristic of all these techniques is the self-sectioning property due to the generation of signals only near the focal point of an objective permitting optically sectional imaging and 3D reconstruction of the specimen in a manner similar to confocal microscopy.⁷⁷

2.1.9.2.1 Two-photon and multi-photon excitation microscopy

Two-photon excitation microscopy (TPM) is a promising technique in the fields of biophysics, biology, bio-engineering, material sciences, and medicine for performing 3D imaging. The theory of TPM is based on the nonlinear quantum process of two-photon excitation. Two-photon excitation requires the simultaneous absorption of two long wavelength photons by a dye molecule such that their combined energy induces the excited state. The total energy of the two photons equals the energy required for normal one-photon excitation. It requires the use of longer wavelength laser sources compared to single-photon excitation. Pulsed infrared or near-infrared lasers are the best light source for TPM due to high power to observe two-photon absorption and a sufficiently low average power not to damage biological samples.⁷⁸ The excitation region in TPM is limited to a small volume (femtoliter) centred at the focus of the objective. Only molecules in focal region are excited and contribute to image formation and no out-of-focus fluorescence is generated. So a confocal-like effect is obtained without using pinholes.⁷⁹

There are some advantages of TPM compared to confocal microscopy. First, the photobleaching and phototoxicity of fluorescent molecules are only limited to small volume in TPM. This allows imaging of living specimens for a long time period. Second, the imaging penetration depth is improved in TPM as light scattering is less for long wavelengths. Third, the shadowing effect due to primary excitation light absorption by a fluorophore above the plane of focus is not problematic in TPM. It is because the photon absorption is confined to a very narrow volume at the plane of focus. So, the specimen above the plane of focus is transparent to the excitation beam. Fourth, as TPM does not generate out-of-focus signal there are no scattered photons to

contribute to the background and image contrast is improved compare to confocal imaging.⁶⁰

Three-photon and higher photon excitation is also possible.⁷⁹ By simultaneous absorption of three photons, significant fluorescence can be generated with some compounds such as fluorophores that have maximum excitation between 200-350 nm. The theoretically lateral and axial resolution for an ideal three-photon microscope operating at 900 nm with NA 1.35 is 200 and 500 nm.⁸⁰

Two-photon fluorescence excitation was presented as an optical sectioning separation-free immunoassay method in the literature and will be discussed in more detail in chapter 3. No record has been found for using three-photon excitation as an immunoassay detection method.

2.1.9.2.2 Second harmonic generation (SHG) imaging microscopy (SHIM)

SHG is a second-order nonlinear optical process offering an alternative to two-photon fluorescence. It is a non-absorptive process in which two photons are converted into a single coherent photon of twice the energy, and half the wavelength. Second harmonic light is generated only by molecules with noncentrosymmetric structure such as some inorganic crystals (quartz, lithium niobate and zinc oxide), many structural proteins (collagen, microtubules, and muscle myosin), and lipid bilayers which have inherent asymmetry.⁸¹ SHIM obtains contrast from variations in a specimen's ability to generate second harmonic light.

SHIM requires the same instrumentation as a multiphoton excited fluorescence microscope. It possesses not only all the benefits of TPM such as high resolution, deep penetration (less scattering of illumination light), reduced out-of-plane photobleaching and phototoxicity but also doesn't have the problem of in-plane

phototoxicity of labelling fluorophores can be reduced due to the non-absorption nature of SHG process.⁸²

Surface second harmonic generation is a special case of SHG where the second beam is generated because of a break of symmetry caused by an interface at surfaces of media.⁸³ Surface SHG is possible even for materials which do not exhibit SHG in the bulk. A technique based on the laser induced surface second harmonic generation (SSHG) has been used as a non-labelled immunoassay detection method. SSHG originates from the field and structural discontinuity at the interface of two media. The signal depends on the angle of the incident light and detector, and the molecular orientation and concentration at the surface.^{83, 84}

2.1.9.2.3 Third harmonic imaging (THG) microscopy

Another coherent nonlinear microscopy technique based on the nonlinear optical process is THG. THG is not limited to specific materials as SHG, since all materials have a nonvanishing third-order coefficient.⁸⁵ In THG, three photons with the same frequency (ω) interact nonresonantly with the medium to produce one photon at the third-harmonic frequency equal to 3ω .⁷⁷ In THG microscopy, third harmonic light is generated at the focal point of a focused short-pulse laser beam. When the medium near the focal point is not uniform, such as difference in refractive index or nonlinear susceptibility, a measurable amount of third harmonic is generated. THG imaging is especially suited for 3D imaging of a transparent specimen.^{85, 86} It is a background free imaging technique and there is no need for additional staining of the specimen. Since the excitation wavelength is long ($>1 \mu\text{m}$), it is a nonbleaching and less biologically damaging imaging method.

2.1.9.3 Structured illumination microscopy (SIM)

SIM is a method to obtain optically sectioned images from a conventional wide-field microscopy in real time. It has been suggested firstly to improve the lateral resolution of an optical system in 1963⁸⁷ but has been used in 1997 to improve the axial resolution of a microscope.⁸⁸ It is a wide field illumination technique that using a grid pattern on the sample. The pattern introduces an artificial high frequency spatial modulation of the sample. With a simple image analysis, it is possible to isolate the part of the sample that is modulated and therefore in focus, from the background that is not modulated and thus out-of-focus. The strength of sectioning depends on the pitch and contrast of the stripe. The image analysis removes the stripe pattern from the final reconstructed optical section.⁸⁷

2.1.9.4 4Pi and I⁵M microscopy

4Pi and I⁵M microscopy are far-field microscopy techniques with improved axial resolution of the order 100 nm. The improvement has been done by the coherent addition of two spherical wave fronts of two opposing lenses of high NA.^{89,90} In 4Pi microscopy, a laser beam is used for illumination of sample and PMT is used as detector. But, in I⁵M, the laser is replaced by an incoherent light source such as an arc lamp and a CCD camera is used as detector.⁹¹

At the present state of development, the sample preparation for 4Pi microscope is not as easy as other optical sectioning methods. The sample should be thin to be mounted between two coverslips with a space gap as thin as about 50 μm and the refractive index needs to be similar between sample, embedding medium and immersion medium. It is an expensive microscope and needs trained specialist personnel to operate it. Therefore, using 4Pi microscope as a detection method for an immunoassay sample in conventional format such as microliter well plates is impossible.

2.1.9.5 Stimulated emission depletion microscopy (STED)

STED is a member of a family of concept that use reversible saturable optical (fluorescence) transitions (RESOLFT) showing that in fluorescence microscopy, the diffraction barrier in far-field can be broken. In a RESOLFT, the subdiffraction resolution is provided by the saturation of an optical transition, and the spatial resolution depends mainly on the saturation level instead of just on the wavelength and on the numerical aperture. The resolution achieved by a STED microscope depends only on the available laser power and the quality of the implementation.⁹² STED microscopy can improve the resolution both in the transverse (x, y) and the axial (z) direction. No record has been found of using STED microscopy to detect immunoassay.

2.2 Immunoassay

Immunoassay (IA) is a quantitative analytical technique based on the reaction between an antigen and antibody to measure the concentration of either reactant. IA is widely used in different fields of biochemical assays due to its high sensitivity, high selectivity, rapid detection and possibility of analysing variety of molecules without fundamental changes in the process.

2.2.1 History of immunoassays

Early immunoassays were based on the direct observation of binding reaction product such as forming of antigen-antibody complex precipitation, *e.g.* using red blood cells and subsequent haemagglutination.²⁹ The first immunoassay originated in 1959 by the work of Yalow and Berson in United States who received Nobel prize in medicine in 1977 for measuring insulin in blood plasma using ¹²⁵I in a competitive radioimmunoassay (RIA).^{93, 94} During the same period, Roger Ekins in England was

studying the distribution of thyroxine between albumin and thyroxine binding protein in the blood of a patient treated with high doses of ^{131}I . He was able to demonstrate the measurement of thyroxine in human plasma by a method called saturation assay which was used as a general procedure using specific binding protein.⁹⁵

For one decade, RIA has been used widely in biomedical laboratories and its sensitivity and precision have been optimized by using highly purified antibodies coupled to radioactive tracer and two-site RIA.⁹⁶ Although RIA is reliable and sensitive method, it suffers from potential health hazards, waste disposal problems, expensive reagents and short half-life using ^{125}I as a label.^{97, 98} The first development of IA techniques was the replacement of radioisotope labels with alternative non-radioisotopic labels such as enzyme labels,^{99, 100} fluorescent labels,^{101, 102} chemiluminescence,¹⁰³ and bioluminescent and variety of different labels as well as unlabelled assay formats using biosensors. Thus, a whole variety of immunoassays, instruments and assay formats has arisen and developed to satisfy users in different aspects of immunoassay performance. Speed, sensitivity, reliability, simplicity, specificity, cost, throughput and automation are the main targets of development in immunoassay technology.⁹⁸ There has been a fast growth in the application and assay formats of immunoassay over the years in which some of them have resulted in more sensitive assays to help clinical research and diagnosis.

2.2.2 Classification of immunoassays

There are different aspects for classification of immunoassays in the literature. The classification depends on the variables contributing to the procedure of immunoassays such as sample type, nature of analyte, assay conditions, etc. Based on the major criteria that have most influence on immunoassay performance, it can be classified as:

- (i) limited or excess reagent format; (ii) homogeneous or heterogeneous format and; (iii) labelled or unlabelled assay formats and choice of label.

2.2.2.1 Limited or excess reagent format

2.2.2.1.1 Limited or competitive assays

In limited or competitive assay format, a limited, constant amount of antibody (or antigen) coated on the surface is used for detection of the unknown amount of antigen (or antibody) in a sample with a fixed and known amount of labelled antigen (or antibody)⁹⁶ (Figure 2-2). There is a competition between labelled and unlabelled forms of analytes for the limited number of binding sites on the surface. The amount of fixed and labelled reagents should be limited so that small differences in the amount of analyte can be seen.¹⁰⁴ The concentration of unlabelled antigen in the sample can be determined from the proportion of labelled antigen that is bound to the antibody on the surface. The response of competitive assay is highly dependent on the amount of labelled and coating reagents.

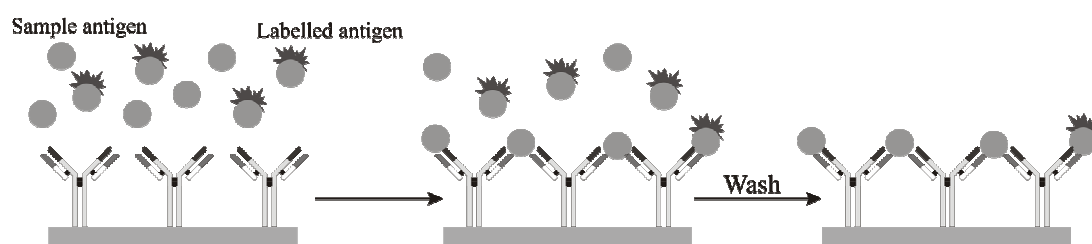


Figure 2-2: A competitive assay for detection of antigen. The competition of a fixed amount of labelled antigen for a fixed amount of antibody on the surface is determined.¹⁰⁴

Competitive inhibition assays are often used to measure small molecules with a single epitope such as hormones, pesticides and drugs.¹⁰⁵ These assays are also used

when a matched pair of antibodies to the analyte to do a sandwich assay does not exist. Radioisotope, enzymes and fluorescent reagents use as the most used labels in competitive format immunoassays.

2.2.2.1.2 Reagent excess assays or non-competitive assays

In this format, antigen binds to an excess amount of antibody. The most common assay in this format is two-site immunometric assay or sandwich assay (Figure 2-3). The plate is coated with excess amount of capture antibody and the sample containing antigen is added. The bound antigen is detected with secondary labelled antibody. The secondary antibody may be labelled directly or detected following addition of an unlabelled antibody specific for the bound antibody followed by a second labelled antibody. Typically, an enzyme or a fluorophore is attached to the secondary antibody followed by absorbance or fluorescence detection. The coating and detected antibodies may be the same or different, may be polyclonal or monoclonal. The two monoclonal antibodies should recognize different epitopes or antigenic binding sites of the antigen.¹⁰⁵ Compared to competitive format assay, metering of reagents is less critical.

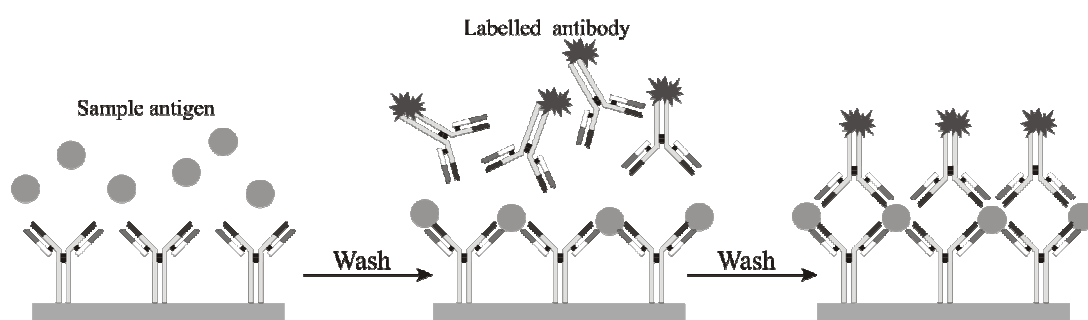


Figure 2-3: Non-competitive or sandwich assay. Antibody coated surface is incubated with sample containing antigen which is subsequently detected by a labelled detector antibody.¹⁰⁴

The two-site assays provide advantages such as speed, sensitivity and specificity. Assay is faster due to using the excess amount of reagents which leads to

shorter incubation times. Higher sensitivity and specificity are due to the two different antibodies needed to bind to the binding sites which decrease the chance of interference by other similar molecules.¹⁰⁶

2.2.2.1.3 Ambient analyte assays

Ambient analyte assays is a novel group of assays introduced by Ekins¹⁰⁷ and comprise assays in which the concentration of analytes is measured directly and independent of sample volume and the amount of antibody when the concentration of the antibody is low enough. The concept of ambient analyte assay is the foundation of current microarray technology.¹⁰⁸

The ambient analyte assay concept is mainly based on the Law of Mass action and antibody binding site occupancy principle. Both competitive and non-competitive assays rely on the measurement of antibody occupancy following its reaction with an analyte. They are different in the way that the fractional antibody binding site occupancy is determined. In non-competitive assays, the occupied antibody sites are measured directly *e.g.* by using a secondary antibody against occupied sites. Conversely, competitive assays rely on indirect determination of binding site occupancy by measuring of unoccupied sites *e.g.* by using labelled analyte.¹⁰⁹ When free antibodies bound to a surface (fAb) capture free analyte (fAg) in a sample to produce an antigen-antibody complex, the fractional occupancy of antibody binding sites (F) according to the law of mass action can be written as:¹⁰⁵

$$F = \frac{[AbAg]}{[tAb]} = \frac{K[fAg]}{1 + K[fAg]} \quad (2-5)$$

where [AbAg], [tAb] represent the concentrations of bound antibody and total antibody at equilibrium and K is the binding affinity constant. The final free analyte concentration is dependent on both total analyte and antibody concentrations. But

when the total antibody concentration is low (less than $0.01/K-0.05K$) there is no significant difference between the free and total analyte concentrations and F tends to:¹¹⁰

$$F = \frac{K[Ag]}{1 + K[Ag]} \quad (2-6)$$

So the fractional occupancy of antibody binding sites only reflects the ambient analyte concentration. Assays based on this concept in which the fractional occupancy of the antibody is independent of sample volume and antibody concentration have been termed as ambient analyte assays. Binding analyte to the antibody causes depletion of the unbound analyte in the sample, but due to the small amount of binding in ambient analyte assays, the reduction in concentration is insignificant and the system is sample volume independent.¹⁰⁵ The concept of ambient analyte assays lead to two further concepts: antibody and dual-label microspot immunoassays.¹⁰⁹

2.2.2.2 Homogeneous and heterogeneous assay

In any labelled format assays, there is a need to differentiate bound from free labelled reagents before measuring the signal of the assay. It can be done either by any means of separating (heterogeneous) or by modulation the signal of the label when analyte is bound to reagent compared to when it is free (homogeneous).⁹⁶

2.2.2.2.1 Homogeneous assays

Homogeneous assays do not require the separation step and therefore tend to be faster, simpler and more amenable to automation. The simplicity of automation is the main stimuli for researchers to continue working on homogeneous assays with better sensitivity.

Homogeneous assays require only the mixing of a sample and immunochemical reagents followed by detection.¹⁰⁵ The binding occurs in the

solution and therefore is homogeneous; detection requires a change in some characteristics (like polarization, anisotropy, FRET, fluorescence /luminescence quenching or enhancement), and this is what is detected. Homogeneous assays take place entirely in the solution phase, while in heterogeneous immunoassays the antibody (or in some cases antigen) is immobilized on a solid support. Heterogeneous assays take advantage of the separation step which occurs before detection - removing unbound antibody or antigen from the site. In this case no change in the above mentioned characteristics is required, and what is detected is the change in the signal due to the separation.

Homogeneous or non-separation fluoroimmunoassays (FIAs) are defined as procedures in which the extent of the antigen-antibody reaction can be quantified without separation of the free tracer from the antibody-bound fraction. The major characteristic of a homogeneous immunoassay is the modulation of the specific signal either by enhancement or quenching when labelled reactant binds to its partner. In particular, homogeneous FIAs are assays in which the antibody-binding reaction significantly alters the fluorescence properties of the label so that it is possible to monitor the extent of the binding reaction at any time from the homogeneous reaction mixture.

2.2.2.2.2 Heterogeneous assays

Heterogeneous formats require separation of bound and free label before signal detection. Although, no separation is a benefit of homogeneous assay regarding of speed and convenience of the assay, but it can be an advantage for heterogeneous assay too. A separation step by introducing a wash step can improve assay detection limits by removing interferes that compromise the detection system and mainly by reducing non-specific binding.⁹⁶

Separation techniques in immunoassay can be classified based on the principles used for separation to different groups such as: physicochemical characterization of antigen or antibody (charge or size), adsorption, fractional precipitation, immunological and non-immunological methods. The immunologically based separation systems using a solid surface are now the most common used. The immunological separation systems can be divided into liquid and solid phase groups. In liquid phase, the immune complex of analyte and secondary antibody separates by centrifugation. The usage of this method was limited due to requiring relatively large amounts of antibody, long reaction time, the need of a refrigerated centrifuge and, great care for washing the precipitate. Development of a solid phase separation method by introducing microparticles, tubes and microtitre plates has enabled frequent washing with no disadvantages compared to the liquid phase method.¹⁰⁵

Various solid phases are used in heterogeneous immunoassays which can be divided into particulate and solid surface matrices. There are two types of particulate matrices: magnetic and nonmagnetic. The advantages of magnetic particles are the high surface area, rapid analyte capture, easy and efficient separation and washing.⁹⁶ Nonmagnetic particulates matrices include latex, glass, Sepharose, Sephadex, nylon particles and beads. Using macro solid surface matrices simplify the protocol of immunoassays. They included membranes (cellulose or nitrocellulose, glass-fibre), coated tubes and microtitre plates. Microtitre plates are the most popular solid phase in use at the present. They are available in different materials (plastic, polystyrene) and formats (96, 384 and 1536).

Chapter 3

Confocal detection of planar immunosorbent assay

This chapter describes the primary goal of the thesis: to demonstrate planar FLISA assays requiring optical sectioning to read out. The assays were based on a model of human IgG sandwich immunoassay. The model system was used to explore the confocal readout process in heterogeneous (two wash steps) and homogeneous (no wash steps) formats. The simplicity of the object shapes arising from the planar format makes the decomposition of analyte signals from the thin film bound to the surface and overlayer straightforward. Confocal readout enables fewer wash and incubation steps compared to conventional planar assays. Hepatitis C has been chosen for investigation of the confocal immunosorbent assay response to a real disease.

The results of this chapter have been published in Journal of Biomedical Optics as “Confocal detection of planar homogeneous and heterogeneous immunosorbent assays” in 2009¹¹¹.

3.1 Introduction

Introduction section of this chapter reviews the existing confocally immunoassay readout methods in the literature by CLSM and other optical sectioning methods. After reviewing each method's prospects, the main aim of this chapter "a planar confocal immunosorbent assay method" is presented theoretically and experimentally. As HCV assay has been used in experimental section, a brief overview of HCV detection methods is also presented.

3.1.1 Optical sectioning immunoassay detection methods

Detection of a FLISA by CLSM has been described previously for bead-based assays (FMAT),^{14-16, 112-114} and spot microarray formats.^{110, 115} Although confocal readout has been described in these papers, they were not carried out in a homogeneous planar format nor have the characteristics of the confocal response from these systems been published. Two-photon excitation has been described as another optical sectioning method for measuring the degree of binding of a fluorescent tracer attached to 3 μ m polystyrene microparticles in a homogeneous immunoassay.¹¹⁶

3.1.1.1 Fluorometric micro-volume assay technology (FMAT)

FMAT is a homogeneous bead or cell based fluorescent immunoassay using a micro confocal imaging system. It is based on volumetric capillary cytometry (VCC) system used for imaging and counting the fluorescently labelled cells in a capillary.¹¹⁷ The homogeneous format of FMAT makes it ideal for HTS and a nonradioactive substitute for traditional HTS assays. It is also capable of doing multiplexed assays using two different fluorescent dyes. The main advantage of FMAT over the traditional ELISA is the minimal requirements of manipulation due to less washing and incubation steps

that makes this method time consuming compared to ELISA and less amount of antibody is needed in this assay.¹⁷ Use of FMAT has been reported in several papers to perform homogeneous multiplexed assays,^{16, 118} receptor-ligand binding assays,^{112, 119} apoptosis and cytotoxicity,¹⁴ HTS,^{120-122, 14, 15, 123, 124} and cell based assays¹²⁵ in the literature. The results of the reports were compatible with traditional ELISA with respect to the linear dynamic range and sensitivity.

The instrumentation of FMAT has been described in detail previously.^{14, 16} The instrument consists of a scanner that uses a 633-nm helium/neon laser as the excitation source that is reflected from a galvo-mirror and is focused through a 20×0.5 NA objective. A *xyz* stage moves the multi-well plates and the area of 1 mm² with a depth of focus of ~ 100 μm in *z*-axis from the bottom of each well of 96- or 384-well plates is automatically scanned.¹¹² Since the depth of focus (100 μm) is small in comparison with the remaining volume of the well, the background fluorescence is minimal compared to the fluorescent assay on cells or beads, and there is no need to wash to remove the overlayer unbound fluorophores.¹²³ The emitted fluorescence is separated from the excitation beam by passing through a dichroic beam splitter and detected by two photomultiplier tubes through the proper filters to detect two independent red dyes emissions simultaneously. The FMAT software processes the digital images and generates a data output of the number of fluorescent cells or beads at the bottom of each well and the intensity of them. The fluorescent signal is directly proportional to the fluorescent antibody attached to cells/beads.

To conduct a sandwich FLISA assay with FMAT system, 6-μm beads are used as a solid surface. Beads covalently attached with goat anti-mouse IgGs are first coated with the first antibody by suspending them and incubation for 16 hours at room temperature. Then the antibody coated beads, biotinylated detection antibody, dye-

labelled streptavidin and the sample or standard are added to the well at the same time together and allow incubation overnight to form sandwich assay and settle down on the bottom of the well. For cell assay, both suspension and adherent cells can be stained with fluorescent antibodies targeted to the cell surface and the amount of the fluorescent on cell surface is quantified with FMAT.¹¹²

3.1.1.2 Two-photon excitation fluoreometry (TPX):

TPX is a homogeneous, separation-free assay technique based on using polystyrene microparticles as the solid phase and detection of two-photon excited fluorescence from the surface of individual microparticles in suspension.^{116, 126} The technique allows quantitative bioaffinity assays from a volume of a few microliters. In two-photon excitation, only fluorescent molecules within a restricted focal volume can be excited and therefore the background signals from the sample outside of the focal volume are not detected so the assay can be detected without washing steps. The applicability of this technique for the detection of virus antigens,¹²⁷ antibodies,¹²⁸ C-reactive protein,^{49, 129} and nucleic acid sequences recognition¹³⁰ has been demonstrated successfully. The authors reported good sensitivity and dynamic range with no washing steps along with the ability to multiplex the assay. Real-time monitoring of the bioreaction and testing of the plasma samples demonstrated the potential of the TPX method for development of clinical immunoassays.⁴⁹

3.1.1.3 Confocal readout of microarray format immunoassays

Confocal readout of microarray format immunoassays has been done previously and there are commercially available scanners for this purpose.^{131, 132} The requirement when using such a confocal microscope system for microarray scanning are a very flat surface for the microarray substrate and sufficient scanning speed to avoid

photobleaching of the fluorophores.¹³³ There is, however, no consensus on the benefits of confocal readout in the literature. For example, confocal readout has been presented as a sensitive method for determination of fluorescent signals emitted from the small detection volume such as spots while rejecting out-of-focus background.²¹ Conversely, it has been argued that most of the background signal on microarrays comes from non-specific binding to the slide surface which is in the same plane of focus as the sample and, thus, confocal read out provides little benefit as a microarray scanning method.¹³³

3.1.1.4 Confocal detection of planar immunosorbent assay

A set of planar FLISA assays requiring optical sectioning to read out was presented. The assays were based on a model sandwich immunoassay consisting of a goat antihuman immunoglobulin G (IgG) immobilized on a glass surface and a goat FITC-labelled antihuman IgG, which are used to detect human IgG. The model system was used to explore the confocal readout process while carrying it out in a spectrum of assays ranging from heterogeneous (two wash steps) to homogeneous (no wash steps). In these model systems, confocal readout enables fewer wash and incubation steps compared to conventional planar assays. By eliminating wash steps, the confocal assay is simpler and potentially more rapid.

3.1.2 Hepatitis C

Hepatitis C is a serious public health problem affecting about 180 million people worldwide.¹³⁴ It is the major cause of acute and chronic hepatitis, liver cirrhosis and hepatocellular carcinoma. Hepatitis C virus (HCV) is a single-stranded RNA virus belongs to the family of Flavivirus. The viral genome is composed of a 5' untranslated region (UTR), a long open reading frame (ORF) and 3'UTR region.¹³⁵ It codes for a

polyprotein of ~3000 amino acids that is subdivided to structural (core, E1, E2, E7) and non-structural (NS) proteins (Figure 3-1).¹³⁶ HCV is classified into 6 genotypes and at least 30 subtypes.

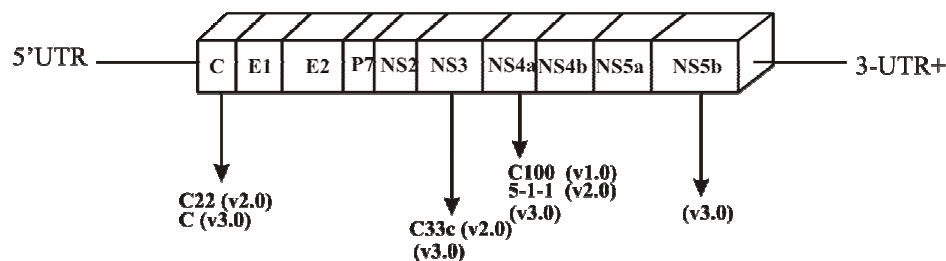


Figure 3-1: HCV genome and location of recombinant antigens used in three generations of enzyme immunoassays.¹³⁵

3.1.2.1 Diagnosis of HCV infection

Following the discovery of HCV genome in 1989,¹³⁷ numerous laboratory tests have been developed and commercialized to diagnose HCV infection and the screening of donated blood. The laboratory diagnostic tests can be categorised into three main classes: (i) serological tests to detect antibody against HCV (anti-HCV) or HCV antigen; (ii) molecular assays to qualify and quantify HCV RNA; and (iii) genotyping assays.

3.1.2.1.1 Serological tests

3.1.2.1.1.1 Anti-HCV screening tests

Antibodies to HCV (anti-HCV) can be detected in serum or plasma 7-8 weeks after infection.^{138, 139} A range of antigens from core and several non-structural proteins is used for detection anti-HCV.¹³⁹ False positive and negative are the main shortcomings of anti-HCV tests which must be confirmed with complementary and molecular techniques. Three generations of enzyme immunoassays (EIA) have been developed to increase the sensitivity and specificity.¹³⁵ The first generation ELISA test contained an epitope from the non-structural region (NS4). The second generation test was

developed with addition of antigens from core and NS3 genes and the third generation test differs by substitution of the NS5 protein and reconfiguration of core and NS3 antigens. The sensitivity of third generation is 97% in population of high prevalence of HCV infection.

3.1.2.1.1.2 Anti-HCV supplementary or confirmatory tests

Supplemental tests have been developed to discriminate the positive result of anti-HCV test. The most commonly used ones are recombinant immunoblot assays (RIBA) which identify the antibodies to individual HCV antigens. The specificity of these tests is higher than ELISA but sensitivity is lower.

3.1.2.1.1.3 HCV core antigen test

Detection of the presence of viral proteins (antigens) is an alternative to HCV RNA detection due to the possibility of detecting antigens in the window period. As the molecular techniques for detection of HCV RNA are labour intensive and expensive, many efforts have been done to find a successful replacement for them. The viral nucleoprotein or core protein was selected due to it is a structural HCV protein and its sequence is conserved across different HCV genotypes.¹³⁸ There are several in-house and commercial HCV core antigen assays in the literature. They are EIA or chemiluminescent assays using monoclonal antibodies to capture HCV core antigen.¹³⁸ The first reported assay had a low sensitivity (a few ng/ml) but the next generation showed better sensitivity comparable with HCV RNA detection assays (about pg/ml).^{140, 141}

3.1.2.1.2 Nucleic acid techniques (NAT)

The presence of HCV RNA in serum or plasma is the direct indication of ongoing HCV infection.¹⁴² Quantification of viral genome is critical in clinical management of

patients. There are expensive methods that need trained personnel to do them correctly. There are commercially kits and in-house methods for detection of HCV RNA. Because of the limited amount of viral RNA in infected persons, a target or signal amplification step is needed.¹⁴³ Reverse transcription polymerase chain reaction (RT-PCR) and transcription-mediated amplification (TMA) are target amplification. The branched DNA (bDNA) test is a signal amplification method which is more stable compared to RT-PCR method but is less sensitive.

3.1.2.1.3 Genotyping tests

Genotyping identification is important in response to treatment and epidemiological studies. Several commercial assays are available to determine HCV genotype by direct sequencing of one of the HCV genome regions (NS5, core, E1 or 5'NCRs) is representative of the whole genome for its genotype.

3.2 Theory of confocally detection of planar immunoassays

The key part of the confocal sandwich immunoassay (Figure 3-2) is a fluorescent layer consisting of three stacked IgG molecules which is < 50 nm in thickness.¹⁴⁴⁻¹⁴⁶ Depending on the orientation of the IgGs within the film, the thickness may range from ~12 to 45 nm. This dimension varies depending on whether it is estimated based on x-ray crystallographic data, scanning probe microscopy, or electron microscopy.¹⁴⁴⁻¹⁴⁶ The value of 50 nm used here is meant to be a conservative estimate indicating that the film thickness is arbitrarily thin under the measurement conditions.

In contrast to beads, the axial position of a planar thin fluorescent film oriented along the bottom of a plate cannot be detected with a conventional microscope. Hence, there is no way to determine the location and relative intensities

of the thin film and overlayer with such a system. In addition, the thickness of this thin fluorescent layer is below the resolution limit of all but the most advanced far-field fluorescence microscopes.¹⁴⁷ Although the thickness of IgGs stacked in a film cannot be measured with a confocal microscope due to the diffraction limit, both the position on the maximum in the axial response curve and the intensity of light from film can be measured with considerable precision.

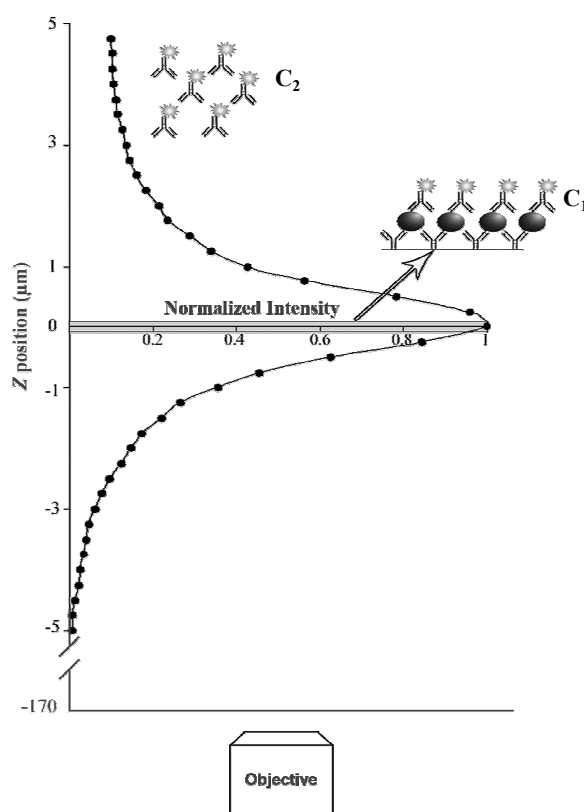


Figure 3-2: Schematic diagram of a confocal sandwich immunoassay. The assay structure consisting of overlayer, thin film, and glass substrate is located above the objective and inverted microscope. To clarify the geometry of the assay with respect to the microscope the graph is oriented relative to the laboratory axes. Subsequent figures plot axial position horizontally.¹¹¹

The response of a planar confocal immunoassay format can be considered as the sum of the responses of a 50 nm thin layer with fluorescent concentration of C_1 and a fluorescent overlayer beginning 50 nm above the glass with concentration of C_2

(Figure 3-2). By using an optical model described in detail in appendix, the concentration dependent intensity, C_1 and C_2 , can be determined respectively.

A semiempirical approach used in which the axial response of CLSM is measured for a thin film in the absence of an overlayer (a FLISA after washing the overlayer) and for the overlayer in the absence of the thin film (a control FLISA). The measured data are then synthesized by making linear combinations of the two measured objects. The best results were obtained by fitting the observed data to Cauchy-Lorentz function and the cumulative Cauchy-Lorentz function. The semiempirical fit used the following form:

$$M(z) = C_1 \frac{1}{\pi\gamma \left[1 + \left(\frac{z-z_0}{\gamma} \right)^2 \right]} + C_2 \left(\frac{1}{\pi} \arctan \left(\frac{z-z_0}{\gamma} \right) + \frac{1}{2} \right) + B \quad (3-1)$$

where, z_0 is the center of the thin film, γ is the width of the response, and B is a constant which corrects for electronic offsets and photomultiplier tube background in the confocal microscope. The first part of this equation measures the concentration related intensity of the thin layer (C_1) and the second part determines the overlayer concentration (C_2).

The other distribution function used for fitting the data was a Gaussian function and the cumulative Gaussian function based on this equation:

$$M(z) = C_1 \frac{1}{\sqrt{2\pi\sigma^2}} e^{-\frac{(z-\mu)^2}{2\sigma^2}} + C_2 \left[\frac{1}{2} \left(1 + \operatorname{erf} \left(\frac{z-\mu}{\sqrt{2\sigma^2}} \right) \right) \right] + B \quad (3-2)$$

where μ is the center of the thin film, σ is the width of the response, and B is a fluorescent background in the microscope.

3.3 Materials and methods

3.3.1 The model assay systems

The first model assay was based on a system consisting of a goat anti-human IgG immobilized on a glass surface and a goat FITC-labelled anti-human IgG which are used to detect human IgG. The model system was used to explore the confocal readout process while carrying it out in a spectrum of assays ranging from completely heterogeneous (2 wash steps) to completely homogeneous (no wash steps). In these model systems, confocal readout allows fewer wash and incubation steps compared to conventional planar assays. The second model assay system was HCV FLISA. Two assay formats of sandwich and indirect were used to detect the HCV core antigen and anti-HCV antibody respectively.

3.3.2 Reagents

Human IgG, goat anti-human IgG (γ -chain specific), goat anti-human IgG (γ -chain specific) FITC conjugate and bovine serum albumin minimum 98% (BSA), phosphate buffered saline pH 7.4 (PBS) was purchased from Sigma-Aldrich Company Ltd (Dorset, UK). Qdot® 605 goat F(ab')₂ anti-human IgG conjugate (H+L) was purchased from Invitrogen (Paisley UK). HCV core antigen (catalogue No. 00115-V), HCV core antibodies (catalogue No. 016-A and 017-A) and HCV core antibody fluorescein conjugate (catalogue no. 017-A-F) were purchased from Virogen company.

To obtain precise and less blurred images from confocal microscopy, it is required to use flat, glass bottom plates. Chambered cover glass slides (Lab-Tek chambered #1.0 Borosilicate, Nalgene Nunc international, USA) and glass bottom 96-

well plates (Nalgene Nunc international, USA) were used as solid supports for the immunoassay.

3.3.3 Instrumentation

3.3.3.1 CLSM

A confocal scanner head (TCS NT; Leica Microsystems, Heidelberg GmbH, Germany) installed on an inverted microscope (DMIRBE, Leica Heidelberg GmbH, Germany) was used for the optical sectioning of the immunoassay. It is a point scanning system that uses dichroic mirrors on a filter wheel to separate the wavelengths of fluorescent light emitted from the sample.⁵¹ Leica TCS NT is equipped with Argon ion and Krypton lasers and has four emission lines at 457, 488, 568 and 647. It had three PMTs which allow simultaneous imaging of different fluorophores in multiple-labelled samples.

The 488 nm line of an argon ion laser was used for excitation and the emission fluorescent intensity was detected using a 530/30 nm bandpass filter. The objectives used were: 10×NA 0.3, 16× NA 0.5, 40×NA 0.6, 40× NA 0.75, and 63× NA 0.7.

3.3.3.2 PAM

The second generation of the PAM in the Department of Molecular biology of the Max Planck institute for Biophysical Chemistry (Göttingen, Germany) was used for 2 weeks to study the confocal immunosorbent assay method. The PAM featured a ferroelectric liquid-crystal-on silicon (LCoS) device (SXGA-R2D, Forth Dimension Displays, Dunfermline, Scotland). The PAM was attached to a camera port on an Olympus IX71 fluorescence microscope (Olympus, Hamburg, Germany). Images are acquired with an emCCD camera (iXon DV897, Andor Technology, Belfast, Northern Ireland). The 488 line of an argon ion laser (~ 200 mW, Coherent Innova 90, Spectra

Physics 2000) was used for excitation and emitted light collected by 595/35 nm band pass filter. The objective used was a water 40×NA 1.15. The camera (Ixon DV 897_BV) was cooled to -100 °C (Julabo Hc F30, Ultratemp 200). EM gain was set at 200 and the exposure time was 250 ms. Data were collected as TIFF files and converted to numerical data using Image J.

3.3.4 Preparation of confocal immunosorbent assay

3.3.4.1 Heterogeneous format of human IgG model

The human IgG immunoassays were conducted by immobilizing anti-human IgG as the capture antibody on the chamber slide overnight at 4° C. The remaining sites for protein binding were blocked with a solution of 1% BSA (1% BSA in PBS) for 2 hour. After washing with PBS human IgG was added as antigen and incubated for 2 hours at room temperature. The chambers were emptied and washed with buffer. Anti-human IgG-FITC was added to the chambers as the secondary labelled antibody and incubated for 1 hour. All steps from blocking to final incubation were performed at room temperature under continuous shaking. The chamber was scanned with the confocal microscope without washing the second labelled antibody.

3.3.4.2 Homogeneous format of human IgG model

For the homogenous format assays, human IgG and goat anti-human IgG-FITC were added simultaneously to the chamber slide and incubated for 2 hours at room temperature.

3.3.4.3 HCV core assay

In this study, HCV assay was chosen as a practical model for using confocal immunosorbent assay for a real disease. Detecting HCV core antigen assay in a

sandwich format with two monoclonal anti-HCV antibodies where one of them is conjugated to an organic dye were selected according to its advantage compare to anti HCV antibody assay.

3.3.4.3.1 Indirect assay

For the indirect assay, HCV core antigen was coated on the surface and goat HCV core antibody was detected with anti-goat IgG-FITC (Figure 3-3). A series of anti-HCV core antibody concentrations was prepared with fixed amount of HCV core antigen (10 $\mu\text{g/ml}$) on surface and was detected with 2 $\mu\text{g/ml}$ of secondary labelled antibody. The assay was scanned with CLSM without washing the fluorescent overlayer.

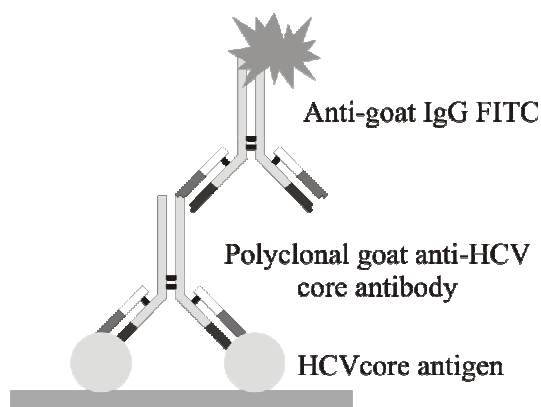


Figure 3-3: The FLISA indirect design for detection of HCV core antibody.

3.3.4.3.2 Sandwich assay

The HCV immunoassay was done in heterogeneous format of sandwich assay to detect the HCV core antigen (Figure 3-4). Polyclonal rabbit anti-HCV core antibody was coated on the surface of 96-well glass plate overnight at 4°C. After washing and blocking the remaining sites with BSA buffer for 2 hours, HCV core antigen was added and incubated for 2 hours at room temperature on a shaker. After washing the excess amount of antigen, polyclonal goat anti-HCV core antibody was added to each

well and incubated for 2 hours. After removing excess amount of secondary antibodies, FITC conjugated anti-goat IgG antibody was added and incubated 1 hour on a shaker at room temperature. The assay was scanned with CLMS without washing the fluorescent overlayer.

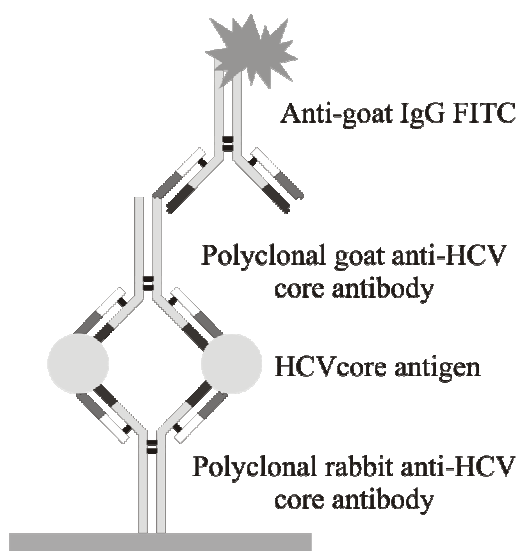


Figure 3-4: The FLISA sandwich design for detection of HCV core antigen.

3.3.5 Analysis

3.3.5.1 Image analysis of CLSM

A software module was developed in C++ language for analysing the fluorescent signals. The sum of the intensity of each image in the stack of confocal images was computed and plotted against z -axis position. These data were fit to Eq. 3-1 for Cauchy-Lorentz distribution function using least squares minimization and to Eq. 3-2 for Gaussian distribution function by Normdist function in Excel.

3.3.5.2 Detection limit

Detection limits were determined in two steps. First, the dose response curve was determined over a range of antigen concentration from 0 to 500 ng/ml with 3 replicates at each concentration. This was used to determine the slope of the linear

portion of the response curve. Second, a further 10 replicates at the lowest detectable concentration from the dose response curve and blank were measured and used to calculate the detection limit, DL:

$$DL = \frac{t \times s}{m} \quad (3-3)$$

where m is the slope of the linear portion of a dose response curve, $t = 2.821$, and s is the standard deviation of a set of 10 sample measurements. Reported “lowest detected concentrations” represent the lowest concentration of sample generating a significant ($p < 0.05$) difference from a set of blank measurements based on a t -test.

3.3.5.3 Adsorption of proteins to a solid phase

The Langmuir equation is widely used to describe equilibrium adsorption phenomena.^{29, 148} The Langmuir isotherm was originally developed to model the adsorption of gas molecules to solid phases but it has been further applied to the adsorption of proteins to a solid phase¹⁴⁹ as follows:

$$F = \frac{F_{Max}[C]}{K_d + [C]} \quad (3-4)$$

In this equation, F is the observed fluorescence intensity, F_{max} is the maximal value of F , $[C]$ the concentration of protein in the solution, and K_d is the thermodynamic dissociation constant at equilibrium.

3.3.5.4 Software and image processing of PAM

In the LCoS-based PAM, the conjugate and the non-conjugate images are recorded simultaneously side-by-side with a single CCD camera. During image acquisition, a background image is first subtracted from the image pair. Optical sectioning by the

PAM is real-time, i.e. the conjugate, nonconjugate and processed, sectioned images are displayed at video rate on the screen.

3.4 Results

3.4.1 Quality assessment of parameters affecting the confocal axial response

Image quality is important when evaluating the performance of a confocal microscope.^{61, 150, 151} The parameters affecting the quality of the response from the confocal microscope relevant to our assays have been investigated: NA, pinhole size, and step size. Step size is discussed in Sec. 3.4.2.3.

3.4.1.1 Numerical aperture

The intensity of a thin fluorescent film resulting from the human IgG model system after removal of the overlayer was measured in the confocal microscope with five different objectives varying in NA from 0.3 to 0.75. The axial response was measured with a 74 μm pinhole every 0.4 μm along the z-axis for a total of 50 images (Figure 3-5). This pinhole size was below one Airy disk diameter and has little or no effect on the resolution for this set of magnifications and NAs. The FWHM was measured for each objective (Table 3-1). As expected, the FWHM decreased with increasing NA with all the objectives showing an axial response to the thin film even at low NA. However, the improved resolution at high NA is advantageous as it will result in less blurring between film and overlayer and thus improve both sensitivity and limits of detection. Based on these results, the 40 \times NA 0.75 objective was selected for subsequent use.

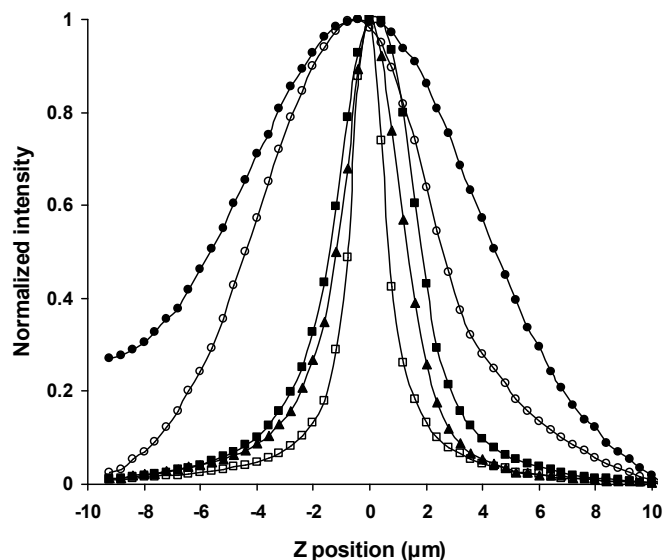


Figure 3-5: The axial response from a thin immunoassay film for a variety of objectives with different magnification and NA ● 10× NA 0.3, ○ 16× NA 0.57, ■ 40× NA 0.6, □ 40× NA 0.75, ▲ 63× NA 0.7.¹¹¹

Table 3-1: Variation of the FWHM of the axial response to a thin film when observed in the microscope as a function of NA for a variety of objectives.

Objective	FWHM (μm)
Leica 10×0.30 HC PL FLUOTAR	10.5
Leica 16×0.5 PL FLUOTAR IMM	7.0
Leica 40×0.60 HCX PL FL L CORR	3.4
Leica 63×0.70 HCX PL FLUOTAR L CORR	2.8
Leica 40×0.75 HCX PL FLUOTAR	1.8

3.4.1.2 Pinhole size

The effect of the pinhole size on the intensity and resolution of the axial response was studied using the 40×NA 0.75 objective using 50 steps of 0.4 μm along the z-axis (Figure 3-6). The intensity of the signal increased nearly linearly with pinhole size but the FWHM of the axial response increased rapidly when the pinhole exceeded 150 μm. The Airy disk diameter in the focal plane for the 40×NA 0.75 objective is approximately 170 μm and the optimal pinhole size is considered to be about 50-60% of this value,⁶¹ in good agreement with the measured data. In addition, since the axial

resolution does not improve significantly below this optimum, there is no benefit to further reduction in pinhole size. The only effect would be to reduce the signal strength from the thin film. Based on these experiments the pinhole size was set to $74\ \mu\text{m}$ in subsequent experiments.

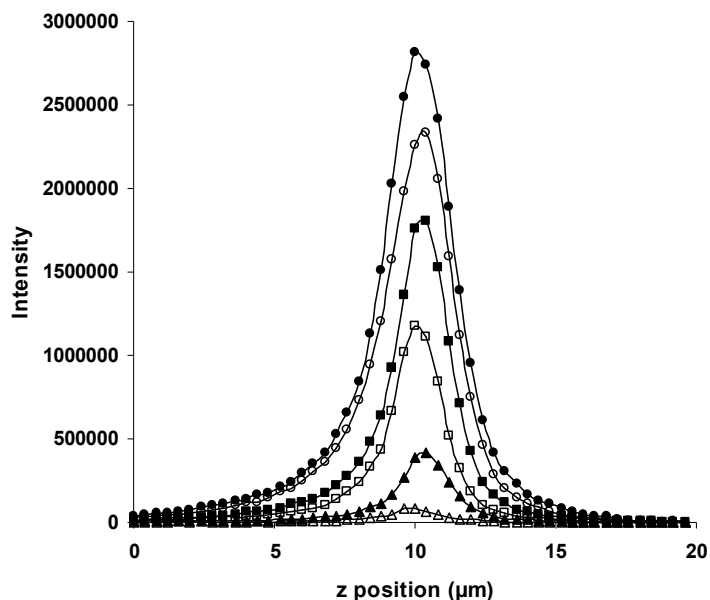


Figure 3-6: The axial response from a thin immunoassay film for a variety of pinhole sizes: ● $250\ \mu\text{m}$, ○ $200\ \mu\text{m}$, ■ $150\ \mu\text{m}$, □ $100\ \mu\text{m}$, ▲ $50\ \mu\text{m}$, △ $20\ \mu\text{m}$.¹¹¹

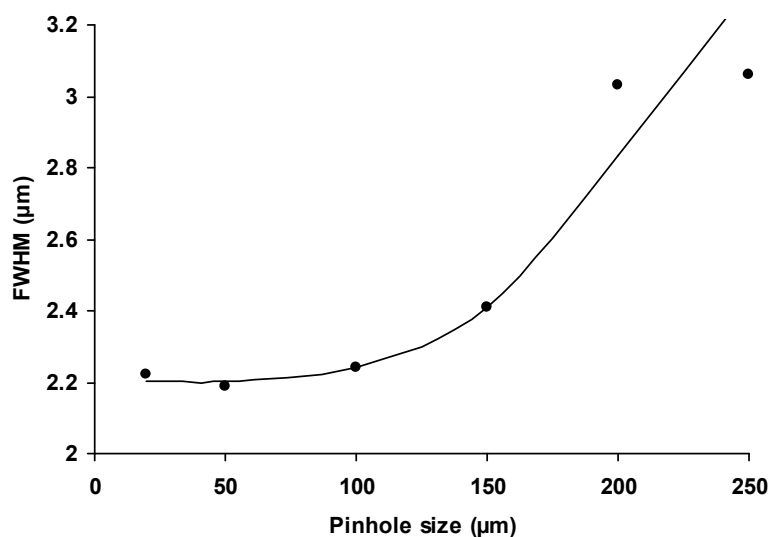


Figure 3-7: Variation of the FWHM of the axial response as a function of pinhole size for the $40\times\text{NA } 0.75$ objective. The axial response begins to degrade when the pinhole is near the diameter of the Airy disk ($\sim 140\ \mu\text{m}$). The line is only to guide the eye.¹¹¹

3.4.2. Heterogeneous Confocal Sandwich Assay

3.4.2.1 Response of film and overlayer

Human IgG as the antigen (1 $\mu\text{g/ml}$) was added to coated chamber slides with the primary antibody (20 $\mu\text{g/ml}$) followed by the secondary antibody (40 $\mu\text{g/ml}$). The chamber was scanned in the confocal microscope using the 40 \times NA 0.75 objective using 50 steps of 0.2 μm along the z axis and a 74 μm pinhole without removing the fluorescent solution. The axial response exhibited three distinct features (Figure 3-8): (I) a region of gradually decreasing signal trending to zero corresponding to the glass surface below the assay (0 to 5 μm); (II) a prominent peak arising from the thin film of concentrated fluorescence on the glass surface (0 μm); and (III) a region of decreasing fluorescence trending to a constant value resulting from the fluorescence of the overlayer of unbound secondary antibody (0 to 5 μm). The FWHM of the peak was 1.75 μm and the measured axial response indicated that the peak height contains signals from both the thin film and the fluorescent overlayer. The presence of overlayer fluorescence indicates that an excess of secondary antibody is present and must be separated from the film signal.

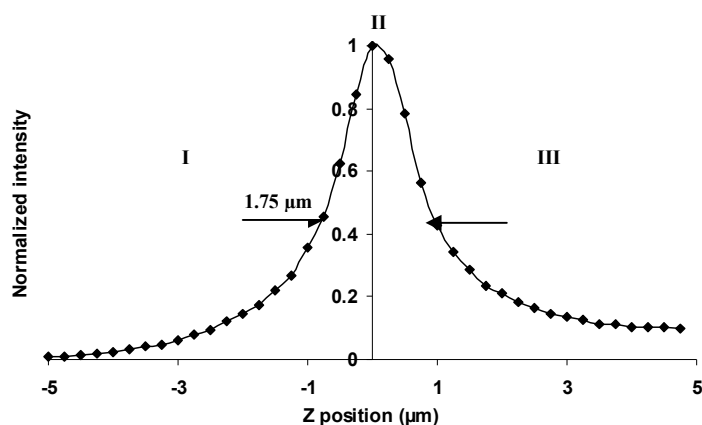


Figure 3-8 : The axial response of confocal sandwich immunoassay has three zones: (I) the negative z position represents locations inside the (~170 μm) thick glass slide; (II) the

location of the thin sandwich immunoassay film (50 nm thick); and (III) the positive z position shows the fluorescent overlayer of unbound secondary antibody.

3.4.2.2 Decomposition of the signals with Cauchy-Lorentz distribution function

The method used for separation was based on distribution functions. Separate scans were generated corresponding to the film and over layer alone. After testing a few functions the Cauchy-Lorentz and cumulative Cauchy-Lorentz functions were found to fit the measured data well (Eq. 3-1). This allowed the decomposition of the two objects when presented together (Figure 3-9).

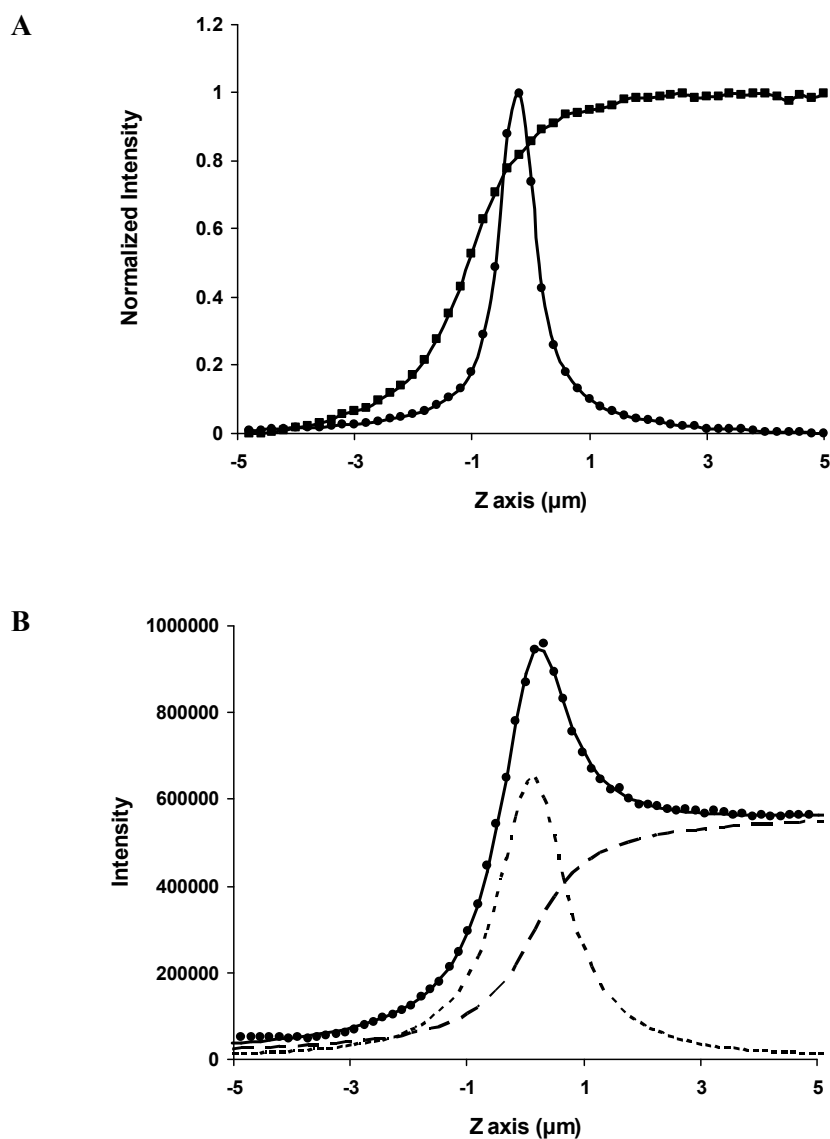


Figure 3-9: Decomposition the signal of confocal immunoassay to the thin film and overlayer based on Cauchy-Lorentz function. A: The axial responses of “thin film” (●) and “overlayer” (■) measured separately. B: The axial response of a sandwich immunoassay: the experimental data (●) is decomposed to thin film (- - -) and (— — —) overlayer after fitting the experimental data to the sum of “thin film” and “overlayer. The line connecting the data points is the best fit to Eq. 3-1 for this set of measurements.¹¹¹

3.4.2.3 Step size optimization

The effect of step size on the separation of signals from the thin film and the fluorescent overlayer was studied by changing the step size in 0.1 μm intervals between 1.6 and 0.1 μm over an approximately 10 μm scan range with a 40 \times NA 0.75 objective. Where 10 μm was not evenly divisible by the step size the closest scan range to 10 μm was selected. This experiment was performed using quantum dots as the reporter fluorophore to mitigate photobleaching problems in repeated scans of the same location encountered with FITC-labelled materials. The results showed that the signal-to-noise ratio (SNR) of the thin film intensity parameter (C_1 in Eq.3-1) decreases in a logarithmic fashion as the step size increased (Figure 3-10) with a tendency to overestimate the intensity of the thin film at step sizes (1 μm). Experiments described in subsequent portions of this report were performed using a 0.2 μm step size, which corresponded to an SNR of 168 in the optimization study.

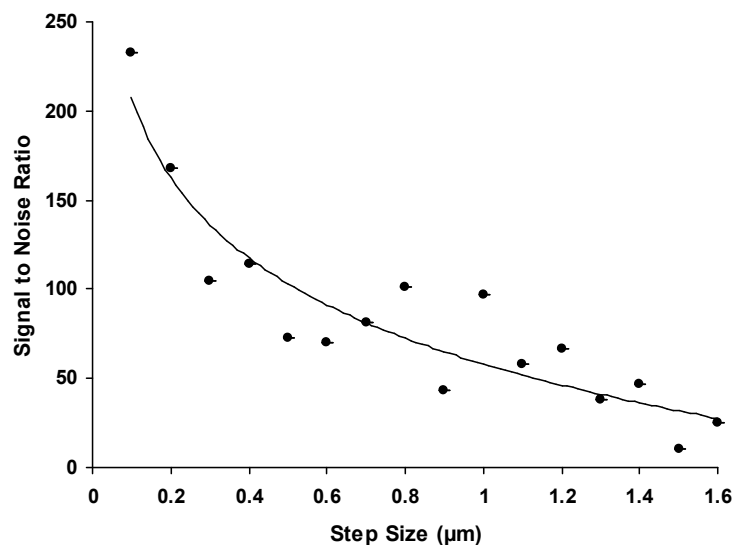


Figure 3-10: Variation in SNR as step size increases over a fixed z axis scan range. Scans were done using a quantum dot reporter in this experiment to enable repeated scans of the same location to be comparable. All other data reported in this chapter used FITC-labelled materials. The line shown corresponds to a logarithmic fit to the measured data. SNR improves as the step size decreases for a fixed scan range. This arises from better sampling of the axial response and an increase in the number of data points in the fit.¹¹¹

3.4.2.4 Heterogeneous confocal sandwich assay optimization

The different steps of the immunoassay procedure were optimized for the widest dynamic range. The concentration of coating antibody (goat antihuman IgG) was tested from 2.5 to 320 $\mu\text{g/ml}$ at a constant saturating level of antigen and secondary antibody (100 $\mu\text{g/ml}$) (Figure 3-11A). Using the protocol, the observed behaviour appeared to follow a Langmuir adsorption process (Eq.3-4). A concentration of 160 $\mu\text{g/ml}$ was chosen as optimal for the first antibody. This is a relatively high loading of the first antibody, but was found to work well for the chamber slides, reagents, and conditions in these experiments. The influence of the FITC-conjugated secondary antibody was investigated between 10 and 100 $\mu\text{g/ml}$ (Figure 3-11B) at a constant

coating of antibody and the antigen yielding an optimal concentration of secondary antibody (50 $\mu\text{g/ml}$).

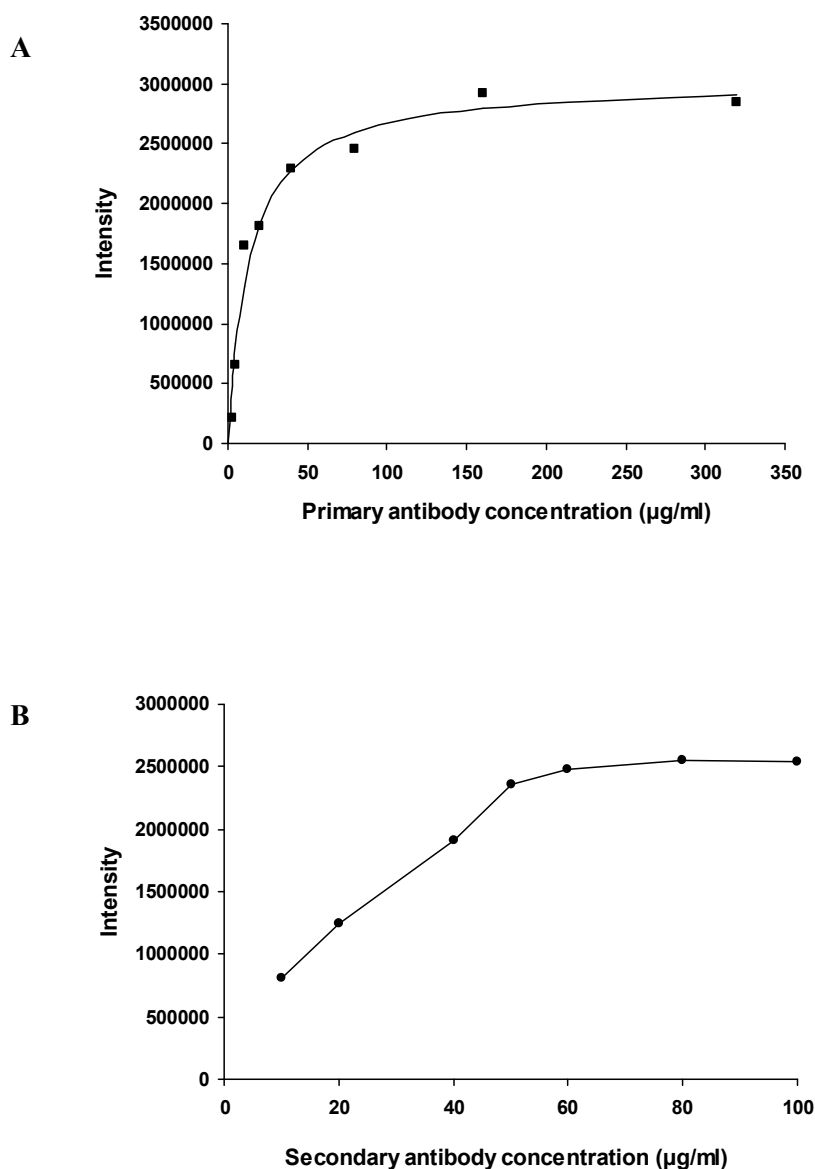


Figure 3-11: Optimization of the model assay system for wide dynamic range: (A) response curve of the primary antibody with Langmuir fit and (B) response curve of the secondary antibody.¹¹¹

3.4.2.5 Heterogeneous confocal planar immunoassay detection limit

A glass 96-well plate was coated with a saturating concentration of primary antibody overnight. After blocking and washing the wells, serial dilutions of human IgG over

the range from 0.5 $\mu\text{g/ml}$ to 0.5 ng/ml , and the same volume of buffer with no human IgG as blank were added to the wells and detected with a low concentration of secondary antibody (0.5 $\mu\text{g/ml}$). Figure 3-12 shows the calibration curve plotted as the difference between intensity of sample and the average of blank signal ($n=3$) versus antigen concentration. The wells were washed with PBS and scanned again to see the effect of washing on responses. The dose response curve before washing the overlayer has a good linear range over the studied range of human IgG concentrations ($r^2=0.9984$). A comparison of average intensities of the low concentrations of antigen and blanks ($n=10$) showed that 5 ng/ml (before washing) and 10 ng/ml (after washing) of human IgG could be detected with 98% confidence. The confidence level reported is from a two-tailed test. The calculated detection limits based on Eq. 3-3 were 5.5 ng/ml (before washing) and 10.4 ng/ml (after washing). The protocol with fewer wash and incubation steps was more sensitive, an effect that ascribed to some second antibody being rinsed from the surface.

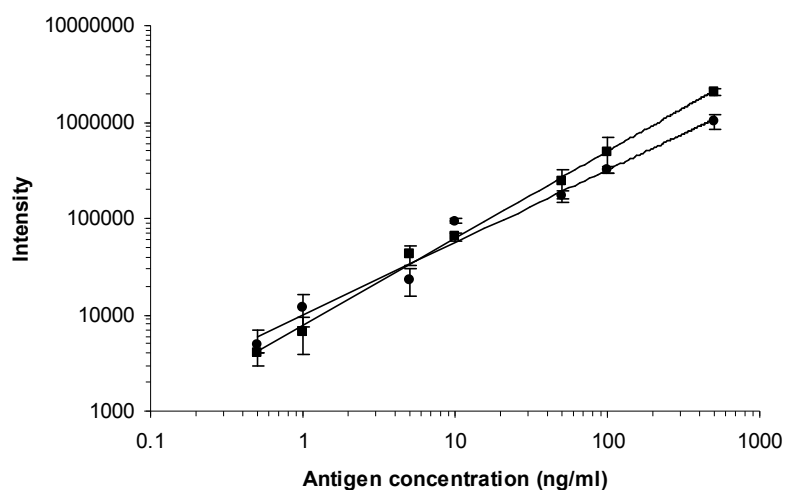


Figure 3-12: Calibration curves of low concentrations of antigen before (■) and after (●) washing the fluorescent overlayer in a heterogeneous format assay.

3.4.3 Homogeneous confocally detected planar immunoassay

To demonstrate the adaptability of the confocally detected immunoassay to a homogenous format, the same model system was adopted to remove all sample and detection wash steps. A serial dilution of antigen over a range from 0.5 $\mu\text{g/ml}$ to 0.5 ng/ml was compared to blanks consisting of PBS buffer with no human IgG. A low concentration of second antibody (0.5 $\mu\text{g/ml}$) was added simultaneously with the prepared antigen solution to the wells of a 96-well plate coated with a saturating amount of primary antibody. The dynamic range of the calibration curve is shown in (Figure 3-13). The homogeneous format approached saturation around 0.5 $\mu\text{g/ml}$, a result consistent with the amount of second antibody (0.5 $\mu\text{g/ml}$) and the ratio of antigen and antibody molecular weights (1:1). The dynamic range of the calibration curve was limited because the concentration of second antibody was intentionally kept low as this was found to improve sensitivity. The assays were subsequently washed for comparison purposes to evaluate the effect of washing on the thin film. The homogeneous assay detection limit was 2.2 ng/ml in the absence of all wash steps. As observed in the heterogeneous assay results, the detection limit increased to 6.0 ng/ml after washing the overlayer. This reinforces the conclusion that wash steps remove analytically important material from the surface and the confocally detected homogeneous planar assay showed better detection limits than the heterogeneous one.

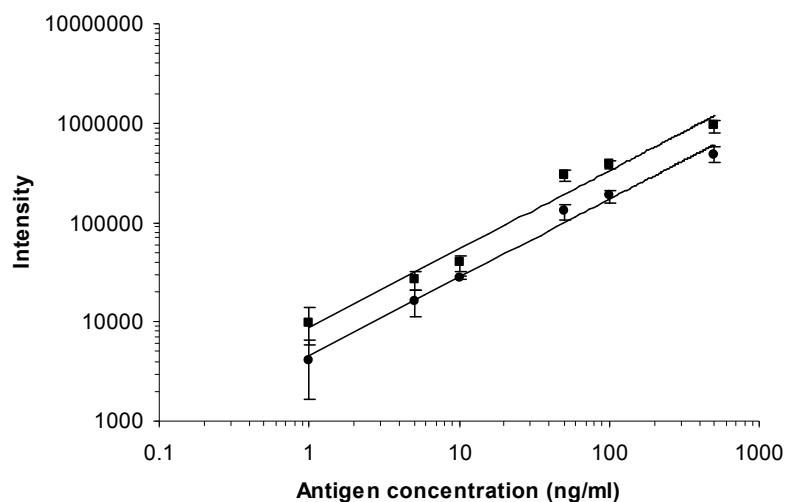


Figure 3-13: Calibration curves of low concentrations of antigen before (■) and after (●) washing the fluorescent overlayer in a homogeneous format assay.

3.4.4 Hepatitis C core immunoassay

3.4.4.1 Sandwich format assay

The two polyclonal antibodies (rabbit and goat anti-HCV core) were tested in a FLISA heterogeneous sandwich assay to select the best one as coating antibody. The result showed the higher intensity for the FLISA assay with rabbit polyclonal antibody as the first antibody on the surface (data not shown). Then a dilution series of HCV core antigen concentrations (60 to 1000 ng/ml) and a control sample were prepared to be sandwiched between a fixed amount of rabbit polyclonal anti-HCV core antibody (20 $\mu\text{g/ml}$) on the surface and goat polyclonal anti-HCV core antibody (10 $\mu\text{g/ml}$). The sandwich assay was detected with 3 $\mu\text{g/ml}$ of secondary labelled antibody (anti-goat IgG-FITC). The dose response curve was fitted to Langmuir isotherm (Eq. 3-4) and is shown in figure 3-14.

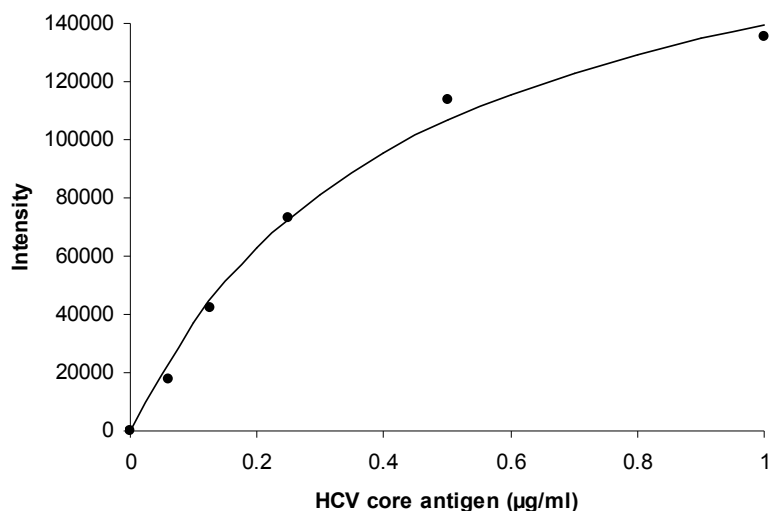


Figure 3-14: Dose response curve of HCV core antigen detected in sandwich assay with confocal immunosorbent assay method.

3.4.4.2 Indirect format assay

A series of goat anti-HCV core antibody concentrations (60 to 2000 ng/ml) and a control sample were prepared with fixed amount of HCV core antigen (10 µg/ml) on surface and were detected with 2 µg/ml of secondary labelled antibody (anti-goat IgG-FITC). The dose response curve was fitted to Langmuir equation and is shown in figure 3-15.

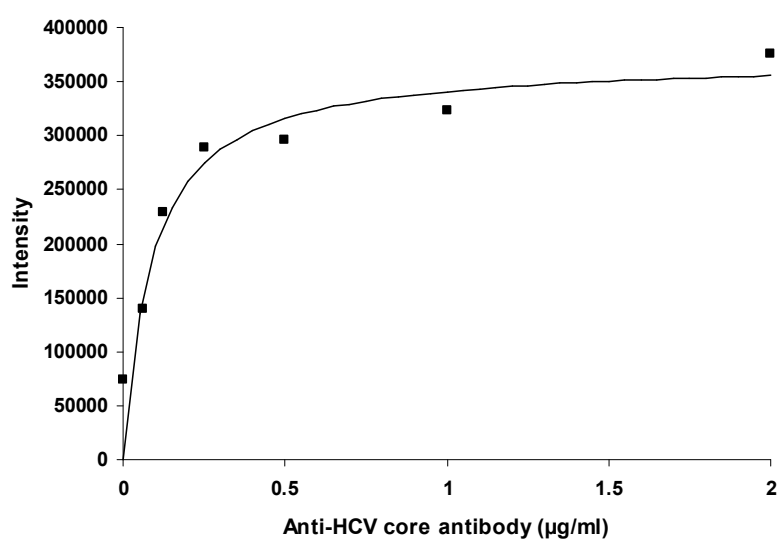


Figure 3-15: Dose response curve of anti-HCV core antibody detected in indirect assay with confocal immunosorbent assay method.

3.4.5 Immunoassay detection with PAM

The heterogeneous human IgG model assay with QD605 anti-human IgG as reporter antibody was selected as a model to study the axial response of PAM. Human IgG as the antigen (1 $\mu\text{g/ml}$) was added to coated chamber slides with the primary antibody (20 $\mu\text{g/ml}$) followed by the QD-conjugated secondary antibody (5 nM). The chamber was scanned by PAM using the 40 \times NA 1.15 water objective using 40 steps of 0.3 μm along the z axis without removing the fluorescent solution. The axial response showed three distinct features (Figure 3-16) the same as the confocal immunosorbent assay response. The FWHM of the peak was 4.21 μm which was broader compared to FWHM of the confocal peak. The presence of overlayer fluorescence indicates that an excess of secondary antibody is present and must be separated from the film signal.

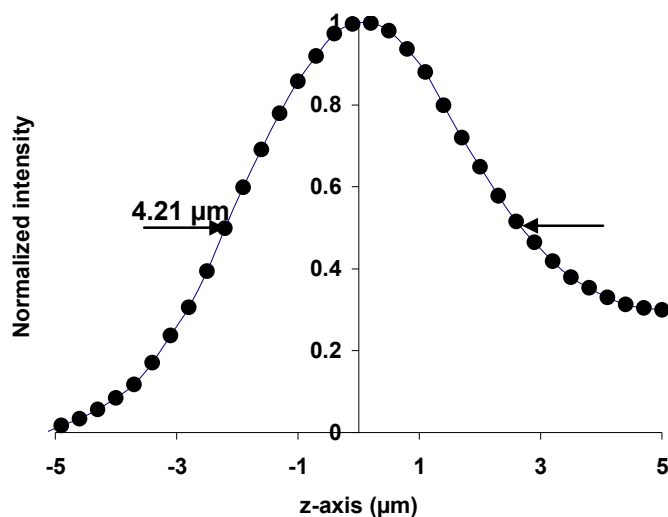


Figure 3-16: The axial response of sandwich immunoassay with PAM has the same three zones as confocal with broader FWHM.

3.4.5.1 Decomposition of signals

The same method for separation signals based on distribution functions was used. The Cauchy-Lorentz and cumulative Cauchy-Lorentz functions were found not to fit the

measured data well. Fitting procedures showed that the shape of axial response of PAM to be well fitted by Gaussian shape (Eq. 3-2), while the response of confocal had a more Cauchy-Lorentz shape. This allowed the decomposition of the two objects when presented together (Figure 3-17).

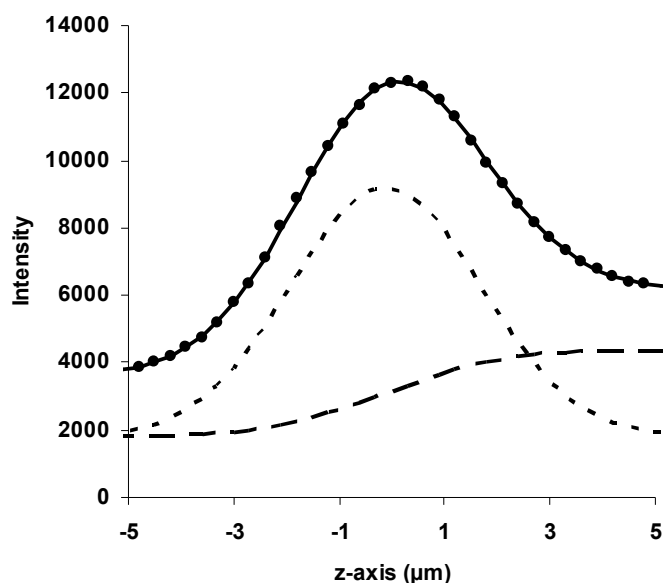


Figure 3-17: Decomposition the signal of the PAM immunoassay to the thin film and overlayer based on Gaussian function: the experimental data (●) is decomposed to thin film (- - -) and (- · -) overlayer. The line connecting the data points is the best fit to Eq. 3-2 for this set of measurements.

3.4.5.2 Dose response measurements

The influence of the different concentration QD-conjugated secondary antibody was investigated between 2 and 80 nM (data not shown) at a constant coating of antibody and the antigen yielding an optimal concentration of secondary antibody (5 nM). The higher concentrations of QD-conjugated antibodies were problematic for scanning without washing the overlayer due to the image saturation.

A 8-well chamber slide was coated with a saturating concentration of primary antibody overnight. After blocking with BSA and washing the wells, serial dilutions of human IgG over the range from 1 $\mu\text{g/ml}$ to 15.6 ng/ml, and the same volume of buffer with no human IgG as blank were added to the wells and detected with 5 nM of QD605 secondary antibody. Figure 3-18 shows the dose response curve followed a Langmuir adsorption process. The results show that all the antigen concentrations could be detected. No more time to do further experiments for determination of low detection limit of human IgG immunoassay with PAM.

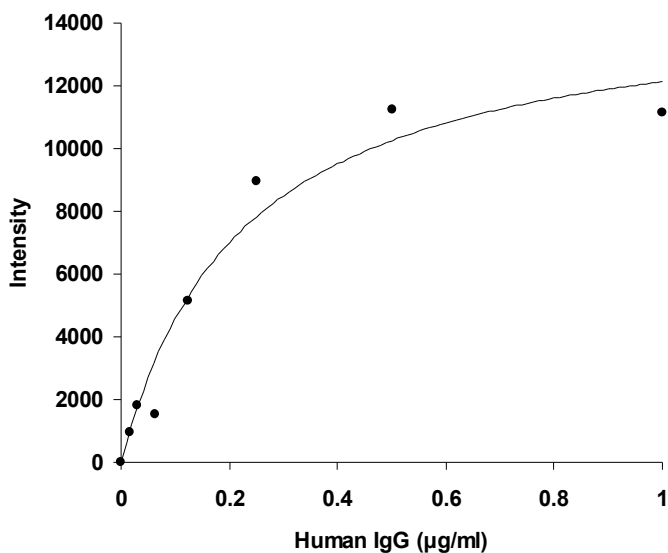


Figure 3-18: Dose response curve of human IgG FLISA assay detected with PAM.

3.5 Discussion:

A confocal readout method for detection of sandwich immunoassays using a human IgG model system has been demonstrated. The response of the confocal system showed an antigen dependent intensity variation originating from a thin film on a glass surface in the presence of an overlayer. The axial response of the thin films generated by the assay to changes of NA and pinhole size was studied and the results showed general agreement with published data on thin films.⁶⁸ These results are general to a wide range of planar format assay systems,^{152, 153} which could be readily adapted to become homogenous assays. These include planar arrays for the detection of genetic material and infectious diseases and many assays currently used in high-throughput screening. Further, other optical sectioning methods, such as two- and three photon excitation and stimulated emission depletion (STED) could be used to similar or better effect to the standard confocal methods used here. Also, using high-speed confocal microscopy systems^{59, 68, 70, 154-157} will improve the slow frame rate of currently available confocal systems.

The consistent trend for improved detection limits observed as the number of wash steps decreased across all of the assay formats implies that weak antigen-dependent interactions were removed by washing. A related trend was seen when comparing the heterogeneous and homogeneous formats. Perhaps uniquely, the homogeneous format reported here exhibited better sensitivity than any of the others. This is due to a combination of preserving interactions between the first antibody and the antigen, between the antigen and the second antibody, and possibly some formation of aggregates in solution between the antigen and the second antibodies prior to binding to the plate. By deleting all washing steps, it is possible to keep and

detect even weak interactions between antigen and antibodies and improving the detection limits. The 2.3 ng/ml detection limit for the human IgG immunoassay is competitive with others reported for this model system. For example, such a model system detected using quantum dots after removing the overlayer was sensitive to 2 $\mu\text{g/ml}$.¹³² Note that the conditions producing the greatest sensitivity differ greatly from those producing a quantitative response over the widest dynamic range. Sensitivity is expected to be fundamentally limited by the Poisson statistics of photons generated by the overlayer. Therefore, sensitivity is enhanced at lower concentrations of secondary antibody because it lowers the noise generated by the overlayer. The widest dynamic range is produced by levels of secondary antibody sufficient to detect saturating levels of antigen. The future improvements in the method are anticipated by optimized instrumentation, the introduction of quantum dots for better photostability,¹⁵⁸ higher NA optics, and additional optimization of the reagent and support surfaces.

A wide range of reports of confocal scanners for readout of fluorescent spots in planar arrays and bead assay systems have appeared in the literature. Despite numerous reports, there is not a paper in which instrumental details are provided for the confocal scanner sufficient to reproduce the experiment together with a measured axial response from an immunoassay. Miriglia *et al.*¹⁴ are exceptional in providing the NA and other optical details of their experiment. More common are reports of “proprietary” systems with few other details.^{159, 160} It is also of interest that, none of these previous studies required a confocal or optically sectioned readout and the confocal readout was of arguable benefit. This work is an attempt to provide a clear example where the confocal readout is required and provides benefit (e.g., no wash

steps and preservation of weak interactions) together with sufficient optical detail to determine how to best take advantage of optical sectioning in assays.

The approach to planar assays shares advantages with other related homogenous and fluorescence-based assays and presents several attractive features. First, compared to conventional ELISAs, the planar homogenous assay could potentially save time due to the reduction of wash steps and the fluorescence readout does not require time for an enzyme reaction to develop. Second, assays can be stored for several days before readout.¹⁶¹ Third, the planar homogeneous assay does not require beads or specialized reagents beyond those commonly available in many laboratories and will not suffer from bead motion during readout. A planar format has two main advantages over beads in this context. First, beads are susceptible to motion during readout unless immobilized. Second, the shape of the bead requires that more complex procedures be used to remove the fluorescent background and determine the intensity arising over the entire volume of the bead. Fourth, due to the ability to eliminate wash steps, the approach is quite attractive for assays based on weaker interactions; such interactions are of very wide interest in high-throughput screening. Highthroughput screening instrumentation already exists for confocally detected cellular assays and could be adapted for other types of screening and use in clinical labs. Fifth, since no washing is required, antigen-antibody reactions can be monitored in real time by measuring the intensity of the thin layer on the well bottom in the presence of free labelled antibody in the overlayer at any time. Evaluation of the rate constants of antigen-antibody pairs is possible under true assay conditions (the aim of chapter 4). Similar studies have been done on microparticles,¹⁶² but not in planar formats. Sixth, it enables assays to be stacked in 3-D arrays followed optically sectioned readout (the aim of chapter 5). Finally, although the planar format using

antibody-antigen interactions was implemented, the approach is general to a wide range of assays that can be presented as a reaction between a surface-bound species and free ligands.

The optical system is designed to work in chamber slides or multiwell plates presenting an optical glass surface with standard refractive index ($n=1.515$) and thickness (0.17 mm). This matches the design criteria for many microscope objectives and minimizes the spherical aberration due to refractive index mismatch. The use of different optical media could result in poor resolution and decreased intensity. For example, when working with polystyrene ($n=1.5917$) or polycarbonate ($n=1.5849$) plates, objectives with a correction collar for variable glass thickness (e.g., 0 to 2 mm) can be used to correct the lack of correct refractive index matching.

The use of air objectives, as described here, simplifies sample-changing automation in an inverted geometry by eliminating immersion fluids. The best separation between film and overlayer was achieved with the highest NA. Further improvement is expected at a higher NA due to better resolution and consequential improvements in detection limits, and better sensitivity are expected under these conditions. Practically, air lenses with longer working distances may be preferable; however, this choice is an engineering related compromise not a fundamental issue. Immersion objectives are somewhat awkward to use in inverted geometries. Finally, for a given a fixed scan range, SNR is improved by decreasing the step size.

To the best of my knowledge, it is the first report of detecting a FLISA with PAM. The biological applications of the PAM has been limited in the field of live cell and tissue imaging,^{69, 163} fluorescence recovery after photobleaching (FRAP) and photoactivation experiments⁷⁶ in the literature. The main advantages of the PAM compared to the CLSM as a read-out method for immunosorbent assays that were

observed here were its higher sensitivity and speed. The concentration of QD605 conjugated antibody used in the dose response curve experiments (5 nM) could not be detected with CLSM. It is a great advantage regarding to the reduced expensive reagents consumption. The overall time required for scanning and analysing the data of a well contained immunoassay was shorter by the PAM compared to the CLSM since the software allowed the user and the computer to interact dynamically with the PAM. There is no specific comparison for the required time for quantitative measurements of FLISA for these two optical sectioning methods. The two-week period for working with the PAM was not enough to study the different aspects of its application for the detection of immunoassays. The PAM has the potential for applications involving optical sectioning with high-speed such as the kinetic analysis of antibody-antigen reactions.

The results of HCV FLISA experiments showed the application of the confocal immunosorbent assay method in a real assay for detection of the HCV core antigen and anti-HCV antibodies. Although the lowest concentrations detected by the confocal method, 60 ng/ml for HCV core antigen and anti-HCV core antibody is not comparable with the range of the detection limits in the literature (\sim pg/ml).^{141, 164, 165}. Most of the reports of HCV diagnostic tests in the literature were used commercial kits or in-house assays using purified monoclonal antibodies from immunized mice with recombinant core antigens.^{141, 164} Different monoclonal anti-HCV antibodies were used with no improvement in the sensitivity of the HCV assay (Data not shown). The application of mixture monoclonal antibodies, using an animal model to develop in-house assay and using the HCV reagents from other available sources could be the alternative approaches to improve the sensitivity of the confocal HCV immunoassay.

Chapter 4

Kinetic analysis of antigen-antibody interactions with CLSM

In this chapter the use of CLSM for monitoring the binding of antigen-antibody reaction in a model of human-IgG assay is studied in heterogeneous and homogenous format assays. According to the separation-free nature of CLSM detection method that has been proved in previous chapter, the kinetic analysis of antigen-antibody reaction on a solid surface should be feasible without interference from free labelled antibodies in the solution. By using two different fluorescent labels conjugated to antibodies (FITC and QDs), the rates of binding to a prepared surface in a sandwich assay are studied and compared. The chapter begins with a review of antigen-antibody interactions and methods for kinetic analysis. Then a simple theory applied to kinetic measurements made on a solid surface format is presented.

4.1 Introduction

Immunoassays based on the specific reaction between an antigen and antibody are quantitative analytical methods with broad applications in biological assays. The use of antibodies as analytical probes is an important part of the immunoassay method in diagnostics and clinics. Understanding antigen-antibody interactions is essential for choosing correct antibodies and presenting well designed assays in clinical diagnosis and therapy in order to obtain proper responses.¹⁶⁶ The kinetics of association and disassociation are important parameters in determining when a system will reach an equilibrium state and predicting the outcome of assays such as detection limits and sensitivity¹⁶⁷.

4.1.1 Antigen-antibody interaction

Antigen-antibody interactions are distinguished by association and disassociation rate constants. Antibodies or immunoglobulins (Ig) are high molecular weight proteins (~150 kDa) which are normally produced by specialized B-lymphocytes after stimulation by an antigen, a substance foreign to the body, such as an immunogen or a hapten. There are five Ig isotypes in mammals known as IgA, IgD, IgE, IgG and IgM and they differ in size, structure, biological properties, and abundance in serum. The IgG molecule is the most abundant class of Ig consisting of two identical heavy (H) and two identical light (L) chains, forming a Y shaped molecule (Figure 4-1). These chains are linked together by disulfide bonds. H and L chains contain variable and constant regions with the variable region located at the amino-terminal domain of each chain. The IgG molecule can be broken down into two regions, the Fc (fragment crystallisable) and Fab (fragment antigen binding). The variable regions in Fab contains two antigen-binding sites known as paratopes which can recognize the

antigenic determinate or epitope of an antigen. The term antigen refers to any substance that can elicit an immune response in a host. There is only one portion of an antigen (epitope) that binds to the paratope of an antibody molecule.¹⁰⁵

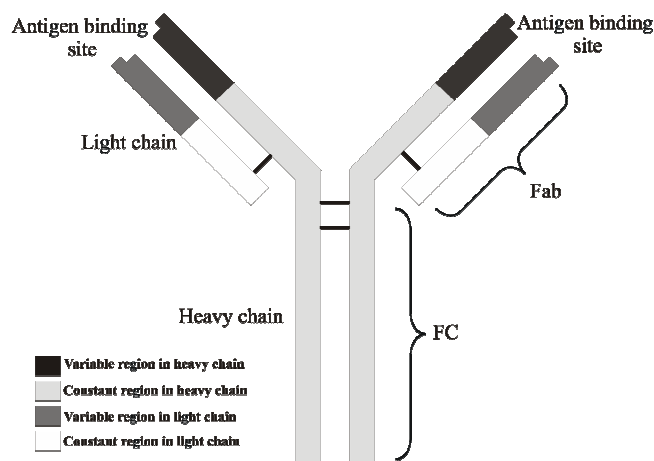


Figure 4-1: Schematic representation of a human IgG molecule.¹⁰⁵

Antigen-antibody interactions are based on hydrophobic interactions, electrostatic forces, hydrogen bonding and van der Waals forces that can be affected by the pH, temperature, concentration and ionic strength of reagents and buffer. The mechanism of antigen-antibody interactions can be explained in two steps. The primary attraction between epitopes and paratopes surfaces with hydrophobic and electrostatic interactions approaches them sufficiently for the secondary step with van der Waals interactions and hydrogen bonds. The hydrophobic interactions occur between hydrophobic nature of the paratope and hydrophilic groups in the epitope. The electrostatic interactions are caused by opposite charges on ionised sites in the epitope and paratope. When they are brought closely enough together, van der Waals interactions occur between all involved atoms and finally hydrogen bonds form across at distances of 2-3 Å.¹⁰⁵

4.1.2 Kinetics of antigen-antibody interaction and rate limitations

The rate of antigen-antibody reaction is more complicated compared to a simple chemical reaction due to the larger size of reactants. The larger size affects the kinetics by several processes, such as mass transport limitations, steric hindrance and heterogeneity of binding sites.¹⁶⁸ The antigen-antibody reaction is considered as a fast macromolecular reaction with rate constant as high as $10^8 \text{ M}^{-1}\text{s}^{-1}$.^{169, 170} Investigation on the kinetics of biomolecular interaction can be divided into two main groups: in solution where both reactants are free to move and at solid surfaces in which one of the reactants is immobilized on the surface either by covalent binding or by passive adsorption. The solid surfaces may vary from sphere, cell and artificial flat surface. The understanding of rate-limiting factors is essential in analysing the kinetics of antigen-antibody binding in these systems. The reaction of antigen-antibody can be reaction-limited, diffusion-limited or influenced by both process.¹⁷¹ If the rate of formation of the antigen-antibody complex is only dependent on the forward and reverse rate constants and the bulk concentration is equal to surface concentration, the system is a reaction-limited which obeys the law of mass action. When the rate of diffusion of reactants to each other controls the rate of the whole reaction and the local concentration in the reaction zone is different from the bulk, the reaction is a diffusion-limited or mass transport-limited. The diffusion limitation has been discussed extensively by Stenberg and Nygren in solution and at solid-liquid interface with various shapes of solid surfaces.^{170, 172, 172-175} The mass transport and binding process are reviewed briefly here for reaction in solution and at solid-liquid interface in the form of a sphere or a flat surface.

Association processes for macromolecules in solution are limited by the time it needs to bring the reactive sites close together by diffusion.¹⁷⁶ Experimental studies

on immunoreactions in solution done mostly on a model of antibodies and free haptens have shown that the reaction is fast and reaches equilibrium.¹⁷⁷ The rate of reaction of antigen-antibody in solution depends on the collision and the orientation of binding sites and is related to the translational and rotational diffusion of biomolecules. The translational diffusion constant, D , is defined by the Stokes-Einstein equation:¹⁷⁰

$$D = \frac{kT}{6\pi\eta r} \quad (4-1)$$

where k is Boltzmann constant, T is absolute temperature, η is viscosity of solution and r is the hydrodynamic radius of a reactant. For two molecules of antigen (Ag) and antibody (Ab), the association reaction is limited by a diffusion rate constant given by:¹⁷⁰

$$k_f = 4\pi(D_{Ab} + D_{Ag})(r_{Ab} + r_{Ag}) = 4\pi DR \quad (4-2)$$

where D is the relative diffusion constant ($D = D_{Ab} + D_{Ag}$) and R is the effective interaction radius ($R = r_{Ab} + r_{Ag}$). For biomolecules with same sizes in solution, the diffusion rate in water is about $7 \times 10^9 \text{ M}^{-1}\text{s}^{-1}$ and for different radii it increases for example when $r_{Ab}/r_{Ag} = 10$ the diffusion rate is about $2 \times 10^{10} \text{ M}^{-1}\text{s}^{-1}$.¹⁷⁰ Since the fastest measured rate constant in solution on a model of antibody-heptan is around $6 \times 10^8 \text{ M}^{-1}\text{s}^{-1}$, the antigen-antibody reaction in solution is not a translational diffusion limited reaction.¹⁷⁰ The other rate limitation factor in solution is the steric factor which can be described by rotational diffusion of biomolecules during the collision to bring their reactive sites close to contact. The rotational diffusion constant for a spherical molecule with radius r is given by the Stokes-Einstein relation:¹⁷⁸

$$D = \frac{kT}{8\pi\eta r^3} \quad (4-3)$$

Studies have shown that the measured rate constants compare favourably to those predicted based on rotational diffusion. They have a similar order of magnitude with prediction which shows the possibility of rotational diffusion limitation on the reaction.¹⁷⁰

The model of solid-phase immunoreaction is closer to the natural *in vivo* conditions in which antibodies react with antigens as parts of virus particles, bacterial or normal cell surfaces which can be considered as solid phases.¹⁷⁷ The rate constants of the antigen-antibody reactions where one of the reactants is immobilized on a spherical or plane solid surface are lower compared to solution reactions due to decreasing the diffusion coefficient of the immobilized reactant to zero. The amount of decrease depends on which reactant is immobilized when the diffusion coefficients are different. If the reactant with higher diffusion coefficient (smaller in size) is immobilized, the decrease in rate constant when compared to a solution phase reaction will be high.¹⁷⁹

An antigen-antibody reaction at the surface of a cell or sphere in solution where one of the reactants is immobilized on the surface is at first limited by the surface reaction which leads to depletion of the reactant near the surface and diffusion limitation.¹⁷⁰ In such cases a parameter called the Damkoehler number, D_a , is used to describe the diffusion limitation of the forward reaction rate constant given by:^{170, 174}

$$D_a = \frac{Rk_f\Gamma_0}{D} \quad (4-4)$$

where R is the radius of the sphere with immobilized reactive sites (such as antigen), Γ_0 is the surface concentration of reactive sites, k_f is the effective forward rate constant. This number is the ratio between the maximum reaction rate at the surface and the maximum rate of diffusion mass transfer. If the Damkoehler number is greater

than one the antigen-antibody reaction is a diffusion-limited reaction and a small Damkohler number shows a reaction-limited reaction.¹⁷⁴

The study of kinetics of biomolecular reactions at a planar surface is important since most routine immunoassay methods take place at planar solid-phase interfaces due to its high sensitivity and providing a simple means of separation of bound and free reactants. These methods can be easily adapted to different surface analysing techniques to obtain quantitative measurements.¹⁷⁰ Most theoretical calculations of kinetic parameters for solid surface immunoassays have been based on the law of mass action assuming they are reaction-rate limited and reversible. However, kinetic measurements of antigen-antibody reactions at solid surface format assays such as ELISA have shown that the reactions are often diffusion-rate limited and irreversible due to depletion of the reactants at the reaction zone near the surface without stirring.¹⁷⁰ The antigen-antibody binding reaction at a planar surface is considered as an initial diffusion-limited reaction followed by a reaction-limited with no equilibrium state in unstirred condition using the routine incubation times of typical immunoassays.

Studies of kinetic reactions at solid surfaces can be divided into two subgroups: solid surface with flow such as those found in most biosensor techniques and solid surface in unstirred conditions such as is encountered in most classical immunosorbent assays in microtiter plates (ELISA, RIA and FLISA). Reaction without stirring will be explained in detail in section 4-2. Here a brief description of the mass transport limitation in flow chambers is presented. In most biosensor techniques, one of the reactants is immobilized covalently on the biosensor surface and the other reactant is transported by flow toward the sensor surface. The transport depends on the flow rate and dimension of the flow chamber. Due to the high density

of immobilized reactant in such methods and high association rate of biomolecules, the mass transport has a significant effect on biosensor measurements. The mass transport limitation can be determined by changing the flow rate, as it is affected by flow but the true reaction rate is flow independent.¹⁸⁰ The mass transport effect has been described theoretically by a numerical model in the literature and the coefficient of mass transport, k_m , is calculated by:¹⁸¹

$$k_m = 1.86 \left(\frac{D^2 \nu}{hL} \right)^{1/3} \quad (4-5)$$

where D is diffusion constant, ν is the flow rate, h , is the height of the flow cell, L is the distance between inlet into flow cell. The binding reaction on a biosensor surface is considered reaction-limited when $k_a g \gg L_m$, where k_a is the measured association rate constant and g is the surface concentration of binding sites.¹⁷¹

4.1.3 Affinity

Affinity is a thermodynamic term for the strength of the interaction of a single epitope of an antigen with a single antibody paratope that is expressed in the form of the equilibrium constant K . It is necessary to know the value of an antibody affinity to understand its immunological activity. A high affinity antibody is more active than a low affinity antibody.¹⁸² The interaction between an antibody and an antigen at equilibrium can be expressed as:



At equilibrium, the rates of association (k_a) and disassociation (k_d) are equal and the affinity constant can be expressed as the equilibrium association constant (K_A) (L/Mol):¹⁰⁵

$$K_A = \frac{k_a}{k_d} = \frac{[AgAb]}{[Ag][Ab]} \quad (4-7)$$

or as the equilibrium disassociation constant (K_D):

$$K_D = \frac{k_d}{k_a} = \frac{[Ag][Ab]}{[AgAb]} \quad (4-8)$$

where $[Ag]$ and $[Ab]$ are free antigen and antibody concentration at the equilibrium and $[AgAb]$ is the concentration of bound antigen. Based on the law of mass action, the Eq. 4-7 can be written:

$$[AgAb] = K_A([Ab]_t - [AgAb])[Ag]$$

or

$$\frac{[AgAb]}{[Ag]} = K_A([Ab]_t - [AgAb]) \quad (4-9)$$

where $[Ab]_t$ is the total concentration of antibodies ($[Ab]_t = [Ab] + [AgAb]$). To obtain the affinity constant, a graph of the ratio of bound to free antigen versus bound antigen is plotted. The slope of this graph which is known as a Scatchard plot is $-K_A$ and the intercept is $[Ab]_t$.¹⁸³

4.1.4 Thermodynamic of antigen-antibody interaction

Thermodynamic data of antigen-antibody reaction provide information about stability, specificity and strength of the reaction. The thermodynamic parameters of an antigen-antibody interaction can be determined by measuring the temperature dependence of its kinetic association and dissociation rate constants. The method of choice used for thermodynamic studies is calorimetry and specifically isothermal titration calorimetry (ITC), which measures the heat exchange during the binding process to obtain the thermodynamic parameters such as enthalpy (ΔH), free energy (ΔG), entropy (ΔS) and the heat capacity (ΔC_p) and binding constant (K_a).^{184, 185}

The change in Gibbs energy of antigen-antibody binding could be calculated by:¹⁸⁶

$$\Delta G = \Delta H - T\Delta S = -RT\ln K \quad (4-10)$$

where R is the gas constant, T is the absolute temperature, K is the equilibrium association constant, and ΔS is entropy. The van't Hoff plot of $\ln K$ versus $1/T$ gives a straight line of slope $-\Delta H/R$:¹⁸⁶

$$\ln K = \frac{-\Delta H}{RT} + \frac{\Delta S}{R} \quad (4-10)$$

4.1.5 Methods for kinetic and equilibrium analysis

Several methods are available for measuring the affinity of antibody-antigen interactions but the number of methods used for kinetic analysis is limited due to the difficulty in finding suitable methods for rapid kinetic measurements. Affinity measurements involve the equilibrium or steady-state, but studying of antigen-antibody kinetics concerns about issues such as the rate and the mechanism of reaction, understanding the intermediate states, and the factors affecting the reaction. For affinity measurements, the free reactant is measured separately after the antigen-antibody reaction reaches equilibrium state. Kinetic analysis is facilitated by methods that allow rapidly separation of free and bound reactants.¹⁸⁷

4.1.5.1 Immunosorbent assays

It is not easy to obtain kinetic information by classical immunoassay involving solid surface method due to the requirement of separation steps and the complexity of kinetic analysis in solid phase reaction. Radio and enzyme immunosorbent assays are suitable for obtaining antigen-antibody affinity constant.¹⁸⁸ The Friguet method¹⁸⁹ and its modification¹⁹⁰ are ELISA methods have been used to measure the disassociation constant in solution phase. In this method an antigen at various concentrations is incubated with constant amount of an antibody. After reaching the equilibrium, the

solution is transferred to a microtitre plate with coated antigen and the concentration of free antibody is determined by an indirect ELISA. The affinity constant and other equilibrium information can be derived by general equations for affinity measurement. There are some records of using ELISA for kinetic analysis by following specific experimental conditions to validate the procedure that make them less practical^{167, 191}.

4.1.5.2 Fluorescence

Application of fluorescent techniques is important in determining the real-time kinetics of molecular binding due to its high sensitivity and capability of making rapid measurements in solution in homogeneous format assay which does not require separation of bound and free components.

4.1.5.2.1 Fluorescence polarization

Polarization of fluorescence is a sensitive and direct method for studying kinetic and equilibrium of antigen-antibody interactions. Fluorescence polarization measurements are based on the observation that fluorescent molecules emit light at different planes of polarized light to that used for excitation due to molecular rotation.¹⁹² In this method, one of the reactants is labelled with a fluorescent dye. Upon the antigen-antibody interaction and complex formation, the size of labelled product is increased which reduces its rotational motion and hence increases polarization.¹⁹³ Small molecules have lower polarization than larger molecules under the same conditions (e.g. the temperature and viscosity of solvent).¹⁰⁵ Intensity of light emitted in the horizontal and vertical planes are measured to calculate the polarisation value. Polarization of fluorescence is also used to measure the rotational relaxation time of macromolecules. The complex of antigen-antibody has a higher rotational relaxation time than its components.¹⁹⁴

4.1.5.2.2 Fluorescence correlation spectroscopy (FCS)

Fluorescence correlation spectroscopy (FCS) is a versatile noninvasive technique to study and measure the dynamics of molecular processes *in vivo* and *in vitro* with high temporal and spatial resolution. FCS utilizes correlation-function analysis of fluorescence intensity fluctuations from a low concentration of laser-excited molecules due to their Brownian motion in a small detection volume of about femtoliter. Any process that causes fluctuations in the fluorescence intensity can be analysed by FCS.¹⁹⁵ The correlation analysis gives information about the diffusion coefficient and concentrations of the fluorescent particles. The time-dependent fluctuations of fluorescent particles with different molecular properties (molecular weight, translational and rotational diffusion time, colour, and fluorescence lifetime) provide the kinetic information required to study the molecular interactions.⁴⁰

The experimental setup of FCS is based on one-photon (confocal) or two-photon excitation modes and can use a single or two channels (dual-colour cross-correlation) detection system.¹⁹⁶ The FCS measurement requires small sampling volumes, high photon detection efficiency and good rejection of background fluorescence. The use of a high numerical aperture microscope objective provides a diffraction limited illumination volume of less than a femtoliter. Also, the development of avalanche photodiodes offers increases in quantum yield compared to common photomultiplier tubes so that single molecules can be detected.¹⁹⁷ Fluorescence excitation in two-photon absorption is confined to a very small volume near the focal plane and has the advantages of reduction of out-of-focus fluorescence without using a pinhole, decreasing of background fluorescence level and minimizing sample photodamage.¹⁹⁸

FCS has been used for studying translational and rotational diffusion^{199, 200}, intermolecular binding and reaction kinetics^{201, 202}, ligand-receptor interactions²⁰³, immuno reaction kinetics²⁰⁴, and conformational dynamics²⁰⁵.

4.1.5.2.3 Fluorescence resonance energy transfer (FRET)

Fluorescence resonance energy transfer (FRET) is a non-radiative energy transfer of an excitation between two different fluorophores (donor and acceptor) whose corresponding emission (donor) and excitation (acceptor) spectra overlap. The efficiency of energy transfer depends on the distance between the donor and the acceptor (20–100 Å), the spectral overlap between the donor emission and acceptor excitation spectra, and the transition dipole orientation. This technique is especially suited for *in vitro* analysis and analysis in living cells.⁴⁰ FRET can be used to follow the association of two interacting molecules or to monitor the distance between two sites within a macromolecule when labelled with two appropriate dyes. FRET-based probes have been used to monitor binding of a ligand labelled with a donor dye to a receptor labelled with an acceptor dye and results in a measurable fluorescence energy transfer from donor to acceptor.²⁰⁶

4.1.5.3 Optical techniques

Optical techniques allow label-free, direct, and real-time detection of macromolecular interactions. These techniques have been categorized as optical biosensors in the literature and provide a direct and rapid readout of both affinity and kinetics. Biosensors convert physical properties of a biological complex into a detectable signal.²⁰⁷ Whereas the other mentioned techniques take place in solution, optical biosensors usually make use of surface sensitive techniques that eliminate the need for any separation.¹⁰⁵ These techniques analyse the behaviour of light at the boundary of

two media with different refractive indices. Generally, a ligand such as an antigen is immobilized on a solid surface of a sensor and an analyte such as an antibody solution is passed over the solid surface at a specific flow rate. Binding the analyte to the ligand increases the mass and makes a change in the refractive index near the solid surface which can be measured by different optical principles. Kinetic parameters can be derived from the time course of the refractive index change.²⁰⁸

4.1.5.3.1 Reflectometric techniques

Reflectometry:

Reflectometry is an optical technique that monitors the polarization of a light beam reflected from an interface. It allows quantification of mass changes on the surface interface due to alternation of polarization by adsorption of materials. This change is measured by determining the ratio between the intensities of parallel and perpendicular components of the reflected beam.²⁰⁹ Reflectometry has been used to study the kinetics of adsorption–desorption process of proteins at solid-liquid interfaces.^{210, 209, 211, 212} The instrument for reflectometry is inexpensive but it is difficult to choose the correct measurement conditions and the amount of calibration required.²¹³

Ellipsometry:

In ellipsometry the change in the state of polarisation of an incident light beam upon reflection at the interface is measured to give information about the thickness and refractive index of a thin film on the surface.²¹⁴ Ellipsometry can be used to study the kinetics of protein adsorption^{215, 216} and immunoreactions at solid–liquid interface^{173, 217}. The immunoreaction studies involve calculation of the thickness of antibody or antigen layer bound to the solid surface. There are some drawbacks with the

ellipsometry technique for monitoring antibody–antigen interactions. The required instrument to monitor antibody–antigen reaction at an acceptable range of sensitivity is sophisticated and expensive.²¹⁸ Ellipsometry is difficult to miniaturize, and suffers from interference by non-specific binding.²¹⁴

Reflectometric interference spectroscopy (RIFS):

RIFS is a reflectometric technique used for direct immunosensing. It determines the thickness of transparent layers by evaluating their reflectance properties. Binding of antigen-antibody at a surface increases in layer thickness and causes a change in the reflectance spectrum which can be monitored by RIFS in real time. Analysis of the spectral distribution of reflected light allows the determination of the optical path length in the layer in the sub-nanometre range. By use of diode array spectrometers, this method allows the rapid monitoring of surface processes in the subsecond range.²¹⁹

4.1.5.3.2 Evanescent wave techniques

The optical techniques of this group are based on total internal reflection (TIR) phenomena that produce an evanescent wave. TIR occurs when light with angle higher than the critical angle (θ_c) strikes the interface between two transparent media from the denser medium ($n_1 > n_2$) is totally reflected to the dense medium (Figure 4-2)²²⁰. An electromagnetic evanescent wave is created perpendicularly to the surface axis and penetrates into the lower refractive index medium by a wavelength's distance from the surface (about 200-300 nanometers).¹⁸¹ The evanescent wave propagates parallel to the surface and decays exponentially with distance from the boundary. The depth of penetration is a distance that the intensity of evanescent wave has decayed to

1/e of its value at the surface and depends on the wavelength, the angle of incident and the ratio of refractive indices. It is approximately 36% of the initial intensity.²²¹ The evanescent wave is only adsorbed by the molecules close to the interface and molecules far from this zone will not be illuminated.²⁰⁷ The dimension of the antigen-antibody complex is in the range of the depth of evanescent wave penetration, so only the immunoassay complex formed on the surface is affected by the evanescent wave and there is no need to wash the unbound reactant before the measurements. This depth dependence separates the bound and unbound reactants in evanescent wave techniques.²¹⁸

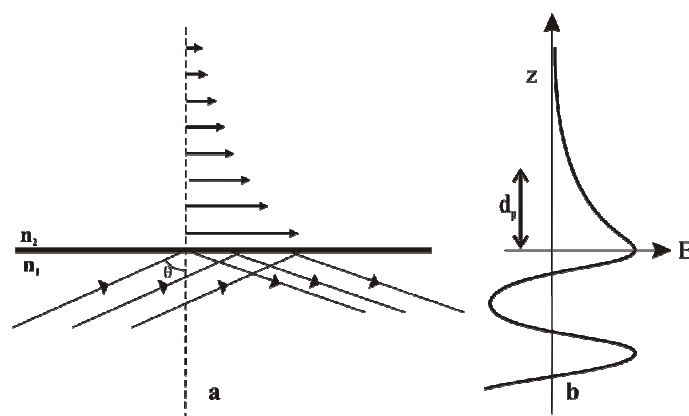


Figure 4-2: Generation of the evanescent wave at an interface. (a) Between two transparent media where $n_2 > n_1$ and θ is larger than the critical angle θ_c ($\theta_c = \sin^{-1}(n_2/n_1)$). (b) Showing the electric field amplitude E on both sides of the interface (Z is the distance from surface; d_p depth of penetration of evanescent wave).¹⁰⁵

The common protocol used for the kinetic analysis of antibody-antigen in these techniques involves four specific steps: (1) covalent attachment of a reactant (antigen or antibody) on the surface, (2) introducing the second reactant with constant concentration into the buffer flow above the sensor surface to monitor the complex formation and binding reaction, (3) disassociation phase by replacement of the buffer solution free of the reactants, and (4) regeneration of the sensor surface to remove remaining complex.²²² The whole process is repeated with different concentrations of

mobile reactant in the buffer to detect the changes in sensor response occurring during association and dissociation to measure kinetics and affinity parameters.²²³

Two main types of optical sensors based on evanescent wave phenomena at the solid/liquid interface are surface plasmon resonance (SPR) and waveguiding techniques. Both are label free techniques that rely on detection of refractive index changes in the evanescent wave zone. There are several instruments based on these techniques on the market in which the BIAcore from Pharmacia Biosensor (Uppsala, Sweden), the IAsys from Fisons (Cambridge, UK) and the BIOS-1 from Artificial Sensor Instruments (Zurich, Switzerland) are the leaders that employ SPR, RM and grating coupled planar waveguiding respectively.²⁰⁷ Evanescent waves can also excite fluorescent molecules on the surface which is the basis of total internal reflection fluorescence (TIRF) methods.²²⁰

Surface Plasmon resonance (SPR):

A monochromatic *p*-polarized light source and a thin metal film coated at the interface of solid/liquid phase are required to observe SPR. A few metals such as gold and silver have free electron clouds called plasmons that can resonate with light in certain conditions. The evanescent wave that has been created at the surface of a metal coated interface of a prism or diffraction grating by a polarized light can provide specific requirements to excite surface plasmons. This resonance condition allows energy transfer from incident light to the surface plasmons and can be recognized by a large drop in reflected light intensity. The maximum adsorption of light occurs at a particular angle of incidence (θ_{sp}) and is sensitive to changes in refractive index and therefore to changes in mass at the surface of the thin metal film. Association or disassociation of reactants at the surface change the refractive index and shift the θ_{sp} which is proportional to the concentration of reactants. The detection of changes in θ_{sp}

during the binding process with respect to time is the basis of SPR biosensors.²²⁰ The instrument demonstrates the changes in resonance unit (RU) during the association and disassociation process as a SPR sensogram with 1 RU corresponding to $\sim 1\text{pg/mm}^2$ and 1×10^{-6} refractive index units (RIU).^{222, 224}

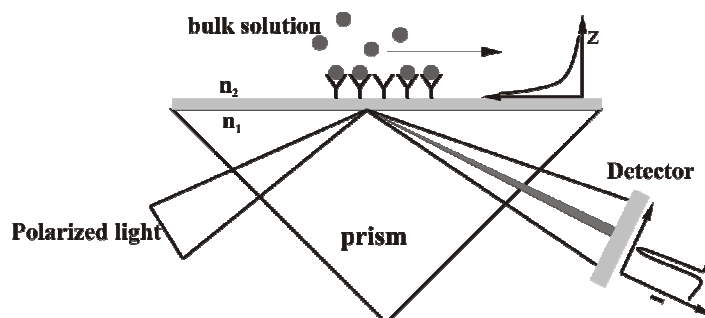


Figure 4-3: Schematic diagram of a prism-based SPR biosensor (Kretschmann configuration). The resonance position is seen as a dip in reflected light.²²²

The most important part of an SPR biosensor is its surface and immobilization process of biological molecules on it. Different surface chemistries are available for different types of biomolecule immobilization. Carboxymethylated dextran coupled with different functional groups is the most common matrix in SPR commercial biosensors due to increased signal by increasing the immobilized binding sites on the surface.²²²

SPR method has some advantages over other techniques used for kinetics analysis. It is fast, allows real-time measurement, needs less sample volume and no requirement for labelling. Although it has been widely used for kinetic and affinity analysis, there are some potential limitations to the use of SPR technique. The major limitation is the lack of sensitivity (detection limit of 1-10 nM) for 20-kDa protein and higher for smaller molecules.²²³ Small molecule antigens such as hormones, drugs and toxins produce poor signal which is hard to distinguish from noise and need special enhancement strategies to generate signals with optimized sensitivity.²²⁵ Some of

these strategies are: (i) labelling small molecules with a high mass label and used them in a competitive assay with unlabelled sample antigens; (ii) immobilization of small antigen on the surface of sensor and detect it with primary antibody labelled with gold nanoparticles; and (iii) usage of linkers to optimized binding of immobilized antigen and antibody in the flow.^{223, 224} Small molecule binding measurements with SPR require accurate design of assay format, immobilization chemistry and labelling to show reliable sensitivity. The other potential difficulty in SPR in kinetic measurement is the mass transport limitation due to insufficient transportation of mobile reactant to and from the biosensor surface which affects both association and disassociation. Kinetic measurements require proper selection of experimental parameters such as flow rate and concentrations of both immobilized and mobile reactants to overcome this limitation.²²² Whereas SPR does not require labelled reactants, one of the reactants has to be covalently immobilized on the surface which may be the source of some artifacts in SPR experiments. The immobilization process affects the reactivity and the native structure of proteins leading to conformational changes in the binding sites.²²² It has been shown that high concentration of immobilized reactant at the surface causes steric hindrance in binding to adjacent binding sites which affect the binding process. Also the orientation of the reactant immobilized on the surface may affect the subsequent antigen-antibody binding process.²²⁶ To overcome this problem, positional immobilization via monoclonal antibodies has been used but this leads to other limitations such as production of target specific monoclonal antibodies against the reactant and removing the monoclonal antibodies during the regeneration step.^{225, 226} The other concerns about SPR method are: severe standardization requirement, need for high purity analytes, non-specific interaction of some proteins with the dextran matrix, proper

washing and regeneration steps and careful experimental design and data processing should be considered to properly carry out a kinetic analysis.²²⁵ Studies to compare the SPR with other methods showed inconsistent results. In some cases good agreement was reported; however, in other reports, significant differences (up to several orders of magnitude) have been observed that may have resulted from the limitations discussed above.²²²

Waveguides:

A simple planar optical waveguide is formed by a higher refractive index layer sandwiched between two regions of lower index. At specific incidence angle ($\theta > \theta_c$), light is coupled into the high refractive index layer and propagates by TIR within this layer produces a standing wave pattern across the layer. This phenomenon is known as waveguiding. The propagating light in a waveguide generates an evanescent field at the surface of the waveguide layer.²²⁷ Any change in this layer causes changes in the resonant waveguide mode that can be measured by different techniques (absorption and fluorescence measurements, grating coupling, interferometry, etc.).

Resonant mirror (RM) is a well-known commercialized waveguide technique that has been used for measuring kinetic parameters. The system has similar construction to the SPR device except that the metal surface is replaced by a dielectric resonant layer of high refractive index (such as titania).²⁰⁷ Unlike SPR, the RM system measures the shift in the phase of the reflected light. Whereas SPR is excited by one input polarization, RM is excited with both TE and TM polarizations and can be used to obtain quantitative measurements of thickness and refractive index at the sensor surface. However, RM is more complex than SPR devices and more difficult to fabricate. So its usage is less common than SPR devices.²²⁸

As mentioned before, the evanescent waves can excite fluorescent molecules attached to the surface in the evanescent wave zone. Use of fluorescent labels in planar optical waveguides presents better sensitivity and specificity due to detection within the evanescent field. This minimizes the disadvantages associated with high backgrounds.²²⁹

4.1.5.4 Magnetorelaxometry

Magnetorelaxometry is based on using magnetic nanoparticles (MNP) as labels in a magnetic field and the direct measurements of their relaxation magnetisation following the switch-off the magnetic field. After switching off the magnetic field, the moments of MNP return to equilibrium by a decay in the magnetisation which is called relaxation. There are two different mechanisms for relaxation: Néel relaxation and Brownian relaxation.²³⁰ The difference between the magnetic relaxation mechanisms of free and bound MNP due to their different mobility are detected magnetically by sensitive sensors such as superconducting quantum interference devices (SQUIDs).⁴⁶ A magnetic relaxation immunoassay (MARIA) method based on magnetorelaxometry technique was established as a homogeneous assay. MARIA provides the quantity of bound antibodies in the presence of the unbound ones because these two signal contributions can be separated.²³¹ MARIA has been used for detection of C-reactive protein (CRP) in serum,²³² quantification of agglutination of bovine serum albumin (BSA),²³³ biotin and avidin²³⁰ and the binding kinetics of biotin and streptavidin.²³¹

4.1.5.5 Optical sectioning methods

Two photon excitation microscopy:

Two photon excitation immunoassay system (TPX) as a separation-free microparticle based assay has been used to measure the kinetic parameters of models of human thyroid stimulating hormone (hTSH)¹⁶² and C-reactive protein (CRP)¹²⁹. The results showed that TPX-system enabled the evaluation of the kinetic parameters due to separation-free nature of this method which allows detection of the two-photon excited fluorescence from the surface of individual microspheres in the presence of unbound fluorescent tracer molecules in solution and background signals from the optical system and from the sample outside the focal volume are not detected.

CLSM:

The application of CLSM in kinetics study of immunoassays has not been reported yet. In this part of my thesis, the feasibility of using CLSM for kinetic analysis of a human IgG assay model was studied. Two fluorescent probes (FITC and QD565) as reporter secondary antibodies and two formats of FLISA assays (homogeneous and heterogeneous) have been used in this section. The main goals were the investigation and application of CLSM to kinetic analysis of antigen-antibody reactions and observation of the kinetic behaviours in different fluorescent probes and assay formats. According to the non-separation nature of the confocal immunosorbent assay method the quantitative measurement of the kinetic parameters on a solid surface was practicable. As it was proved in previous chapter, CLSM allows the optical detection of the fluorescent products at the interface of the thin layer of the antigen-antibody complex on the surface and the unbound fluorescent markers in the solution without interference signals of the solution.

4.2 Theory

In this section, the theory of the kinetics of antibody-antigen reactions at a solid surface in a model fluorescent sandwich immunoassay is described in heterogeneous and homogenous formats. As it was explained in chapter 3, the main difference between these two formats is the step of adding antigen. In heterogeneous format, each step of the sandwich assay protocol is performed sequentially. But, the two steps of adding antigen and secondary antibody are conducted simultaneously in the homogeneous assay.

4.2.1 Heterogeneous format

The main reaction to be studied in this format is the reaction between an antigen (human IgG) which is immobilized on the surface via binding to a first antibody (anti-human IgG) and a fluorescently labelled secondary antibody (QD565 or FITC conjugated anti-human IgG) in the solution.

The reaction of antibody-antigen at a solid surface takes place at the boundary of two phases of liquid and solid. The reaction is the sum of several sub-reactions and the slowest sub-reaction determines the rate of total reaction. The subreactions can be summarized as the diffusion reaction of the reactant (fluorescent antibody) in the solution to the surface, the binding reaction between antigen-antibody, the disassociation reaction of immunoassay complex and the diffusion of mobile reactant to the solution (Figure 4-4).

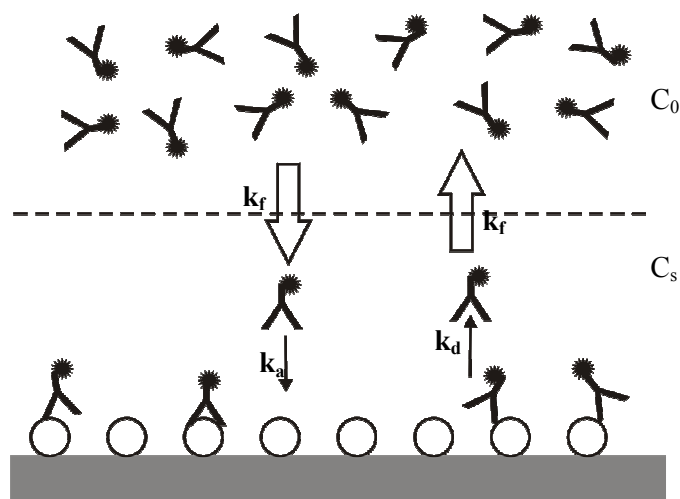


Figure 4-4: Schematic illustration of diffusion-limited binding of labelled antibodies in solution with immobilized antigen on a solid surface in heterogeneous format assay.¹⁷⁷

C_0 and C_s are the labelled antibody concentrations in the solution and at the surface respectively. k_{dif} is the diffusion rate constant that describes the mass transport of the labelled antibody to the surface. k_a and k_d are the forward and reverse kinetic rate constants. To assess if the reaction is reaction-limited or diffusion-limited, the diffusion limitation of the labelled antibody bound to a flat surface for an unstirred solution is calculated based on Fick's law of diffusion for a planar surface for:¹⁷²

$$C_s = \frac{2}{\sqrt{\pi}} C_0 \sqrt{Dt} \quad (4-11)$$

where C_s is the surface concentration of bound antibody, C_0 is the concentration of labelled antibody in solution and D is its diffusion constant (cm^2/s) and t is time (s). The comparison between the theoretical and experimental amount of bound antibody at the surface will determine whether the reaction is limited by diffusion.^{172, 173}

The model of a sandwich immunoassay used for the experimental section may be schematized as following steps:

- (1) Coating a coverglass chamber slide with the first antibody (Ab);
- (2) Washing step to remove non-adsorbed antibody to the solid surface;

(3) First incubation with antigen (Ag)



(4) Washing step to remove unbound antigen;

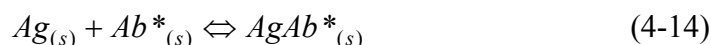
(5) Second incubation with a fluorescently labelled secondary antibody (Ab*)



(6) Studying the kinetics of the reaction (4-13) by CLSM which allows measurement of the intensity related to the concentration of $AbAgAb^*$ complex without washing the unbound or free secondary antibodies.

There are some assumptions to be considered for the simplicity of the kinetic model:

(a) All the side reactions will be ignored. The most important ones are:



since it is assumed that all unbound antigen are removed during the given washing step (4) so there is no free antigen in solution (Ag_s) to react with the labelled antibody, and:



due to the assumption of removing all non-adsorbed first antibody from the reaction chamber slide during the first washing step.

(b) Since the same concentration of the first antibody has been used for all kinetic experiments in this thesis, the concentration of $AgAb$ is proportional to the concentration of Ag .

(c) The antigen and antibody have 1:1 interaction.

By considering all the assumptions, the interaction of immobilized antigen on the solid surface of a chamber slide with a fluorescent labelled antibody is simply described as:



Kinetic data can be analysed based on different kinetic models to obtain the best description of experimental data and measure the kinetic parameters. The kinetic models tested varied from a simple model such as exponential curve fitting which has been used to analyse of biosensor data²³⁴⁻²³⁶ to mathematical models based on numerical methods to solve nonlinear ordinary differential equations.^{162, 168, 237} The association reaction is expected to be a pseudo-first-order process as the labelled antibody is present in excess and therefore its concentration remains constant during the reaction time. The experimental studies on the kinetics of antigen-antibody reaction on the solid surface have shown that disassociation rate constant is low so the contribution of disassociated antibodies from surface to solution near the surface is minimal.¹⁷⁷

The rate of formation of the antigen-antibody reaction as shown in equation 4-16 at time t may be written as:

$$\frac{d[AgAb^*]}{dt} = k_a[Ag]_t[Ab^*]_t - k_d[AgAb^*]_t \quad (4-17)$$

where k_a is the association rate constant, k_d is the disassociation rate constant, $[Ag]_t$, $[Ab^*]_t$ and $[AgAb^*]_t$ are the concentration of antigen, labelled antibody and antigen-antibody complex at time t respectively. The concentrations of antigen and antibody at any given time t are:

$$\begin{aligned} [Ag]_t &= [Ag]_0 - [AgAb^*]_t \\ [Ab^*]_t &= [Ab^*]_0 - [AgAb^*]_t \end{aligned} \quad (4-18)$$

where zero denotes the initial concentrations of reactants. Since the concentration of labelled antibody is in excess which means $[Ab^*]_0 \gg [AgAb^*]_t$, so the equation 4-17 may be written as:

$$\frac{d[AgAb^*]}{dt} = k_a[Ab^*]_0([Ag]_0 - [AgAb^*]_t) - k_d[AgAb^*]_t \quad (4-19)$$

In CLSM detection method, the change in fluorescent intensity, I , which is proportional to $[AgAb^*]$ is measured, thus:

$$\frac{dI}{dt} = k_a [Ab^*]_0 (I_{max} - I_t) - k_d I_t \quad (4-20)$$

Where I_{max} is the fluorescent response at complete saturation of the antigen binding sites when $t \rightarrow \infty$. By rearrangement:

$$\frac{dI}{dt} = k_a [Ab^*]_0 I_{max} - (k_a [Ab^*] + k_d) I_t \quad (4-22)$$

The solution of this equation results in a pseudo-first order equation.²³⁶

$$I_t = (I_{max} - I_0)[1 - \exp(-k_{obs}t)] + I_0 \quad (4-23)$$

I_t is the intensity at time t , I_0 is the initial intensity at time zero which could be related to the background fluorescence from the solid surface and k_{obs} is the observed rate constant (s^{-1}) is given by:

$$k_{obs} = k_a [Ab^*] + k_d \quad (4-24)$$

From Eq. 4-23, the CLSM intensity should increase in a single exponential manner which describes the one-to-one interaction of the reactants. However, it is possible that the interaction is not well described by a monophasic model based on one k_a or k_d . Studies have shown that in some cases the experimental kinetic data of the antigen-antibody interaction was described better by more complex relationship such as biphasic association which can be described by Eq. 4-25:^{236, 238, 239}

$$I_t = A[1 - \exp(-k_{obs1}t)] + B[1 - \exp(-k_{obs2}t)] + I_0 \quad (4-25)$$

Here, I_t varies with two association rate constants (k_{obs1} and k_{obs2}) and the magnitudes of the intensity of two phases are A and B respectively such as $I_\infty = A + B + I_0$. The biphasic interaction curve is made up of two monophasic interaction curves, phase 1

and phase 2 with fast and slow association rate constants, respectively. Mechanisms involved in multiphasic association rate constants will be discussed later.

The disassociation rate constant could be measured by washing the fluorescent overlayer of unbound conjugated antibody and substituting buffer (PBS) then scanning the chamber slide for a period of time with CLSM. The disassociation reaction is a pseudo-first order decay reaction which may be obtained by fitting the desorption data to this exponential equation:²³⁸

$$[AgAb^*]_t = [AgAb^*]_0 \exp(-k_d t)$$

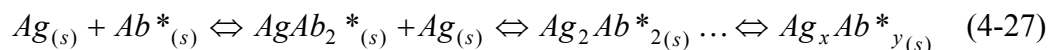
or:

$$I_t = I_a [\exp(-k_d t)] \quad (4-26)$$

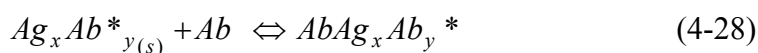
Where $[AgAb^*]_0$ is the concentration of bound antibody at the starting point of the disassociation period and I_a is its proportional intensity at that time.

4.2.2 Homogeneous format

The theory behind homogenous format is not as straightforward as the heterogeneous. Here, the main step of the sandwich assay takes place in the solution where the antigen binds to the fluorescent labelled secondary antibody (Eq 4-18). The excess amount and free movement of antigen and polyclonal antibodies in solution may cause more complex reactions occur such as aggregation (Figure 4-5):



The next reaction is diffusion of the antigen-antibody complex ($Ag_xAb_y^*$) from solution to the surface to react with immobilized first antibody. The product of this reaction can be measured by CLSM at the interface of the solid surface:



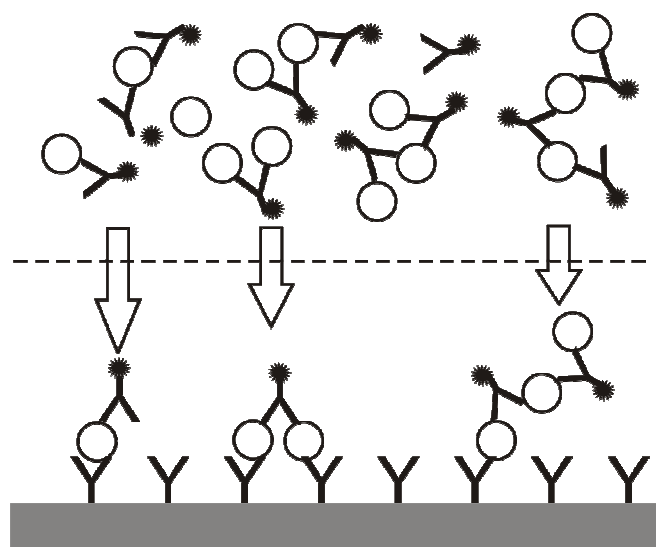


Figure 4-5: Schematic illustration of diffusion-limited binding of labelled antibodies in solution with immobilized antigen on a solid surface in a homogeneous format assay. Reaction of antigen and labelled antibody start in solution and then the complexes diffuse to bind to antibodies on the surface. The arrow size is related to the magnitude of diffusion.

In a homogeneous system, the issue of mass transfer by diffusion of antigen-antibody complex in solution toward the first antibody on the surface is important and may be the rate-limiting step of the whole reaction. A simple comparison of homogeneous and heterogeneous format assays regarding the diffusion from solution to surface shows that the rate of diffusion should be slower in homogeneous format due to the bigger size of the molecule and smaller diffusion coefficient.

4.3 Materials and methods

4.3.1 Reagents

Human IgG, goat anti-human IgG (γ -chain specific), goat anti-human IgG (γ -chain specific) FITC conjugate and bovine serum albumin minimum 98% (BSA) and phosphate buffered saline pH 7.4 (PBS) were purchased from Sigma-Aldrich

Company Ltd (Dorset, UK). Qdot® 565 goat F(ab')₂ anti-human IgG conjugate (H+L) was purchased from Invitrogen (Paisley UK). Chambered cover glass slides (Lab-Tek chambered #1.0 Borosilicate) were used as a solid surface of immunoassays.

4.3.2 Instruments

A confocal scanner head (TCS NT; Leica Microsystems) installed on an inverted microscope (DM IRBE, Leica Heidelberg GmbH) was used for the optical sectioning of the immunoassay. The 488 nm line of an argon ion laser was used for excitation and the emission fluorescent intensity was detected using a 530/30 nm bandpass filter. For quantum dots 565, the 476 and 488 nm lines of the argon laser were used for excitation and the emission intensity detected using LP550 nm filter. The objective used was 40× NA 0.75 and scanning was done by using 50 steps of 0.2 µm along the z-axis with a 74 µm pinhole size.

4.3.3 Preparation of sandwich FLISA for kinetic measurements

The human IgG immunoassays were conducted by immobilizing anti-human IgG (40 µg/ml) as the capture antibody on the chamber slide at 4°C overnight. The remaining sites were blocked with a solution of 1% BSA for 2 hours at room temperature. After washing with PBS, human IgG (10 µg/ml) was added as antigen and incubated for 2 hours at room temperature. The chamber was washed and the antibody-antigen reaction was started by adding anti-human IgG conjugated to FITC or QDs 565 as the secondary labelled antibody to the chamber to produce the sandwich complex of anti-IgG/ IgG/FITC(QD)-anti IgG. The reactions were followed for 2 hours without stirring with CLSM. Data were collected every minute for the first hour and then every 2.5 minutes for another hour (85 kinetic data sets for each concentration). There

was no specific consideration for controlling temperature in the kinetic experiments. The confocal microscopy room was equipped with air conditioning which provided a fixed temperature of 21°C during all measurements. The disassociation reaction of antigen-antibody complex has not been studied by CLSM. The antibody and antigen concentrations used in kinetic experiments were chosen according to the dose response experiments in chapter 3.

4.3.4 Homogenous versus heterogeneous format assays

The comparison between two assay formats (heterogeneous and homogenous) has been done with QD565 labelled antibody. The kinetic experiments of both assays were carried out in a same day with identical instrumental conditions and reagent concentrations (40 µg/ml anti-human IgG and 10 µg/ml human IgG). The only difference between the heterogeneous and homogenous experimental procedures was the step of adding antigen to chamber slides. In homogenous format after blocking the chamber with 1% BSA for 2 hours at room temperature, the human IgG (10 µg/ml) and anti-human IgG conjugated with FITC or QD565 were added simultaneously not sequentially. The chamber slide containing the homogeneous format assay was scanned first for two hours and then the heterogeneous one was scanned.

4.3.5 Data analysis

Data were collected in the form of digital images in TIF format. Images were analysed by the custom software that has been described in section 3.3.8.1. The fluorescent intensity related to the thin layer of the bound antibody was determined based on Eq. 3-7. The Graphpad Prism version 5.02 was used to fit the data based on one-phase and two-phase association exponentials. The statistical analysis F test was performed in order to assess the best fit for each data series.

4.4 Results

4.4.1 Association rate constant analysis

4.4.1.1 Heterogeneous FLISA with FITC conjugated secondary antibody

To calculate the association rate constant of the reaction between surface-bound human IgG and anti-human IgG-FITC in solution, kinetic binding experiments were carried out at various concentrations of anti-human IgG-FITC (0, 40, 80, 160 and 270 nM) with the fixed amount of human IgG bound to anti-human IgG coated chamber slides. After decomposition of the fluorescent signals, the time responses of fluorescence intensity of the thin layer of the immunoassay complex at different concentrations of labelled antibody were measured and shown in Figure 4-6. For scanning FITC labelled samples, the point of scan had to be moved for each data point to avoid decreasing intensity due to the photobleaching of FITC.

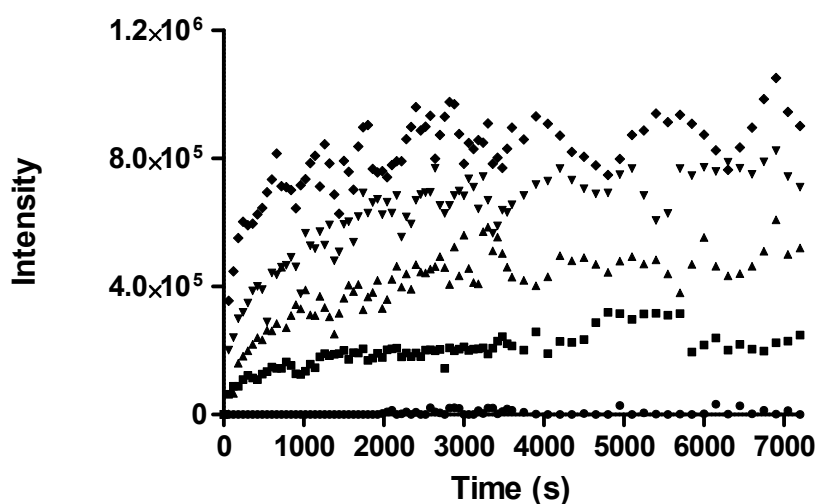
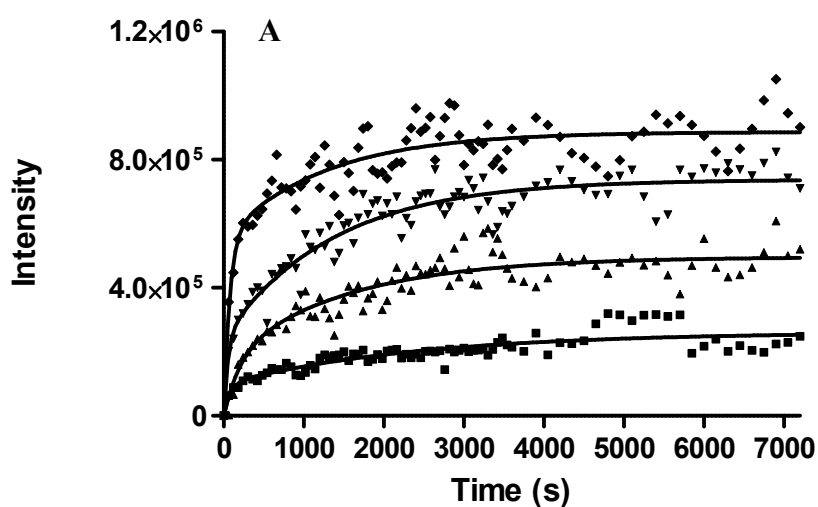


Figure 4-6: Binding curves of different concentrations of anti-human IgG-FITC to immobilized human IgG: (●) zero, (■) 40, (▲) 80, (▼) 160 and (◆) 270 nM.

The result of zero concentration of the fluorescent antibody in solution shows that the non-specific binding has no effect on the kinetic binding experiment and the observed intensity is only related to the interaction of antigen and antibody. The confocal response upon binding labelled antibodies to the immobilized antigen increases in an exponential manner. The equations 4-23 and 4-25 were used to fit the experimental data to determine the single or double exponential association processes of the kinetic reaction. The result of fitting the data is shown in Figure 4-7. The data of all concentrations fit best to a double exponential association equation according to the F test resulting in two distinct rate constants. The values of k_{obs1} and k_{obs2} vary with the concentrations of labelled antibodies in solution. The results of fitting are summarized in Table 4-2.



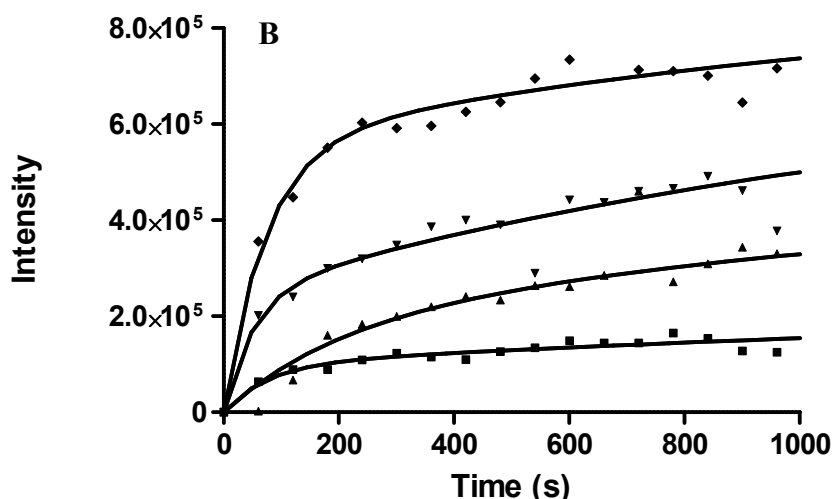


Figure 4-7: Binding curves of different concentrations of anti-human IgG-FITC to immobilized human IgG fitted to double exponential Eq. 4-25: (■) 40, (▲) 80, (▼) 160 and (◆) 270 nM. B shows the initial part of the curves before reaching equilibrium.

Table 4-2: Best-fit kinetic parameters of the binding of human IgG and anti-human IgG-FITC in heterogeneous format assay.

Secondary Antibody (nM)	Kinetic parameters					
	k_{obs1} (s ⁻¹)	k_{obs2} (s ⁻¹)	%A	%B	k_a (M ⁻¹ s ⁻¹)	k_d (s ⁻¹)
40	$(4.7 \pm 0.2^a) \times 10^{-3}$	$(5.3 \pm 2.3) \times 10^{-4}$	38	62	$(5.8 \pm 1.0) \times 10^4$	$(4.0 \pm 1.7) \times 10^{-3}$
80	$(1.1 \pm 0.6) \times 10^{-2}$	$(2.7 \pm 1.6) \times 10^{-4}$	36	64		
160	$(1.3 \pm 0.3) \times 10^{-2}$	$(7.4 \pm 2.2) \times 10^{-4}$	37	63		
270	$(1.9 \pm 1.1) \times 10^{-2}$	$(7.0 \pm 1.0) \times 10^{-4}$	33	67		

a: \pm Std error

A plot of k_{obs1} values versus concentration was used to obtain the association rate constant from the slope and the dissociation rate constant from the y-intercept based on Eq. 4-24. A linear equation was obtained as $y = (5.8 \pm 1.0) \times 10^4 x + (4.0 \pm 1.7) \times 10^{-3}$ ($R^2 = 0.94$) in Figure 4-8. Thus, the association and disassociation rate constants are $k_a = 5.7 \times 10^4$ and $k_d = 4 \times 10^{-3}$ (s⁻¹) respectively.

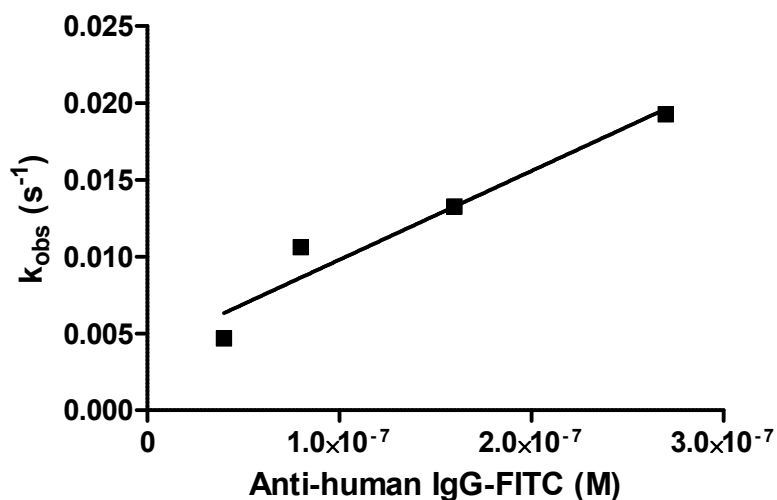


Figure 4-8: Concentration dependence of k_{obs1} values derived from double exponential curve fitting of human IgG binding to of anti-human IgG-FITC

4.3.1.2 Heterogeneous FLISA with QD565 conjugated secondary antibody

The kinetic reaction of heterogeneous FLISA with QDs was studied with different concentrations of anti-human IgG-QD565 (0, 20, 60, 160 and 270 nM) with the fixed amount of human IgG bound to anti-human IgG coated chamber slides. The same procedure for decomposition of the fluorescent signals has been done to obtain the fluorescence intensity of the thin layer of the immunoassay complex at different concentrations of QD565 labelled antibody shown in Figure 4-9. The confocal scanning in these series of experiments with QDs was limited to one point at the solid surface during the time course due to photostability and resistance to photobleaching properties of QDs.

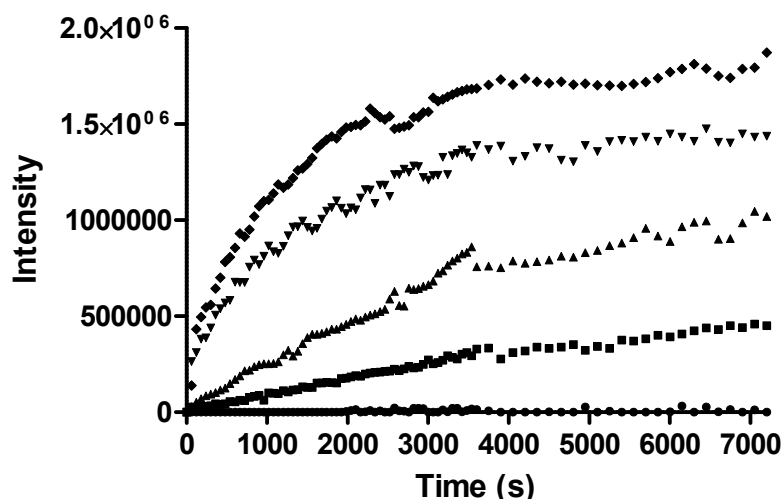


Figure 4-9: Binding curves of different concentrations of anti-human IgG-QD565 to immobilized human IgG: (●) zero, (■) 20, (▲) 60, (▼) 160 and (◆) 270 nM.

The binding curves of human IgG to different concentrations of QDs conjugated antibodies show differences in the shape of kinetics response compared to FITC experiments and can be divided to two groups of low concentrations (20 and 60 nM) and high concentrations (160 and 270 nM). At low concentrations there is no change in the shape of the curves during the time course and the plot is nearly linear shows the reaction of antigen and QDs conjugated antibody did not reach equilibrium. At high concentrations of QDs labelled antibodies significant difference in the shape of binding curve is obvious. The binding started with a sharp increase in the bound antibody concentrations followed by a transition to equilibrium step. The kinetic parameters of the binding reactions were quantified by fitting the data points with equations of 4-23. The F test showed that lower concentration binding curves fitted well with a single exponential binding equation but higher concentrations better fitted to double exponential binding kinetics. The result of fitting the data is shown in Figure 4-10. The plot of k_{obs} as a function of QD565 anti-human IgG was drawn based on the K_{obs1} result to determine the association and disassociation rate constants

(Figure 4-11). A linear equation was obtained as $y=(2.6\pm 0.4)\times 10^4x+(3.5\pm 0.6)\times 10^{-6}$ ($R^2=0.96$). Thus, the association and disassociation rate constants are $k_a=2.6\times 10^4$ ($M^{-1}s^{-1}$) and $k_d=3.5\times 10^{-6}$ (s^{-1}) respectively. The results of fitting and rate constants are summarized in Table 4-3.

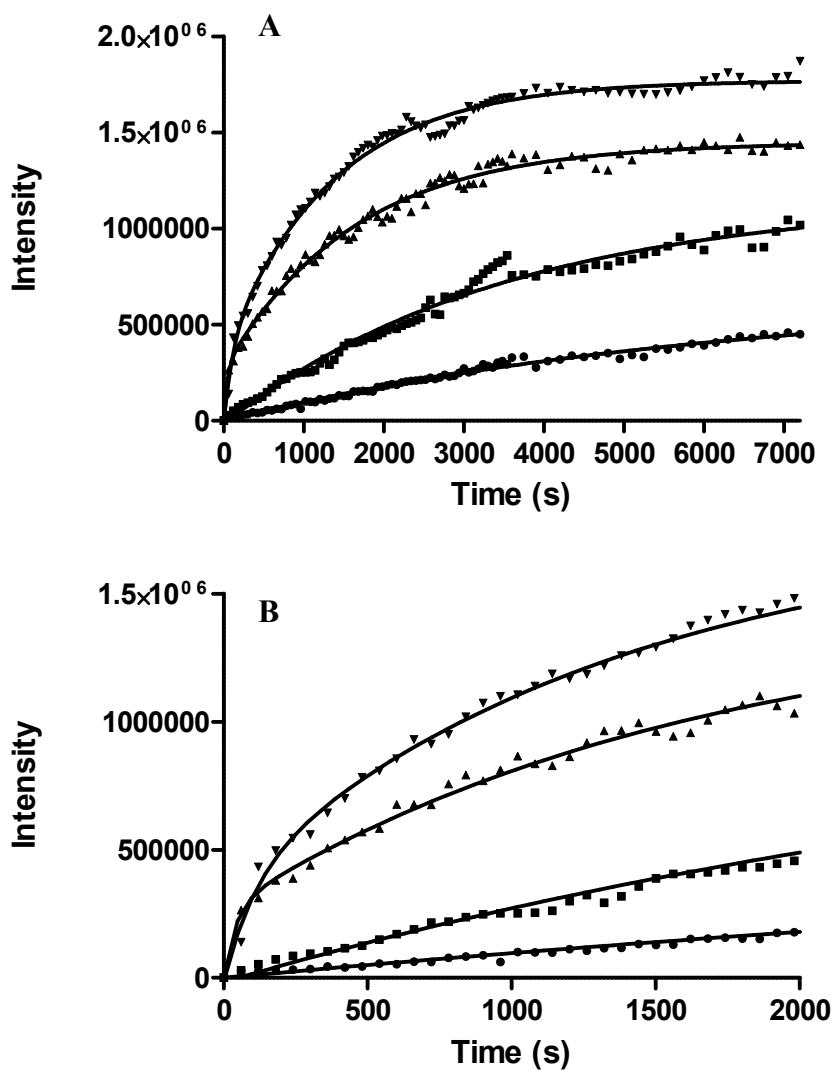


Figure 4-10: Binding curves of different concentrations of anti-human IgG-QD565 to immobilized human IgG fitted to double exponential Eq. 4-25: (■) 20, (▲) 60, (▼) 160 and (◆) 270 nM. B shows the initial part of the curves before reaching equilibrium.

Table 4-3: Best-fit kinetic parameters of the binding of human IgG and anti-human IgG-QD565 in heterogeneous format assay.

QD656 (nM)	Preferred model	k_{obs} (s^{-1})		Kinetic parameters			
				%A	%B	k_a ($M^{-1}s^{-1}$)	k_d (s^{-1})
40	Single	$(1.6 \pm 0.1^a) \times 10^{-7}$		-	-	$(2.6 \pm 0.4) \times 10^4$	$(3.5 \pm 0.6) \times 10^{-6}$
80	Single	$(1.3 \pm 0.1) \times 10^{-4}$		-	-		
160	Double	$(1.5 \pm 0.4) \times 10^{-2}$	$(5.2 \pm 0.3) \times 10^{-4}$	80	20		
270	Double	$(7.3 \pm 0.1) \times 10^{-3}$	$(6.6 \pm 0.4) \times 10^{-4}$	77	23		

a: \pm Std error

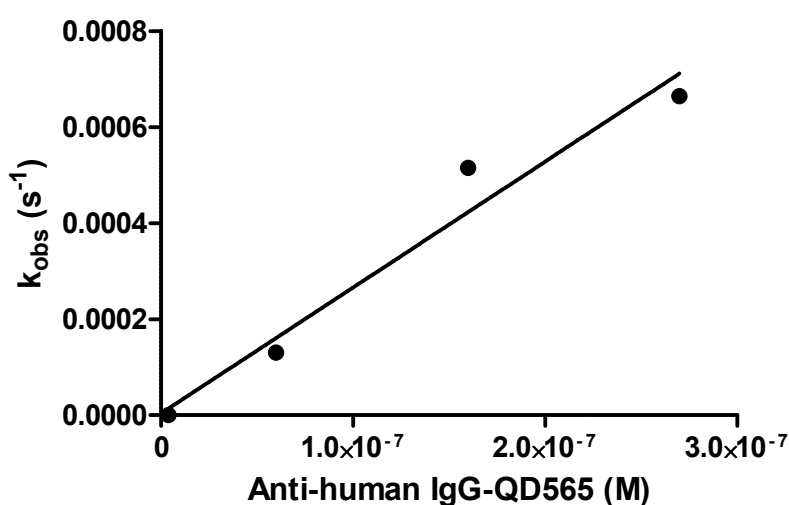


Figure 4-11: Concentration dependence of k_{obs} values derived from fitting parameters for the reaction of human IgG binding to of QD565 anti-human IgG

4.3.2 Diffusion or reaction limited

The rate constants that were determined experimentally in previous section should be clarified whether they reflect the intrinsic kinetics of the binding reaction or diffusion influenced by the diffusion limitation.

4.3.2.1 FITC conjugated secondary antibody

The diffusion-limited amount of FITC labelled antibodies bound to the surface of the chamber slide was calculated according to Eq. 4-11. The diffusion constant for IgG antibodies was taken to be approximately $4 \times 10^{-7} \text{ cm}^2 \text{ s}^{-1}$.^{170, 175} The amount of

calculated diffusion-limited bound labelled antibody versus time was simulated (Figure 4-12). Then the fitted values of concentration-dependent intensities of different concentrations of the labelled antibody were normalized and plotted together with normalized diffusion-limited amounts (Figure 4-13).

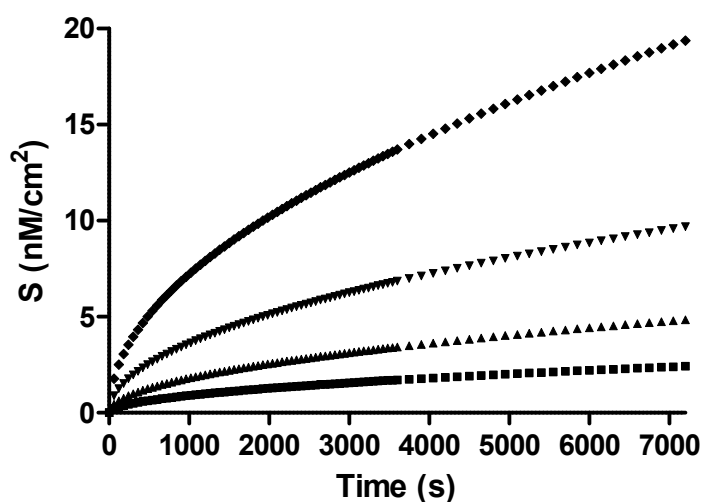


Figure 4-12: Theoretical values of bound anti-human IgG-FITC on the surface of the chamber slide calculated from the diffusion-limited amount of bound antibody Eq. 4-11: (■) 40, (▲) 80, (▼) 160 and (◆) 270 nM.

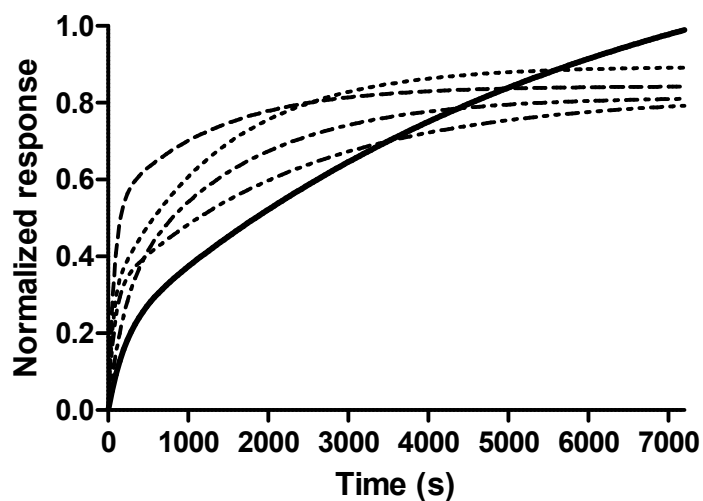


Figure 4-13: Quantitative description of the amount of bound anti-human IgG-FITC antibody at the surface. Solid line is the normalized theoretical amount of bound antibody calculated based on Eq. 4-11. Dash lines are the normalized fitted concentration-dependent intensities of confocal microscopy response of bound antibody on the surface: (---) 40, (- - -) 80, (- . -) 160 and (---) 270 nM.

In this plot (Figure 4-13) it is possible to show whether the binding reaction of human IgG and anti-human IgG-FITC is reaction or diffusion limited. The solid line corresponding to the theoretical amount of diffusion-limited bound antibody and the other dash lines are experimental findings. As can be seen, for all labelled antibody concentrations the experimental results are higher than diffusion-limited amounts at the first hour course of the experiment. When the ratio of reaction rate and diffusion rate is greater than 1 ($I_t > S$) the reaction is diffusion-limited which means the diffusion or mass transfer is the slowest reaction step.¹⁶⁹ Therefore, all the binding reactions of human-IgG to anti-human IgG-FITC in the concentration range of 40-270 nM were diffusion-limited at least in the first hour of the experimental time course.

4.3.2.2 QD565 conjugated secondary antibody

Each particle of QD565 from Invitrogen company consists of three antibodies (anti-human IgG) attached to one QD with CdSe/ZnS composition. The size and weight of QD are about 15-20 nm and 2500 kDa respectively.²⁴⁰ It was not possible to find literature values about the diffusion coefficient of the used QDs from the company. There is a paper using confocal fluorescence correlation spectroscopy (FCS) to characterize different QDs from Invitrogen in solution.²⁴¹ It was reported that the tested QDs had larger hydrodynamic radii and slower diffusion coefficients compared to the tested organic dye, Alexa 488. The measured diffusion coefficient for QD565 in this report was $15.9 \times 10^{-8} \text{ cm}^2 \text{ s}^{-1}$ with 13.9 nm hydrodynamic radius which was used here to calculate the diffusion-limited amount of QD565 labelled antibodies bound to the surface of the chamber slide. The amount of calculated bound labelled antibody versus time was plotted as shown in Figure 4-13. The theoretical values of the amount of bound QD565 conjugated antibodies on the surface are lower compared to FITC

antibodies due to a smaller diffusion coefficient (maximum 10.3 compared to 19.4 nM/cm^2 for FITC antibodies). Then the fitted values of concentration-dependent intensities of different concentrations of the QD565 antibody were normalized and plotted together with normalized diffusion-limited amounts (Figure 4-14). The results showed that for two binding curves (20 and 60 nM) belong to lower concentrations of QD565 conjugated antibodies the mass transport did not limited the reaction ($S > I_t$) but for the higher concentrations (160 and 270 nM) the binding reactions are diffusion-limited.

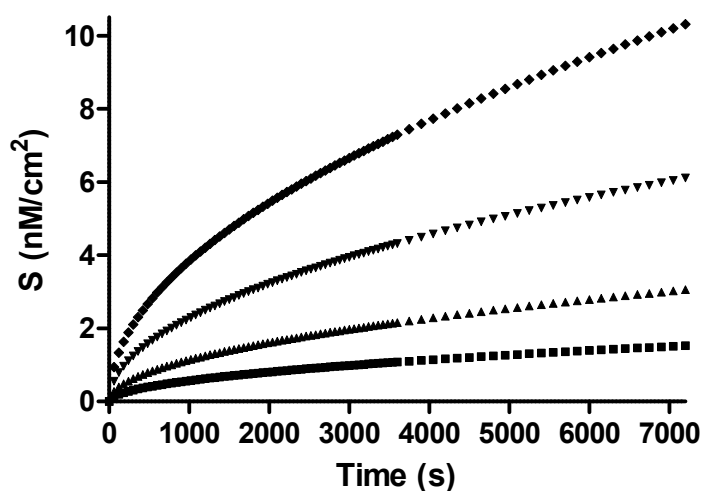


Figure 4-14: Theoretical values of bound anti-human IgG-QD565 on the surface of the chamber slide calculated from the diffusion-limited amount of bound antibody Eq. 4-11: (■) 20, (▲) 60, (▼) 160 and (◆) 270 nM.

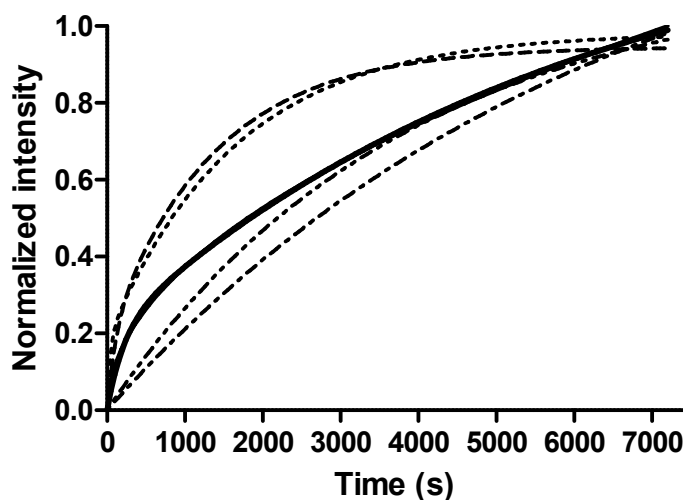


Figure 4-15: Quantitative description of the amount of bound anti-human IgG-FITC antibody at the surface. Solid line is the normalized theoretical amount of bound antibody calculated based on Eq. 4-11. Dash lines are the normalized fitted concentration-dependent intensities of confocal microscopy response of bound antibody on the surface: (---) 20, (- - -) 60, (- . -) 160 and (- . . -) 270 nM.

4.3.3 Heterogeneous versus homogenous assay formats

The effect of different assay formats on the binding reaction of human IgG and anti-human IgG-QD565 was studied by analysing their kinetic parameters. The comparison between homogeneous and heterogeneous format assays has been done on two different concentrations of anti-human IgG-QD565, 40 and 160 nM. Figure. 4-14 shows the intensity profiles of both formats over the time course after decomposition of signals and fitting. The possibility of aggregation of antigen-QD labelled antibody in the homogeneous format assays was supported by the fact of observation of bright aggregated microscale structures during scanning with CLSM which has not been observed in the heterogeneous format assays. In general, aggregation causes hiding of the binding sites on both antigen and antibody and therefore slows down the binding reaction. As can be seen the observed intensity of the homogenous assay in both concentrations was lower than heterogeneous which gives a lower bound complex formation in homogeneous format. The difference in

shape of binding curve is observed in lower concentrations of QD565. The heterogeneous format follows a linear response in experimental time course that have been seen previously for other low concentrations of QD565 while the homogeneous format reaches equilibrium state in this period. The binding curve of both concentrations of homogeneous format assays fit better with double exponential equation. The kinetic parameters of both formats are summarized in Table 4-4.

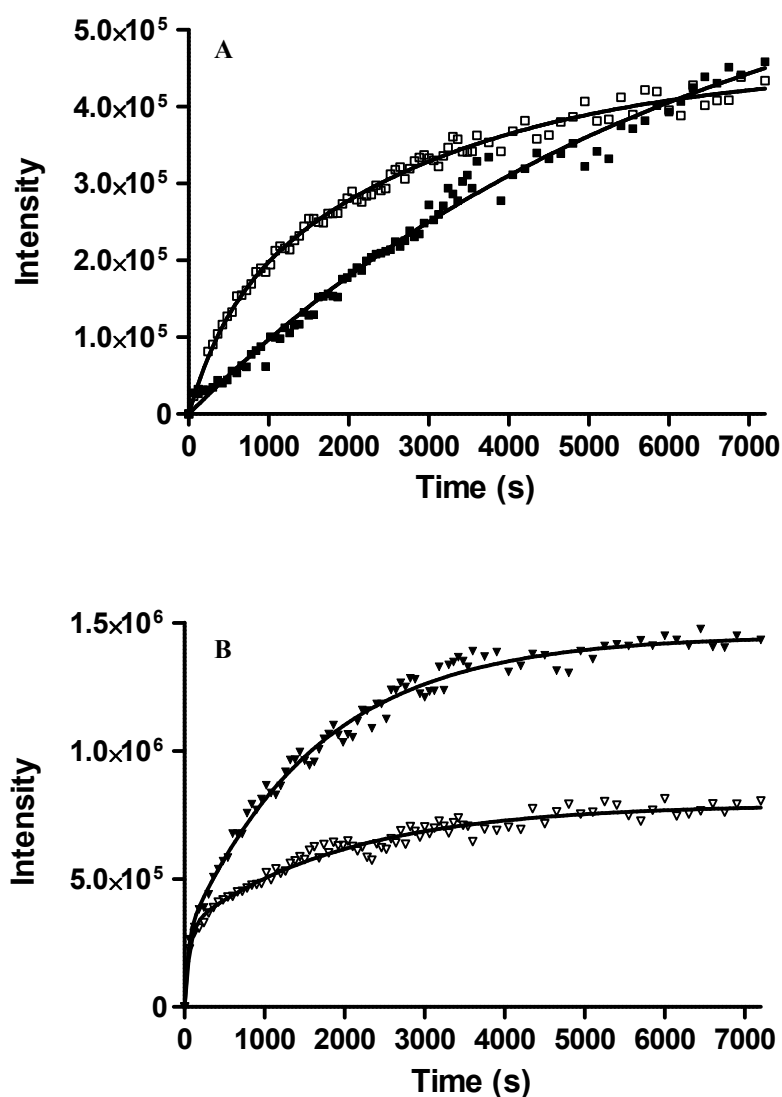


Figure 4-16: Binding curves of different concentrations of anti-human IgG-QD565 to immobilized human IgG on the surface in heterogeneous and homogeneous format assays. (A) 40 nM of anti-human IgG-QD565 (■) heterogeneous and (□) homogeneous. (B) 160 nM of anti-human IgG-QD565 (▼) heterogeneous and (▽) homogeneous.

Table 4-4: Best-fit kinetic parameters of the binding of human IgG and anti-human IgG-QD565 in homogeneous and heterogeneous format assays

QD656 (nM)	Assay format	Preferred model	k_{obs} (s^{-1})		Double model parameters	
					%A	%B
40	Heterogeneous	Single	$(1.6 \pm 0.1) \times 10^{-4}$		-	-
	Homogenous	Double	$(2.2 \pm 0.5) \times 10^{-3}$	$(3.3 \pm 0.4) \times 10^{-4}$	25	75
160	Heterogeneous	Double	$(2.5 \pm 1.1) \times 10^{-2}$	$(6.1 \pm 0.2) \times 10^{-4}$	18	82
	Homogenous	Double	$(1.6 \pm 0.3) \times 10^{-2}$	$(5.1 \pm 0.3) \times 10^{-4}$	40	60

4.4 Discussion and conclusion

To the best of my knowledge, this is the first report of using CLSM in kinetics analysis of antigen-antibody reaction. A model of human IgG FLISA was chosen to demonstrate the application of CLSM in measurement of kinetic parameters of the binding of human IgG immobilized on a solid surface and labelled anti-human IgG in solution. The results suggest that the confocal immunosorbent assay detection method is a suitable method for real-time investigation of immunoreaction between immobilized antigens on the surface and labelled antibodies in the solution. Using the proposed method of decomposition of the signals from the fluorescent immunoassay thin layer and overlayer in chapter 3, the changes in fluorescent response over the time can be obtained which is correlated to the concentration of the formed immunoassay complex on the solid surface. The separation-free CLSM detection method enables the measurement of the binding kinetics by measuring the amount of bound reactant in the presence of unbound ones by separating the two qualitatively different signals. The acquisition of kinetic constants is an advantage of the confocal immunosorbent assay method and adds valuable insight into this method compared to the classical routine immunoassay methods that require unbound reactant to be

washed out to obtain the signal of bound reactant. The application of the confocal immunosorbent method to quantify the kinetics of binding could be extended to measure the kinetics of any kind of the ligand-receptor or cell-based reactions where the binding reaction occurs at the boundary of liquid-solid surface.

The confocal immunosorbent assay method does not require specific geometries such as microsphere or bead and any format of planar solid surfaces can be used without specific requirements for sample preparations which are required for some binding detection methods such as some optical biosensors and bead based assays. The immobilization process of one of the reactants on solid surface is an important issue regarding its influence on binding kinetics. Most optical biosensors use covalent attachment of the reactant for immobilization which has its own benefits and disadvantages. The physical adsorption (passive method) which has been used for immobilization of proteins onto the glass surface of chamber slides in this thesis is the most common method for coating in standard laboratory immunoassays. Although there are some disadvantages for this method such as variability and reversibility in unstable environmental conditions (e.g., pH, buffer) it is still the most commonly used immobilization method for proteins.^{242,243} It is not only due to its simplicity but also because of the availability of the active or binding site of the proteins to interact with their targets.

The QDs conjugated antibodies were used in this study due to the bright emission and higher signal to noise ratio and better signals compared to FITC labelled antibodies. Also their high photostability against photobleaching presented a great advantage in the kinetic experiments as it enabled the scan of one point on the solid surface for the whole period of incubation (2 hours). But for FITC experiments, the scanning position had to be repositioned regularly to mitigate photobleaching effects.

The kinetic curve of QDs labelled antibodies (Figure 4-10) shows less fluctuation and noisy appearance compared to FITC conjugated antibody kinetics (Figure 4-6). The research studies on applications of different kinds of nanoparticles for therapeutic and diagnostic purposes have been increased intensively in recent years but quantitative kinetic studies of nanoparticle based immunoassays are limited in the literature.^{231, 244, 245} It is important to investigate the kinetics aspects of their binding interaction with biomolecules to develop and optimize performance. The kinetic of the adsorption of CdSe/ZnS quantum dots to different functionalized self-assembled monolayers (SAMs) was investigated for characterization nanoparticle-substrate interactions which showed the binding constant dependency to the nanoparticle-substrate chemistry and pH.²⁴⁶ The nanoparticle based immunoassays have been introduced as sensitive detection methods in existing immunoassay systems.^{247, 248, 249, 250} But little information about the kinetics behaviour of nanoparticle conjugated antibodies in immunoassays such as the kinetic rate and affinity constants is available which is essential to design a sensitive immunoassay.²⁴⁵ Magnetorelaxometry is one of the homogeneous immunoassay methods specifically applied for measuring the binding of biomolecules by labelling them with magnetic nanoparticles.^{231, 233} A study on kinetics binding of europium (III) chelate nanoparticles conjugated antibodies and monovalent antigen has shown that the association rates of nanoparticle conjugated antibodies were two fold higher than the original antibodies due to higher number of binding sites (130) on nanoparticles surface which needed fewer collisions with antigens for binding reaction.²⁴⁵ It has been mentioned that the association rate constant for the nanoparticle conjugated antibody with only a single binding site was very low, about 10^4 which is in the range of magnitude with the measured association rate constant for QD565 anti-human IgG. The comparison of kinetics parameters of

FITC and QDs binding reaction in this thesis may not be directly comparable due to the difference in type and source of anti-human IgG (γ -chain specific and F(ab')₂). Indeed, due to using a polyclonal antibody in this research it is hard to compare the results of kinetic parameters with that in literature. Polyclonal antibodies are combination of different subtypes with different affinities. Here, they were used only to demonstrate the feasibility of CLSM in measuring kinetic data. Therefore, the estimation of the order of magnitude of kinetic parameters should be satisfying.

The measured results for IgG-anti IgG binding reaction by different optical biosensors in the literature are in the range of 1.3 to $55 \times 10^6 \text{ M}^{-1}\text{s}^{-1}$ for association and 1.8 to $20 \times 10^{-4} \text{ s}^{-1}$ for disassociation rate constants.²⁵¹ It should be mentioned that the measurements were done under flow condition without the influence of diffusion or mass transport limited reaction.²⁵² The calculated results for the association constant with CLSM is about one order of magnitude less than what reported in the literature. By considering the actual differences between confocal immunosorbent method and optical biosensors such as the close and unstirred conditions in confocal method, the slower association rate constant should be possible. More experiments especially on different antigen-antibody systems may help to have more precise comparison between confocal and other methods.

Of the applied fitting models, the double exponential model appears to best describe most of the kinetic data. The single exponential model assumes a pseudo-first-order kinetics using the 1:1 binding model. The two component model suggests the existence of two surface populations for the bound antibody (anti-human IgG), one fast, and the other slow. Several studies have been conducted on deviations from pseudo-first-order kinetic behaviour in analysing antigen-antibody reactions at solid surface.^{169, 235, 236, 238, 239, 253} Several factors have been mentioned as the causes of

deviations. The heterogeneity and multivalency of the binding sites of immobilized antigen and antibody in solution were identified as the main sources of the deviation. The random distribution of immobilized antigen molecules along the solid surface which is feasible in case of passive absorption may be one the reason of heterogeneity of antigen binding sites.²³⁸ The IgG antibody is bivalent, able to bind to two antigenic sites. Actually, on solid surface immunoassays, IgG antibodies are in a mixture of bound states, monovalent and bivalent. Previous studies have shown that IgG antibodies do not bind homogeneously to antigens immobilized on a solid surface and that binding is a mixture of monovalent and bivalent states.²⁵⁴ In both cases of heterogeneity of antigen or antibody, the chance of deviation from pseudo-first-order kinetics increases with increasing the concentrations of reactant in solution due to the binding reaction between bivalent sites beginning after saturation of monovalent sites.²³⁸ Mass transport or diffusion-limited effects are also mentioned as a source of deviation.²³⁸ In such situations the assumption of constant concentrations of the reactant in solution is not valid anymore and the binding kinetics shows different behaviour. Also, the binding reaction limited by diffusion can be considered as two phenomena taking place simultaneously.²³⁹ The masking problem of binding sites is another reason for deviation due to the immobilization of excess amount of antigens on the surface additional to actually involved in the binding reaction. This problem also could be seen in binding a large molecule of antibody to immobilized antigen that may lead to masking of the adjacent binding sites.²³⁸ The other sources of deviations could be: non-specific binding, steric effects, and other binding process such as conformational changes.^{235, 254}

The binding reaction in homogenous format assay with QD565 labelled antibodies presented in this thesis was accompanied by aggregation that affected the

binding kinetics as observed in the results. The results of two different concentrations of QD565 conjugated antibodies showed the same kinetic curve trend that was not affected by the concentration of QDs labelled antibodies in the solution significantly. The formation of aggregates in solution with larger sizes and hydrodynamic radii compared to initial antigens and antibodies molecules influences the kinetic mechanism by decreasing the diffusion coefficients of the aggregated particles. The results should be a mixture of biomolecules with different sizes, diffusion coefficients and rates of diffusion toward the immobilized antibodies at the surface. The overall rate of association reaction is determined by the slowest rate reaction. Also the steric hindrance due to aggregation and binding of larger molecules to the surface decreased the observed intensity and therefore the concentration of bound antibodies which may be the reason that the homogenous format assays showed less reactivity and reached the steady state sooner than for the heterogeneous format (Figure 4-14). It is probably due to the saturation through steric hindrance at the surface in the homogeneous format. In order to estimate the kinetics parameters of this format properly, modelling and quantification of the aggregate formation such as the size and number of molecules in aggregates are required. Since the main part of the reaction between antigen and labelled antibody takes place in the solution where it could not be detected by CLSM, utilization of other techniques enabling the investigation of aggregate behaviour in solution leads to better understanding of the whole process of binding. The kinetics of QDs conjugated to polyclonal antibodies through the streptavidin-biotin reaction with specific antigens in solution has been investigated by flow cytometric analysis to characterize aggregation formation in detail.²⁵⁵ The results showed a sigmoid kinetic curve with three different phases for the aggregation process: a slow initial rate, a rapid phase and the equilibrium aggregate stage which

has been mentioned as a normal kinetic behaviour for most self-assembly processes. Integration of flow cytometry or any light scattering techniques with CLSM to investigate the kinetics of QD-conjugated antibody aggregation in solution may improve the theoretical and experimental understanding of these nanoparticles interaction mechanisms.

Chapter 5

Z-axis multiplexing immunosorbent assays with CLSM

In this chapter, the novel idea of detection of more than one immunoassay along the z-axis with CLSM is studied theoretically and experimentally. The idea arose from the unique optical sectioning ability of CLSM. By replacing standard substrates with multiple 30 μm layers of glass or mica, a high density array of immunosorbent assays is created within a stratified medium. Stacks of up to 5 modified thin mica substrates of model immunoassays were analysed with CLSM. The results showed a decrease in fluorescent intensity with increasing number of substrate layers and a concomitant broadening of the axial resolution. Z-axis multiplexing of planar format immunosorbent assays using CLSM readout was demonstrated by detection of two model assays consisting of human and mouse IgGs on different mica layers.

5.1 Introduction

Detection of fluorescent immunosorbent assays (FLISA) by confocal laser scanning microscopy (CLSM) for planar format assays has been presented in chapter 4. Confocal FLISA can detect a thin layer of fluorescently bound material arising from antigen binding in the presence of an unbound fluorescent overlayer. In this chapter, detection of more than one FLISA along the z-axis is demonstrated. To prepare a layered structure, standard thickness (170 μm) substrates should be replaced by thin substrates due to the maximum depth of imaging of the used CLSM which is about 170 μm . Thinner substrates could provide more layered structure. Mica and glass with approximately 30 μm thick could be suitable substrates to create a multilayer structure for the aim of this chapter. Such layered structure can be studied as a stratified medium consisting of alternating layers (substrate and gap) of different indices of refraction. To the best of my knowledge, similar immunoassays arrayed along the z-axis of an optical system have not been reported previously.

5.1.1 Volume measurements in CLSM

In thick specimens, performance of CLSM is degraded by aberrations caused by the refractive index mismatch between the immersion medium of the objective lens and the specimen. As the focus depth in the mismatched medium increases, the axial response of the CLSM degrades and the intensity decreases. In addition, a focal anomaly caused by the refractive index change generates a discrepancy between real and optical distance.^{256,257} The effect of refractive index mismatch on volume measurements in confocal microscopy created by the immersion medium and the object's embedding has been studied extensively in the literature.^{56, 256-259} The induced aberration has been analysed for objectives designed for different immersion fluids.^{56,}

^{260, 261} Measurement of the thickness of transparent plates, films and coatings has been done with optical methods such as low-coherence interferometry²⁶²⁻²⁶⁴ and confocal microscopy^{257, 265}. An optical method based on a reflection dual-confocal fiber-optic sensor was used for absolute measurement of refractive index and thickness of a glass microscopic plate.²⁶⁶ Also optical methods based on combining confocal microscopy and low-coherence interferometry have been used to measure the thickness and refractive indices of multilayered structures.^{267, 268}

5.1.2 Confocal detection of stratified media

Theoretical treatment of standard confocal imaging of well-defined stratified media has been limited with few follow-on experimental studies, particularly in the case of fluorescence. In an earlier study, confocal reflection microscopy of a simplified object consisting of different thicknesses of SiO₂ thin films on Si substrates was investigated and the thickness measured with 0.80 and 0.95 NA air objectives.²⁶⁹ The authors proposed a theory for imaging a stratified medium in which the refractive index varied continuously with depth but experimental results were presented for only a single layer.

Rajadhyaksha *et al.* reported using a video-rate CLSM for imaging human skin *in-vivo* and showed that thin sections of human skin can be visualized without biopsy and histological process.^{270, 271} The immersion medium and three layers of human skin was modelled as plane parallel layers with different refractive indices to determine the axial shift in objective focal plane. The optimum range of parameters for CLSM to improve the resolution and increase the field of view and depth of imaging in human skin were determined.

5.1.3 Multiplexing assays

Detection of multiple biomarkers is important in genomics, proteomics, disease detection and epidemiological and environmental studies.^{272, 273} The ability to screen multiple analytes in a single assay offers many advantages: multiplexed assays are simple, rapid, cost effective, less prone to sampling and detection errors and more economical on reagents and time.²⁷⁴ Generally, there are three main methods of multiplexed assays: mass spectrometry,^{275, 276} nucleic acid amplification assays such as polymerase chain reaction (PCR) and real-time PCR (RT-PCR),²⁷⁷ and immuno and affinity assays. These are further subdivided into fixed and mobile support assays.²⁷² In fixed support assays, the probes are arrayed in x and y over a surface²⁷⁸ or microwell²⁷⁹. Mobile support assays consist of probes moving freely in solution or attached to microspheres.^{280, 281} Existing fixed support multiplexed assays have been constructed in arrays within a single plane.

5.1.4 Mica as substrate

Glass and plastic surfaces are common fixed supports for immunoassays. Arrayed substrates (glass, polystyrene, mica, etc.) having refractive indices and overall thickness close to that of a standard coverslip (n_D 1.515 and 170 μm) may be stacked to create a z-axis array that may be read using optical sectioning. Glass is commonly used for optical microscopy, with applications of mica in this context comparatively rare. However, mica has been used extensively as a substrate for imaging, probing and quantifying proteins and DNA adsorption at solid-liquid interfaces with atomic force microscopy (AFM) due to its atomic-scale flatness. The surface chemistry of mica allows it to bind to DNA strongly.²⁸²⁻²⁸⁵ Binding of proteins is less effective on bare mica,²⁸⁶ however, mica can be modified with aminosilanes such as (3-Aminopropyl)-

triethoxysilane (APTES) to become more hydrophobic and to present amino groups on the surface. Such modified mica surfaces provide good substrates for protein immobilization, patterning, and immunoassay.^{287, 288}

5.2 Theory

A limitation of CLSM is the degradation occurring when focusing into a medium with a different refractive index than that specified by the design conditions of the objective lens. Such a refractive index mismatch generates focal anomalies and blur. The focal anomaly resulting from a single refractive index change has been described with emphasis on the case of light moving from a high refractive index medium into one of lower refractive index.^{256, 258, 289} This condition is often encountered when observing biological specimens with oil objectives. In this case, objects appear stretched along the z-axis. Similarly, objects appear compressed when moving from low to high refractive index media (Figure. 5-1). This latter situation is encountered when an air objective is used to measure the thickness of a glass or mica substrate based on thin fluorescent layers on the top and bottom surfaces. Understanding the optical behaviour of layered structures is important for designing assays arrayed along the z-axis and assessing the practical limitations of measurements made on stacked substrates.

5.2.1 Measuring the thickness of a single substrate with CLSM

Given a cone of light having radius x_1 , at an incident angle θ_1 , with respect to an interface between a low refractive index medium n_1 , and a high refractive index medium n_2 , the angle of refraction θ_2 , may be calculated using Snell's law (Figure 5-1):

$$n_1 \sin \theta_1 = n_2 \sin \theta_2. \quad (5-1)$$

Given a high refractive index medium of thickness (t), the displacement (Δz), along z sufficient to move the focus of the cone of light from the front to the back surface can be computed:

$$x_1 = t \tan \theta_2, \quad (5-2)$$

and

$$\Delta z = \frac{x_1}{\tan \theta_1}. \quad (5-3)$$

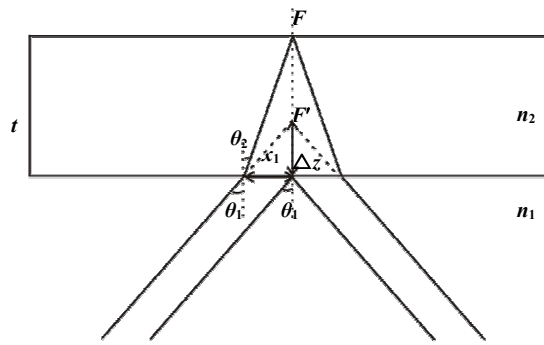


Figure 5-1: Ray traces for light focusing on the front (ray 1) and rear (ray 2) surface of a substrate assuming ($n_1 < n_2$). For a specific ray, the radius of the cone of light, x_1 , at the interface together with n_1 , n_2 , θ_1 and θ_2 determine the focal point, F , of the rays. This position differs from the nominal focus, F' , expected from a given displacement Δz , of the microscope stage. The focal anomaly is the difference $t - \Delta z$. If $n_1 = n_2$, the light rays follow a straight trajectory (dashed line) and $F = F'$.

The difference $t - \Delta z$ is the focal anomaly. The displacement (Δz) may be expressed in terms of numerical aperture ($NA = n_1 \sin \theta_1$).

$$\Delta z = t \frac{\tan \theta_2}{\tan \theta_1} = t \frac{n_1 \cos \theta_1}{n_2 \cos \theta_2} = t \sqrt{\frac{n_1^2 - NA^2}{n_2^2 - NA^2}}. \quad (5-4)$$

It should be noted that equation 4 is a high angle approximation which is closest to the position of minimum spot size and that a distribution of angles will be encountered from a real lens, an effect giving rise to aberrations and reduced resolution.

For an air objective ($n_1 \sim 1$), the confocal stage displacement required to focus on the back of the substrate simplifies to:

$$\Delta z = t \sqrt{\frac{1 - NA^2}{n_2^2 - NA^2}}. \quad (5-5)$$

5.2.2 Measuring z-position within a stack of substrates

A specimen consisting of a stack of two or more of the same substrates with variable thickness separated by fluid layers of variable thickness presents a more complex optical problem (Figure 5-2). For simplicity, just the front side of each layer is labelled. The refractive index n_3 , of a fluid layer such as distilled water or phosphate buffered saline (PBS) generates a third angle of refraction, θ_3 . For a stack of two substrates, consider a displacement, Δz_1 , along z such that the light focuses onto the second layer in a stack of substrates. Such a cone of light (cone 2 in Figure 5-2) has a radius of $x_1 + x_2$. The light is refracted twice along its path at angles θ_2 and θ_3 .

$$\Delta z_1 = \frac{x_1 + x_2}{\tan \theta_1} = \frac{t_1 \cdot \tan \theta_2 + d_1 \cdot \tan \theta_3}{\tan \theta_1} = \sqrt{n_1^2 - NA^2} \left[\frac{t_1}{\sqrt{n_2^2 - NA^2}} + \frac{d_1}{\sqrt{n_3^2 - NA^2}} \right]. \quad (5-6)$$

For a stack of three substrate layers, the light ray is refracted four times on the way to focus onto the front surface of the third layer in which the third and fourth refraction angles are the same as θ_2 and θ_3 as the refractive indices are the same as n_2 and n_3 (light ray number 3). The stage displacement, Δz_2 , required to place the focus onto the front surface of the third substrate is given by:

$$\begin{aligned} \Delta z_2 &= \frac{x_1 + x_2 + x_3 + x_4}{\tan \theta_1} = \frac{(t_1 + t_2) \tan \theta_2 + (d_1 + d_2) \tan \theta_3}{\tan \theta_1}, \\ \Delta z_2 &= \sqrt{n_1^2 - NA^2} \left[\frac{t_1 + t_2}{\sqrt{n_2^2 - NA^2}} + \frac{d_1 + d_2}{\sqrt{n_3^2 - NA^2}} \right]. \end{aligned} \quad (5-7)$$

For a stack of m layers of a substrate with refractive index n_2 and thickness t_m having gap thicknesses d_{m-1} , the axial displacement required to position the focus onto the front surface of the m^{th} layer is:

$$\Delta z_{m-1} = \frac{x_1 + x_2 + \dots + x_{2(m-1)}}{\tan \theta_1} = \frac{(t_1 + t_2 + \dots + t_{m-1})(\tan \theta_2) + (d_1 + d_2 + \dots + d_{m-1}) \tan \theta_3}{\tan \theta_1},$$

$$\Delta z_{m-1} = \sqrt{n_1^2 - NA^2} \left[\frac{\sum_{m=2}^m t_{(m-1)}}{\sqrt{n_2^2 - NA^2}} + \frac{\sum_{m=2}^m d_{(m-1)}}{\sqrt{n_3^2 - NA^2}} \right] \quad (5-8)$$

where m is the number of substrate layers, θ_1 , θ_2 , and θ_3 are the incident and refracted angles shown in Figure. 5-2, n_1 is the refractive index of the objective medium, n_2 is the refractive index of the substrate and n_3 is the refractive index of the gap filler.

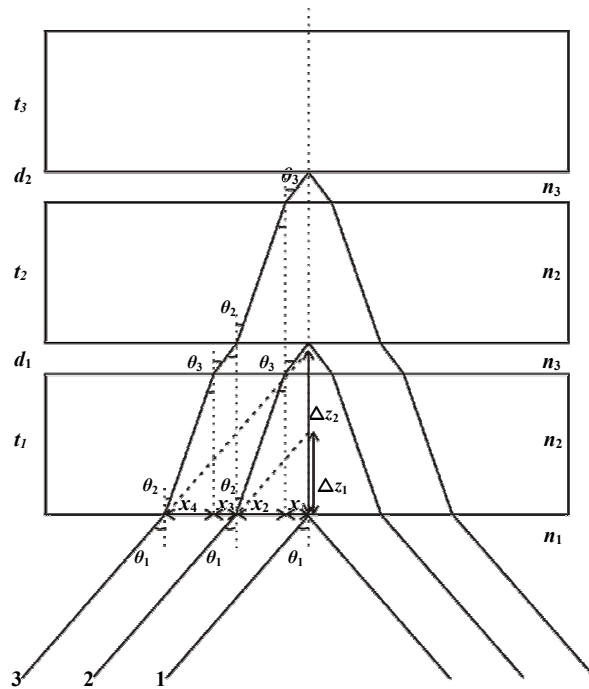


Figure 5-2: Rays traces for light interacting with a layered system consisting of uniform substrates separated by a variable fluid layer assuming $n_1 < n_3$ and $n_3 < n_2$. Light focusing on the front surfaces of the first (ray 1), second (ray 2), and third (ray 3) substrates all are incident on the system at the same angle, however, the cones they represent have variable radii (0, x_1 , and x_2). The confocal stage displacements, Δz_1 and Δz_2 , are those required to focus on the front surface of the second and third layer. For simplicity, only the front surfaces of the substrate are considered.

5.3 Materials and Methods

5.3.1 Instrumentation

A confocal scanner head (TCS NT; Leica Microsystems, Wetzlar GmbH, Germany) installed on an inverted microscope (DMIRBE, Leica Microsystems Wetzlar GmbH, Germany) was used for the optical sectioning of the immunoassay. The 488 nm argon ion laser line was used for excitation and the fluorescence detected using a 530/30 nm bandpass filter. For quantum dots 565, the 476 and 488 nm lines of the argon laser were used for excitation and the emission intensity detected using LP550 nm filter. All CLSM measurements were made with an 63×NA 0.7 air objective (Leica Microsystems, Wetzlar GmbH, Germany).

5.3.2 Reagents

Human IgG, goat anti-human IgG (γ -chain specific) (Lot no. 095k6026), goat anti-human IgG (γ -chain specific) FITC conjugate (Lot no. 086H8822), mouse IgG, anti-mouse IgG, anti-mouse IgG-FITC, casein (Batch no. 037K0202), phosphate buffered saline pH7.4 (PBS) (Lot no. 069K8204), 3-aminopropyltriethoxy silane (APTES), were purchased from Sigma-Aldrich Company Ltd (Dorset, UK). Qdot® 565 ITK™ carboxyl quantum dots (Lot no. 705132) and Qdot® 565 goat F(ab')₂ anti-human IgG conjugate (H+L) was purchased from Invitrogen (Paisley UK).

5.3.3 Substrates

Muscovite mica (Shree GR Exports Private Limited, India) has structural formula $\text{KAl}_2(\text{AlSi}_3\text{O}_{10})(\text{OH})_2$, with about 30 μm thickness and refractive index of 1.58. Muscovite mica is a flat and transparent substrate. It is a biaxial birefringent material and the refractive index has three eigenvalues as $\alpha = 1.552$ -1.576 $\beta = 1.582$ -1.615 and

$\gamma = 1.587-1.618$.²⁹⁰ Glass substrate, D263 T borosilicate thin glass (Prazisions Glas & Optik GmbH, Iserlohn, Germany) with thickness of 30 μm was cut to $1 \times 1 \text{cm}^2$ pieces with CO_2 laser before use.

5.3.4 Modification of substrates

Mica and glass substrates were cleaned with sulfuric acid and functionalized by immersing in a solution of 2% 3-APTES in dry acetone for 30 min at room temperature. After washing with dry acetone and distilled water, the substrates were dried in an oven for 1 hour. Modified substrates were always prepared just before carrying out the experiment. The modification of mica substrate is shown in Figure 5-3. The reaction involves the covalent binding of APTES to hydroxyl groups on the mica surface.

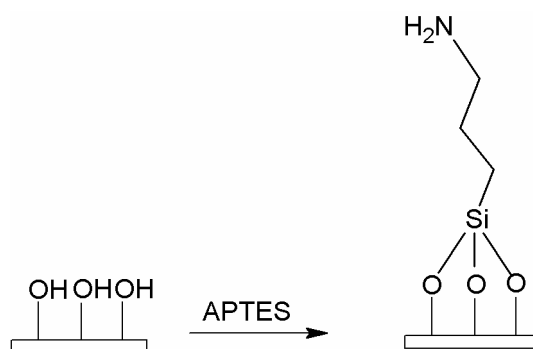


Figure 5-3: Mica modification with APTES.²⁸⁶

5.3.5 Labelling with carboxyl terminated quantum dots

Carboxyl terminated quantum dots were coated onto both sides of $1 \times 1 \text{cm}^2$ sections of modified substrates by immersion in a solution of quantum dots (80 nM) in a small glass vial for one hour. The substrates were then rinsed with distilled water and dried by air. For coating of one side of a substrate, 20 μl of quantum dot solution was placed in the middle of a $1 \times 1 \text{cm}^2$ substrate and was spread with a pipette tip. After drying, the substrate was rinsed with distilled water and dried by air. Stacks of two,

three, and four mica layers were prepared with distilled water filling the gap between layers.

5.3.6 Preparation of sandwich immunoassay on mica

Model immunoassays using human and mouse IgGs were prepared by incubating anti-human (or mouse) IgG overnight on a $1 \times 1 \text{ cm}^2$ modified mica substrate at 4°C . The remaining sites for protein binding were blocked with a solution of 1% casein (1% casein in PBS) for 2 hours at room temperature. After washing with PBS, human (or mouse) IgG was added as antigen and incubated for 2 hours at room temperature. After washing with PBS, anti-human (or mouse) IgG-FITC was dropped onto the surface as the secondary labelled antibody and incubated for 2 hours at room temperature. After washing the secondary antibody and drying by air, the mica was fixed to a microscope slide with nail polish and scanned with CLSM. CLSM data were presented as the sum of the intensity of each image in the stack plotted against z-axis position.

5.4 Results

5.4.1 Modification of substrates

The substrate modification procedure produces covalently linked amine groups from APTES on the surface. After being exposed to water solution, the surface of mica becomes positively charged and thus protein molecules with negative charges such as glutamate and aspartate residues bind via ionic interaction.²⁹¹ Glass and mica were modified with APTES and exposed to carboxyl functionalized quantum dots for 2

hours at room temperature. Attachment was evaluated based on the intensity of the signal after washing the quantum dots on modified and non-modified mica (Figure 5-4). The quantum dots adsorbed to the untreated mica but most were removed from surface after washing (data not shown). The modified mica surface exhibited greater attachment indicating stronger binding of carboxyl groups on the quantum dots to amino groups on the modified surfaces.

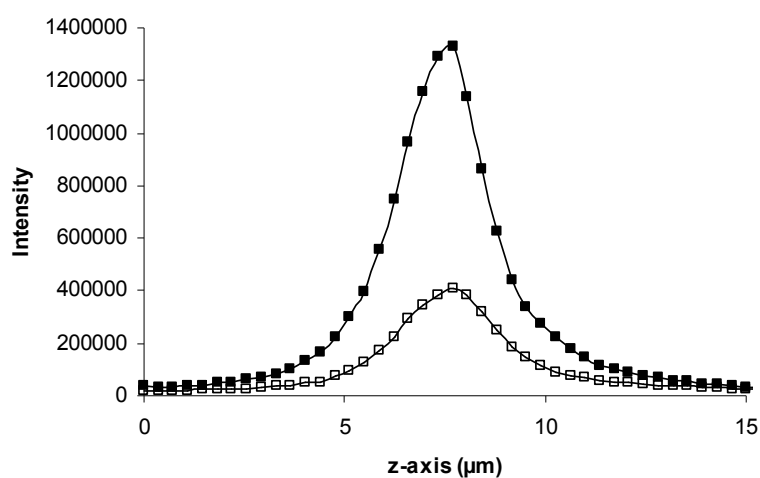


Figure 5-4: The axial response of modified (■) and non-modified (□) mica labelled with QDs.

5.4.2 Measurement of substrate thickness and refractive index

5.4.2.1 One layer of substrate:

The confocal response of mica and glass substrates coated with quantum dots exhibited two peaks (Figure 5-5). Axial scaling factors computed via equation 5 for mica and glass (0.504 and 0.529, respectively) were applied to the data to obtain the geometrical thickness. The results obtained from CLSM listed in Table 5-1.

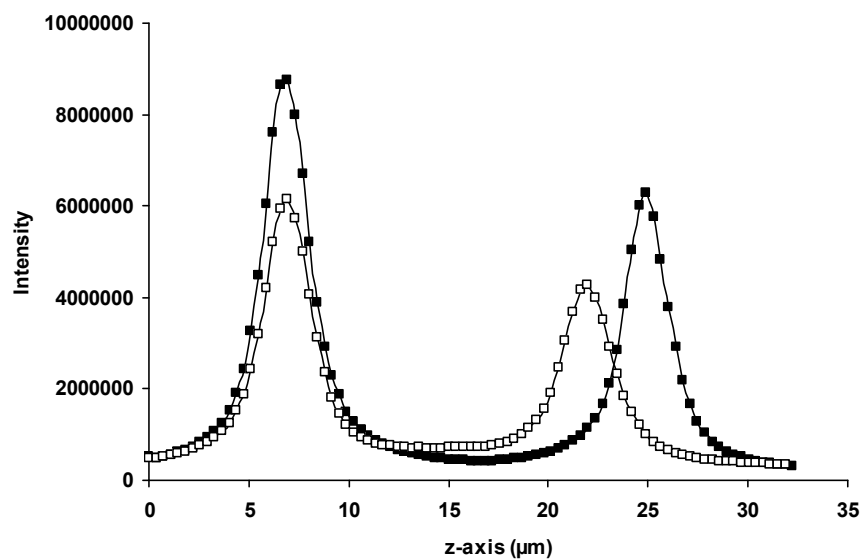


Figure 5-5: Axial response of substrates labelled on both sides with carboxyl quantum dots on glass (■) and mica (□).

Table 5-1: Measurement the thickness of glass and mica substrates with CLSM.

Method	Glass thickness (μm)	Mica thickness (μm)
Manufacturer's data	30	30
CLSM	$32.7 \pm 0.9^*$	30.4 ± 0.6

* Standard deviation of $n=3$

5.4.2.2 Stack of the substrates

One side of the glass and mica substrates were modified and coated with quantum dots. Each mica layer thickness was measured with a micrometer separately. Stacks of two, three and four mica layers separated by distilled water were prepared and scanned with CLSM. A stack of two glass substrates was prepared and measured; however, the thickness of each individual glass layer could not be measured with a micrometer without breaking it. The axial response from a stack of up to four mica layers could be measured by CLSM (Figure 5-6). There is a marked decline in intensity and broadening in width in the deeper layers. This was ascribed to

aberrations arising in the layered structure. However, within each layer the measured intensities were comparable. The equation 5-8 was used to calculate the gaps based on measurements with a micrometer. The measurements of the thickness of each layer and the gap between made with a micrometer and CLSM are listed in Table 5-2.

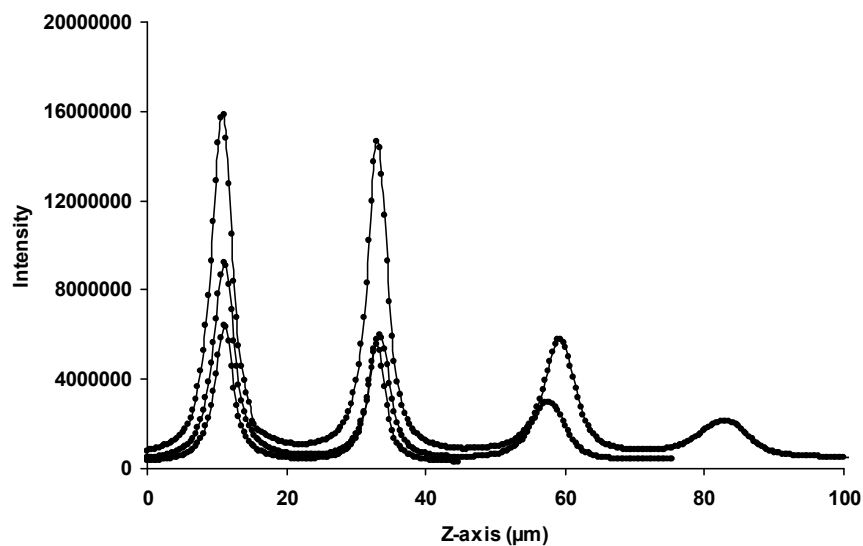


Figure 5-6: Axial response of the stack of two, three and four mica layers labelled with carboxyl quantum dots by CLSM.

Table 5-2. Measurements of layered of mica and glass substrates with micrometer and CLSM.

Method No. of stack	Micrometer (μm)	CLSM [‡] (μm)
2 mica	$t_2^* = 31 \pm 1^{\dagger}$ $t_1 = 32$	$d_1 = 9$
3 mica	$t_3 = 31$ $t_2 = 32$ $t_1 = 30$	$d_1 = 11$ $d_2 = 12$
4 mica	$t_4 = 31$ $t_3 = 32$ $t_2 = 30$ $t_1 = 30$	$d_1 = 12$ $d_2 = 18$ $d_3 = 11$
2 glass	No data	$d_1 = 13$

*: Ordering of layers is based on the Figure 5-2. Closest layer to the objective is called t_1 and so on.

†: The resolution of the micrometer was $\pm 1\mu\text{m}$

‡: d_1 , d_2 and d_3 are derived quantities based on the thickness of the mica measured by a micrometer, the total distance between fluorescently labelled front surfaces, and equation 5-8.

5.4.3 Immunoassays on mica

Modified mica substrates ($1\times 1\text{cm}^2$) were used to conduct immunoassays based on human and mouse IgGs. The sandwich immunoassay protocol was performed on a mica surface in a heterogeneous format including final wash step after incubation with the fluorescently labelled antibody. Binding of IgG molecules to modified mica was strong enough to sustain several wash steps with buffer.²⁹²

5.4.3.1 Dose response of IgG immunoassay on mica layers

A range of antigen concentrations from 0 to 10 $\mu\text{g/ml}$ of human IgG with fixed amount of first antibody (20 $\mu\text{g/ml}$) and secondary antibody conjugated to FITC (20 $\mu\text{g/ml}$) were prepared on mica layers. The mica was fixed on a glass microscope slide with nail polish and scanned with CLSM. Then a bare mica substrate (without immunoassay) was put on each mica substrate containing immunoassay and scanned with CLSM to study the effect of deeper z-axis on the intensity of the immunoassay. A dose response curve obtained from the human IgG sandwich immunoassay on one and two mica layers (Figure 5-7) fit well to Langmuir isotherm equation (section 3.3.5.3). The measurements made through successive mica layers gave decreased intensity consistent with previously calculated z-axis responses with change in nominal focal position.²⁵⁷ The Langmuir parameters of the dose-response curve was observed to be constant with the exception of the maximum intensity (e.g. the binding parameters were unchanged).

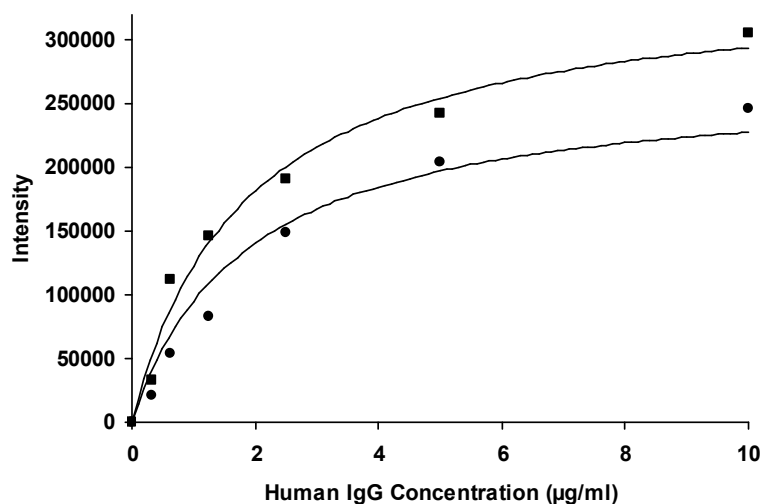


Figure 5-7: Dose response curve of human IgG on the first (■) and second (●) layers of a stacked mica system.

5.4.3.2 Sandwich immunoassays on multilayer of mica

Five modified mica substrates with sandwich human IgG immunoassay on each were prepared. To avoid photobleaching of fluorescent intensity during scanning of multilayer of substrates, QD-conjugated secondary antibody was used instead of FITC. The same concentration of first antibody (20 µg/ml), antigen (1 µg/ml) and QDs conjugated secondary antibody (50 nM) was used for all substrates. After conducting the immunoassays, the mica substrates were washed, dried and fixed on a microscope slide. Stacks of two, three, four and five mica layers were prepared and scanned with CLSM. The results showed the possibility of detecting up to five immunoassays. Although the fifth layer showed the lowest intensity and broadest peak width compared to the other layers it is still distinguishable from baseline (Figure 5-8).

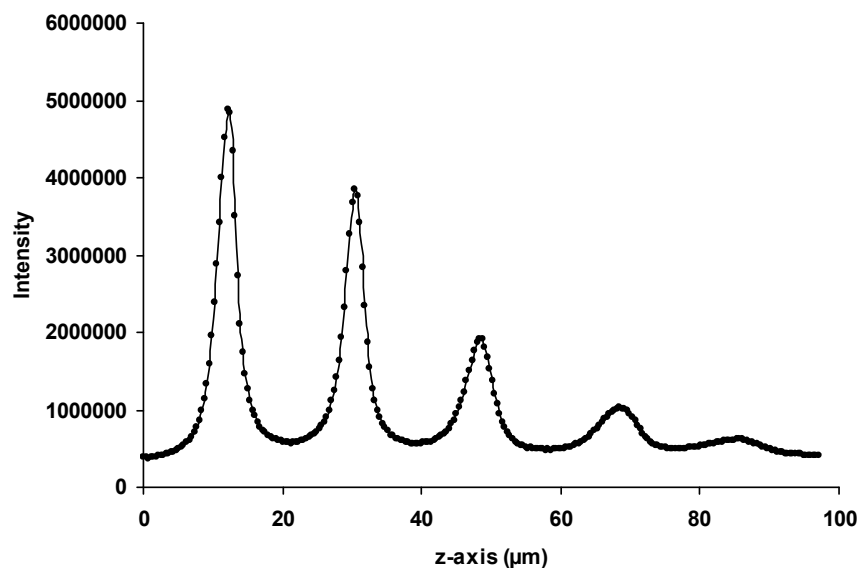


Figure 5-8: Axial response of the stack of five mica layers containing human IgG immunoassays by CLSM.

5.4.3.3 Multiplexed sandwich immunoassays on mica layers

To demonstrate the multiplexing ability of the method, two model assays using different IgGs were prepared. The human and mouse IgGs were prepared and the dose response curve for each was obtained separately over the range from 0 to 10 $\mu\text{g/ml}$ of antigen (mouse and human IgG). Then the stack of two mica substrates containing mouse IgG assay (10 $\mu\text{g/ml}$) in the bottom and human IgG (10 $\mu\text{g/ml}$) on the top was assembled, fixed on a microscope slide with nail polish, and scanned with CLSM. The axial response (Figure 5-9) gave a clear fluorescent signal from each layer in the axially arrayed model immunoassay. The peak of the human IgG assay was lower and the profile broader compared to the mouse IgG assay due to its z-position. Quantitative results were obtained from both layers.

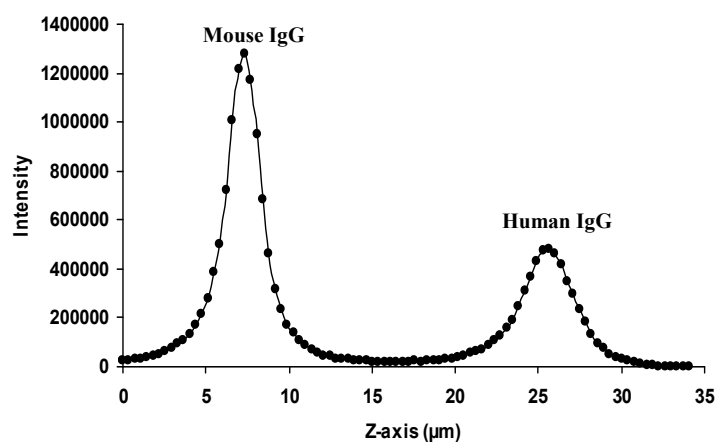


Figure 5-9: Multiplexed confocal immunosorbent assays arrayed along the z-axis. Axial response of the stack of two mica layers containing human and mouse IgG with CLSM. The first and second peaks correspond to assays detected with mouse IgG and human IgG, respectively.

5.5 Discussion and Conclusion

This first demonstration of a confocal readout of a multiplexed assay arrayed along the z-axis highlights the advantage of confocal detection of immunosorbent assay versus conventional immunoassay detection methods. Optically sectioned readout of assays allows the detection of more than one signal along the z-axis. This method potentially increases the analysis speed and array intensity compared to single layer assay. Conventional multiplexed assay methods are typically arrayed in the xy -plane based on position or color.²⁷⁴ The current study indicates that the assay density can be increased by at least a factor of five by arraying along the z-axis. Improved substrate materials and optics should minimize the refractive index mismatches, and yield further improvement. The proposed detection method would find application in screening of analytes when the presence or absence of a wide range of biomarkers, is required. There is a patent regarding to the methods for fabrication, and screening of

combinatorial libraries of materials arranged as 3D arrays by deposition a variety of samples onto at least one substrate in which each sample is characterized by its 3D coordinate (x,y,z) .²⁹³ The experimental part of this patent consists of the confocal laser scanning of arrays of fluorescent polymer materials in the form of thin coatings on a cylinder dielectric waveguide demonstrating 3D arrays probed at different spatial depths (lower, upper and side surfaces of the cylinder). There is no research paper about the content of this patent in the literature.

Mica has been widely used as a solid surface for studying protein and DNA adsorption processes at solid/liquid surfaces by AFM.^{284, 288, 294} Using mica as a solid surface for an immunoassay was reported for investigation of antigen-antibody binding with AFM²⁹⁵ and studying the modification of mica by conducting immunoassays with microcontact printing techniques.²⁸⁸ A competitive immunoassay was used in these papers; however, in this report the use of mica in sandwich assays was demonstrated which are generally more sensitive and specific than competitive ones.¹⁰⁵ It is also the first report of the antigen dependent dose response curve on mica demonstrating that it is a suitable solid surface for immunoassay. The results demonstrated that it is possible to use both sides of a substrate; however, this remains to be implemented. They also show the feasibility of non-conventional solid surface material in immunoassay detection methods. Further work on substrate materials other than mica or glass such as thin plastic films and polydimethylsiloxane (PDMS) may yield more suitable synthetic material.

To the best of my knowledge, this is the first report of assays arrayed along the z-axis of an optical system: the most extensive study of fluorescence in stratified media, and the most comprehensive treatment of axial distance in layered systems to date. The work of Sheppard *et al.* who studied the imaging of the stratified film

structures of SiO₂ by confocal microscopy is notable; however, this was limited to presentation of theory.²⁶⁹ Previous studies on confocal imaging of thick biological specimens showed that point spread function (PSF) tends to be broader, more asymmetric and the axial resolution gets worse with increasing the focal depth in a mismatch medium.²⁵⁹ As shown previously the two main effects of mismatching refractive indices between the immersion medium and sample are focal anomaly and intensity fall-off.²⁹⁶ Similar behaviour was seen in the results of this chapter with the intensity of the axial response showing depth-dependent attenuation. Spatial distortion and blurring in deep layers within a stack arise from aberration leading to intensity attenuation. Partial correction could be done by adaptive aberration correction and minimization of the refractive index mismatches by careful selection of materials. This attenuation can be overcome by calibration of the intensity response as demonstrated with human IgG immunoassays.

The presented stratified assay could also be studied with two photon excitation microscopy and other optical sectioning method. Some advantages may be obtained from the lack of pinholes and the improved depth of penetration.⁶⁰ A study on theoretical PSF calculation through a stratified medium showed that in deeper focus (100 μm below the cover glass) the illumination PSF is less blurred in two photon microscopy compared to confocal.²⁹⁷

Chapter 6

3D z-axis multiplexing immunosorbent assay with CLSM

This chapter demonstrates an extension of the confocal immunosorbent assay into two dimensional and three dimensional formats. The microcontact printing method was chosen to print antigens on modified mica substrates to carry out indirect immunoassays with QD-conjugated antibodies. Stacked layers of mica with patterned immunoassays were scanned with CLSM and 3D image was produced. By fabricating arrays of multiprotein immunoassays on mica substrates and analysing them by CLSM, the capacity of simultaneous immunoassay detection was increased.

6.1 Introduction

This chapter focuses on microcontact printing (μ CP) as a microfabrication technique for patterning proteins on surfaces. At first, a brief description of microfabrication techniques in general and soft lithography specifically is presented. Then μ CP as a soft lithographic technique for printing on different surfaces is discussed in the context of protein patterning. The main theory supporting the work in this chapter was presented in chapter 5. The main prospective goal of this chapter is a feasibility study expanding the spatial density of immunoassays by detection in three dimensions by integration of μ CP and z-axis scanning by CLSM. QD-conjugated antibodies were used to detect antigens in all experiments in this chapter due to their unique photostability allowing them to maintain brightness during the long term measurements. A review of the literature produced no record of 3D detection of immunoassay.

6.1.1 Microfabrication technology

Microfabrication is a process used to create microscopic structures and patterns with micrometer to millimetre range of dimensions. Microfabricated objects or devices consist of a range of miniature structures, such as microelectromechanical systems (MEMS), micromachining, lab-on-a-chip, microsystems, and micro-total analysis systems (micro TAS) which have been developed with several successful commercial and scientific applications.²⁹⁸ In recent years, micro- and nanofabrication have emerged as essential and key techniques for further progress in the fields of physics, chemistry, material science and biology.²⁹⁹ They have made a great impact on biology and medicine due to presenting the ability to design and control experiments at the

micrometer scale which has attracted interest in fundamental studies using this technology.

Microfabrication products offer several advantages compared to conventional macroscopic structures. Miniaturization and creation of small size devices that are portable and can be placed in constrained spaces are the main advantages of microfabrication. Increased surface area to volume ratio in micro-scale size devices lead to remarkable physical enhancements that result in better performance of microfabricated devices. High-throughput devices made of miniaturization such as protein and DNA microarrays have decreased the analysis time and presented the multiplexing ability of genomic and drug discovery research. Reduction of the required volume of sample in microfabricated devices is an attractive advantage leading to the cost effective and extended use of limited amounts of some medical samples. Microfabrication also allows accurate geometrical and spatial control which is hard to do in macroscopic size.²⁹⁸

Micro- and nano-scaled materials can be fabricated by two main strategies: bottom-up and top-down.³⁰⁰ In top-down method, bulk material has been used to create new small structures based on miniaturization. Lithography techniques such as photolithographic and non-photolithographic methods are the most successful techniques in top-down fabrication.³⁰¹ Bottom-up methods create highly organized small structures from smaller functional components. The most important applied bottom-up method is self-assembly of molecules. Creation of self-assembled monolayers (SAMs) by microcontact printing method has opened new ways to fabricate cheap, easily accessible, and multifunctional micro- and nano-scale structures.³⁰²

Microfabrication uses a sequence of processes to fabricate a microstructure. Generally four basic processes are used in microfabrication: patterning, thin-film growth or deposition, etching, and bonding.²⁹⁸ Photolithography is a well-known patterning technique that was initially used to generate patterns in electronic circuits, but has been extended to pattern other materials such as biomolecules. In photolithography, a photomask is used as a master to transfer patterns onto a thin film of photosensitive material (photoresist) upon UV irradiation followed by chemical process.³⁰³ It is a highly developed patterning technique but its major limitations are the high costs, the requirement of clean room facilities and chemical treatments, fabrication of only two-dimensional microstructures, and limitations for patterning on non-polar surfaces and patterning of some chemical functional groups, make this technique inconvenient specifically for biological applications.³⁰³⁻³⁰⁵

6.1.2 Soft lithography

Soft lithography techniques are a set of non-photolithographic microfabrication techniques based on self assembly and molding that use stamps or channels made of an elastomeric material for transferring high quality micro- and nano-scale features. Soft lithography techniques offer several advantages compared to photolithography techniques: cost-effective, procedurally simple, patterning on variety of planar and non-planar surfaces, patterning on solid materials other than photoresists, patterning of surface functional groups, patterning of liquid materials, and 3D microstructure formation.³⁰³

All soft lithography methods share a common characteristic of using a patterned elastomer material such as a poly(dimethylsiloxane) (PDMS) as the form of a stamp or mold. Various soft lithographic techniques based on the way of using stamps or molds have been presented in the literatures in particular by the Whitesides

group at Harvard University. There are: microcontact printing (μCP)³⁰⁶, microfluidic networking (μFN),³⁰⁷ replica molding (REM),³⁰⁸ microtransfer molding (μTM),³⁰⁹ micromolding in capillaries (MIMC),³¹⁰ and solvent-assisted micromolding (SAMIM).³¹¹

6.1.3 Microcontact printing technique

Microcontact printing (μCP) is one of the soft lithographic techniques that have been developed for micro- and nanofabrication. It is an inexpensive and simple method for patterning microstructures and has the advantages of patterning arbitrary and multiple patterns by fabricating proper master structures.³⁰⁰ μCP uses an elastomeric stamp to transfer chemical or biological ink to various substrates by conformal contact to print high resolution patterns without a clean room environment or special chemical treatments.³¹² The elastomeric stamp is made of PDMS which acts as a mold to form a negative replica of a silicon master. The stamp is coated with a given ink and transfers molecules from the patterned region of the stamp to a substrate. This transfer is made by conformal contact between the PDMS stamp and the substrate. For effective transfer, the interaction of the molecules with the substrate should be stronger than with the stamp.³¹² Therefore, the surface chemistries of the stamp and substrate are important in determining transfer efficiency and must be tailored carefully based on the application of μCP . For instance, choosing alkanethiols and alkylsilanes as inks for μCP on gold and glass respectively is due to tight coordination of sulfur atom with gold and covalent binding of alkylsilanes with Si-OH group of glass.³¹² The surface of both stamp and substrate can be modified in order to transfer the ink to the surface of the substrate effectively.

μCP described by the Whitesides group in 1993 was originally used to produce microstructures by self-assembled monolayers (SAMs) of alkanethiolates on

a gold surface.³⁰⁶ Since then, it has been widely used by researchers in different fields to pattern organic solvents,³¹³ metals,³¹⁴ polymers,³¹⁵ DNA,³¹⁶ proteins,³¹⁷ and cells³¹⁸ on different solid surfaces.

Masters are key parts of the μ CP technique and can limit its utility due to the availability of size features on the master. The masters are usually prepared by thin film photolithography of conventional resists to make submicron features. Micromachining,³¹⁹ commercial diffraction gratings, etching in silver films, and assembling polystyrene microspheres on a flat surface are other methods that have been used to make masters with features down to ~ 100 nm.³²⁰ It is hard to pattern features size below 100 nm due to the deformation of elastomeric stamp.³²¹

6.1.3.1 PDMS stamp

The chemical formula for PDMS is $\text{CH}_3[\text{Si}(\text{CH}_3)_2\text{O}]_n\text{Si}(\text{CH}_3)_3$, where n is the number of repeating monomer $[\text{SiO}(\text{CH}_3)_2]$ units. PDMS is a flexible silicone elastomeric polymer that is commonly made from a Sylgard® 184 kit. The kit consists of a base and a curing agent both of which are liquid at room temperature. The two part resin system containing vinyl groups (part 1) and silicon-hydride groups (part 2). The base includes a platinum-based catalyst that cures the elastomer by an organometallic cross-linking reaction. Mixing the two resin components leads to a cross-linked network of dimethyl sioxane groups by the addition of the Si-H bonds of part 2 across the double bonds of part 1 to form Si-CH₂-CH₂-Si linkages (Figure 6-1).³²² The product is a crosslinked polymer with the -Si(CH₃)₂-O- structural unit.

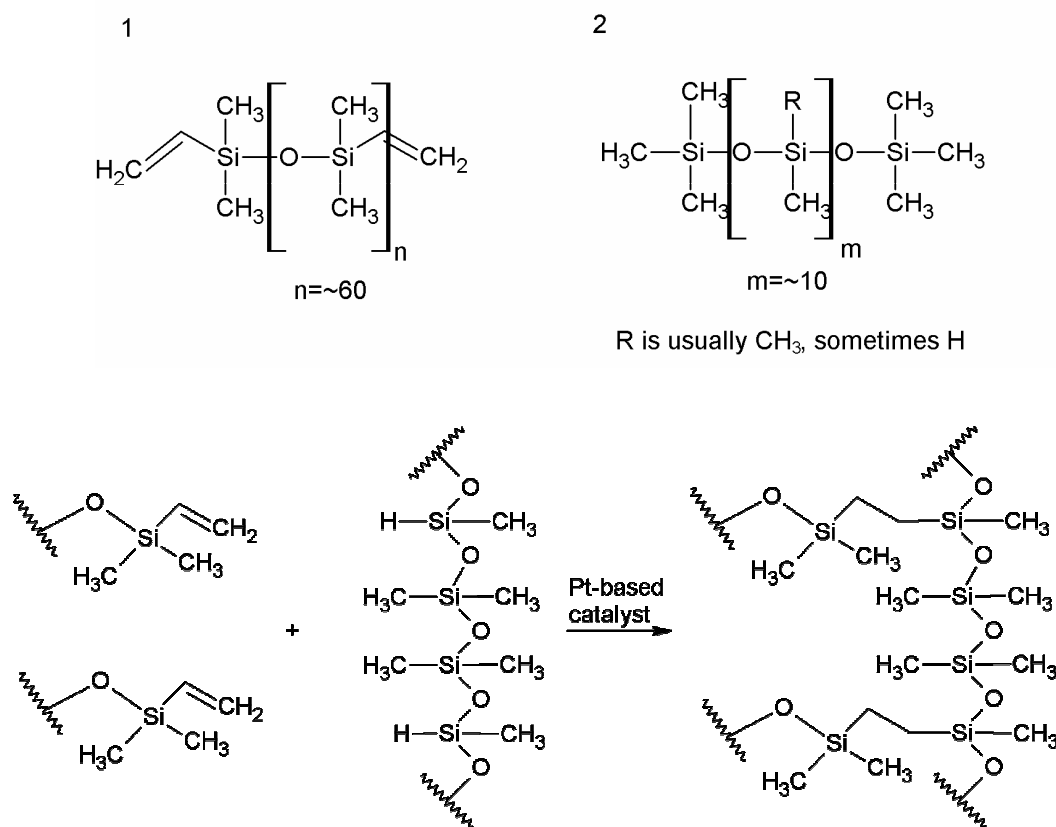


Figure 6-1: PDMS chemical structure before and after crosslinking. Mixing the base (1) and curing agent (2) together leads cross-linked network of dimethyl siloxane groups.³²²

PDMS has several unique advantages making it suitable for μCP and microfluidic devices as well: 1) reproduction of high accuracy micro- and nanometer scale features by replication molding; 2) optically transparent; 3) non-toxic; 4) reversible binding and a range of other materials via Van der Waals and covalent binding after exposure to air plasma; and 5) no damage to the conformal surface due to its elastomeric property.³²³ Its biocompatibility and gas permeability make it well suited to be used in μCP of proteins and cells.³⁰⁴

Transferring molecules from a stamp to a substrate by μCP depends on modification of both surfaces. The PDMS surface is hydrophobic and polar inks cannot wet its surface restricting the use of inorganic and biomolecules. Several

studies have been done to change the hydrophobicity of PDMS stamp by replacing it with new stamp materials or modification of the surface.³⁰⁰ Exposure to reactive oxygen species by oxygen plasma or UV ozone treatments increases the hydrophilicity of the PDMS surface.^{324, 325} Oxidation of the PDMS surface forms a hydrophilic thin silica-like surface layer rich in SiCH₂OH groups and makes it usable with polar inks.³⁰⁰ This layer is usually unstable and loses its hydrophilic character quickly unless the stamp is kept under water.³²⁶ Some methods have been tested to maintain the hydrophilicity of the oxidized stamp surface for longer period of time by chemical attachment of silanes or covalent attachment of polymer layers.³⁰⁰

6.1.3.2 Protein patterning with μ CP

The ability to position proteins, DNA and cells in a specific pattern on a substrate has been an important issue in the development of biosensor technology,³²⁷ microarrays and tissue engineering.³²⁸ Microarray technology is a common method to pattern biomolecules on different surfaces that offers several advantages to proteomic and genomic research. Biochemical reactions in small volumes are not influenced by diffusion-limits and would be more efficient.³²⁹ Assays in microarray formats can be performed quickly in large numbers plus the ability of multiplexed detection. Also less reagents and samples are used which makes this method cost effective. There are several techniques for making micro-scale 2D arrays of proteins and DNA on special surfaces that can be categorized into two main groups of contact printing³³⁰ and non-contact printing³³¹ which is limited based on the surface chemistry available for protein attachments.³³² Contact printing relies on dispensing biomolecule solutions through a set of metallic pins that physically contact the surface. This method has the advantage of exact drop position on the surface, but has the disadvantage of possible damaging of the coated surface by direct contact. In non-contact method such as ink-

jet printing the sample solution is dispensed without direct contact between a print head (such as a piezoelectric head) and a substrate. This method is less invasive than contact printing but lacks the accuracy of drop position. Both contact and non-contact printing methods are expensive and need special equipment.

μ CP has expanded to pattern biomolecules due to low fabrication costs, simplicity and possibility of patterning of different types and concentrations of biomolecules compared to other patterning techniques such as ink-jet printer and lithography.³³³ Two important factors in printing proteins on a surface by μ CP are the efficiency of transfer and maintenance of the structure and biological activity of the proteins during the printing process. Studies have shown that surface modifications that increase the hydrophilicity of the substrate or increase the hydrophobicities of the stamp appeared to improve μ CP.³¹² There are several ways to pattern proteins onto solid surfaces which can be divided into two main groups: indirect and direct methods. In the indirect method, patterned SAMs created by μ CP have been used as templates for selective protein adsorption and cell attachments on various surfaces.^{312, 314} The pattern of hydrophobic alkanethiols generates sites on the surface where proteins can deposit from solution after blocking the unprinted parts.³³⁴ μ CP has been applied successfully to direct patterning of proteins on a variety of surfaces without losing biological activity.^{329,312, 335} The exact mechanism of protein transfer by μ CP is not fully understood. It has been demonstrated that both stamp and substrate wettability is crucial for protein transport.³¹² It was shown in the literature that many proteins (e.g. IgG) easily adsorb to non-modified PDMS surfaces through van der Waals interactions.^{335, 336} The strategies of protein patterning on surfaces relies on: inking of the non-modified stamp with protein solution, incubation, drying the stamp and bringing the stamp into conformal contact with the (modified) substrate (Figure 6-2).

Bernard *et al.* pioneered work on direct transfer of proteins from non-modified PDMS stamps to a target glass surface resulting in patterns with high surface coverage.³¹⁷

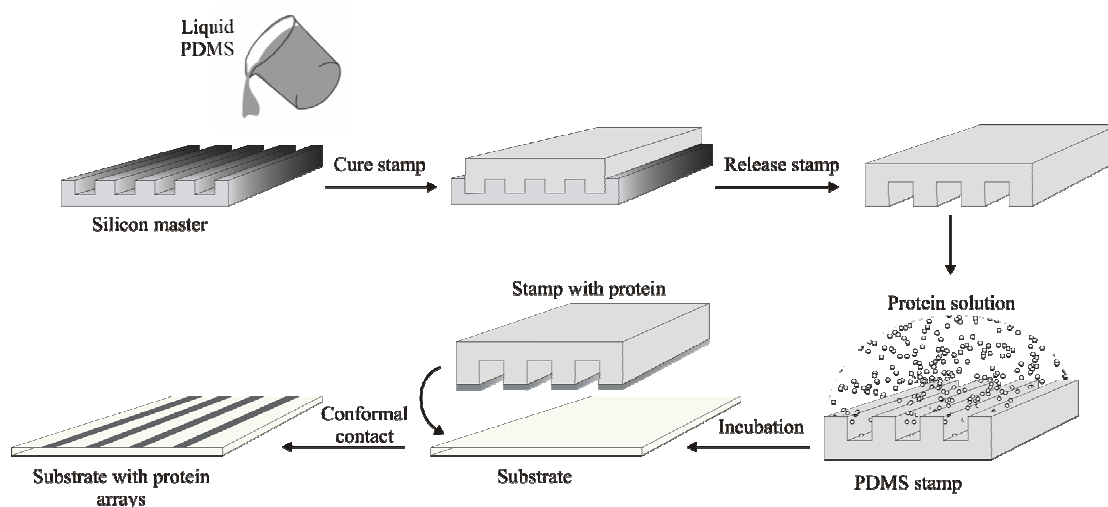


Figure 6-2: Schematic representation of fabrication of a PDMS stamp and its use in μ CP of proteins. The relief pattern of a silicon master is replicated by pouring prepolymer of PDMS and curing it. After releasing the stamp, it is used to transfer the protein solution to a substrate by conformal contact.³¹⁷

6.1.3.3 Multiprotein patterning with μ CP

The range of μ CP applications can be expanded by patterning a single surface with different proteins. In general, there are two methods for printing different proteins on a single substrate using μ CP: (i) sequential inking and printing and (ii) parallel inking of a stamp followed by single printing.³²⁹ In sequential printing, different stamps (stamps with different patterns or different inks) can be printed several times onto a same substrate. The printed patterns have been kept stable due to the fact that the stamp does not pick up proteins that have already been printed. Using this method, arbitrary protein patterns can be easily printed and during each printing step a completely different pattern than the previous printing step can be used.³³³ In the parallel inking, a stamp must be inked with different proteins on different regions. The

stamp is a vehicle for transferring proteins, so planar stamps (without surface relief) can be used. The main technical requirement of this method is fabrication of a stamp inked locally with different proteins. Microfluidic networks (μ NF) has been used to define the area of patterning.^{337, 338} Delmarche and co-workers have demonstrated such multiprotein patterning by sequential printing as well as single step printing methods.³²⁹

6.1.3.2 Substrates for μ CP of proteins

μ CP has been used to generate patterns on different substrates such as glass, silicon, metals, and polymers. Glass slides are the most popular substrates for protein patterning due to several advantages.³³⁹ They are chemically resistant to solvents, having low fluorescent background, optical transparency, and a flat nonporous surface. In addition they are inexpensive and easy to handle. Metals, especially gold, have shown the best properties for functionalization with SAMs patterning.³⁴⁰ The thiol-gold chemistry is well-known and is much easier to control than other surface chemistry. Other metal surfaces such as silver,³⁴¹ titanium,^{342, 343} aluminium and copper,³⁴⁴ have been used for the attachment of biomolecules. Polymers such as PDMS or poly(methyl methacrylate) (PMMA)³⁴⁵ are good candidates for attachment of biologically active molecules. Functionalized PMMA has been used successfully as a substrate for the immobilization of proteins.³⁴⁶

In this study, mica has been used due to the requirement of the thin layer of substrate to show the z-axis ability of CLSM (chapter 5). The structure and properties of mica as a solid surface has been reviewed in detail in chapter 5 as well. In the literature, only one record of using mica as a substrate for μ CP to pattern proteins for immunoassay application has been found.²⁸⁶

6.2 Material and methods

6.2.1 Reagents

Human IgG, casein (Batch no. 037K0202), phosphate buffered saline pH7.4 (PBS) (Lot no. 069K8204), 3-aminopropyltriethoxy silane (APTES), were purchased from Sigma-Aldrich Company Ltd (Dorset, UK). Qdot® 565 ITK™ carboxyl quantum dots (Lot no. 705132), Qdot® 605 goat F(ab')₂ anti-human IgG conjugate (H+L) (Lot no. 691987), Qdot® 655 goat F(ab')₂ anti-human IgG conjugate (H+L) (Lot no. 512135) and Qdot® 565 goat F(ab')₂ anti-mouse IgG conjugate (H+L) (Lot no. 617325) were purchased from Invitrogen (Paisley UK). Sylgard® 184 silicone elastomer kit was purchased from Dow Corning (Dow Corning Limited, UK).

6.2.2 Instrumentation

A confocal scanner head (TCS NT; Leica Microsystems, Wetzlar GmbH, Germany) installed on an inverted microscope (DMIRBE, Leica Microsystems Wetzlar GmbH, Germany) was used for the optical sectioning of the immunoassay. The 488 nm argon ion laser line was used for excitation and the fluorescence detected using a 530/30 nm bandpass filter. For quantum dots 565, the 476 and 488 nm lines of the argon laser were used for excitation and the emission intensity detected using a 550 nm long pass filter. All CLSM measurements were made with an 63×NA 0.7 air objective (Leica Microsystems, Wetzlar GmbH, Germany).

6.2.3 Substrate

Approximately 30 μm thick muscovite mica (Shree GR Exports Private Limited, India) has a structural formula $\text{KA}_2(\text{AlSi}_3\text{O}_{10})(\text{OH})_2$ and a refractive index of 1.58. Muscovite mica is a flat, transparent and biaxial birefringent material.

6.2.4 Preparation of PDMS stamp

Stamps for μ CP were made by using a casting station, polycarbonate stamp holder, and 15x15mm² Teflon coated silicon master chip (GeSiM, Germany) (Figure 6-3). Since the masters were Teflon coated, they were easily able to release the casting PDMS and there was no need to silanize the master surface to prevent sticking. The silicon master chips were fabricated of 525 μ m thick 4" silicon wafer material and patterns were produced by reactive ion etching (RIE) using SF₆-O₂ plasma (GeSiM, Germany). The silicon master chips have been used for this study having these etched features: strips of 5 μ m separated by 5 μ m (5/5 μ m), strips of 10/10 μ m and donuts etched 20/20/10 μ m as shown in Figure 6-4, all 10 μ m deep.

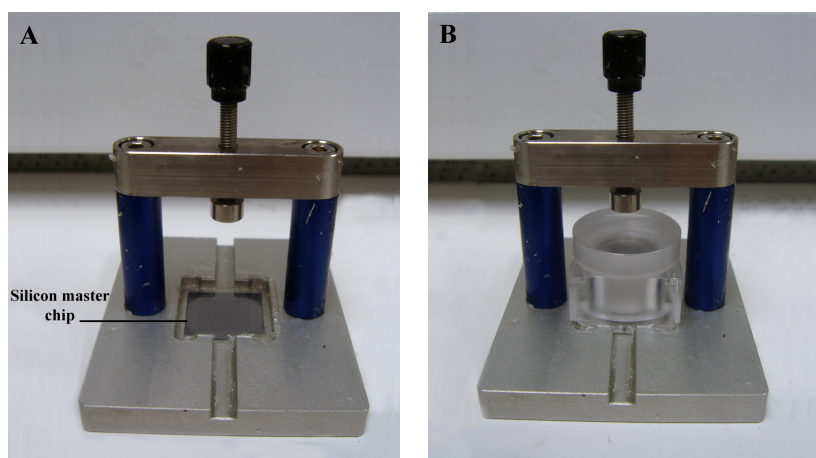


Figure 6-3: The casting station used for PDMS stamp fabrication. A: the place of silicon master chip and B: the place of polycarbonate stamp holder

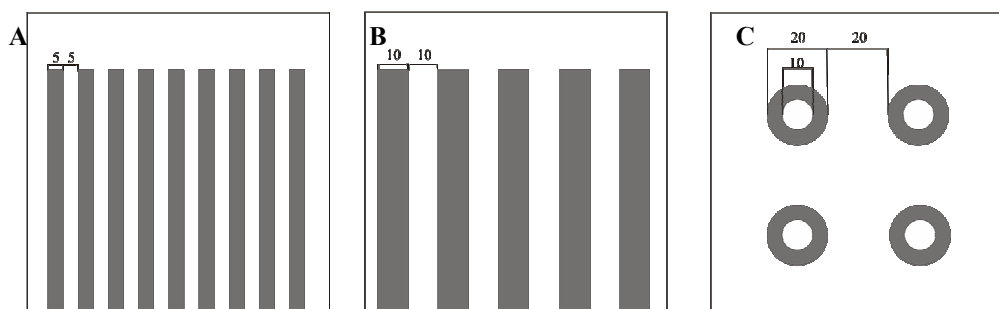


Figure 6-4: The different patterned stamp masters used for μ CP: (A) strips of 5/5 μm (B) strips of 10/10 μm and (C) donuts 20/20/10 μm .

To prepare the PDMS stamps, a mixture consisting of 10:1 (W/W) PDMS elastomer (Sylgard 184) and curing agent was mixed thoroughly and degassed in a vacuum chamber to remove bubbles for 30 minutes. The casting station was used to fabricate the PDMS stamp by injection of the degassed PDMS solution into the inlet port of the casting station containing the silicon master chip inside. A PDMS diaphragm or membrane spanned across a polycarbonate stamp holder (Figure 6-5). The PDMS stamp was cured for 1 hour at 100°C in an oven and cooled to room temperature. The PDMS stamps were obtained by slowly lifting off the silicon master. Each stamp has been used once and was cleaned by sonication in a 2:1 solution of distilled water and ethanol for 15 min, rinsed in distilled water, and dried under N_2 flow prior to the use. Stamps could be reused after cleaned by sonication in water-ethanol mixture.³⁴⁷

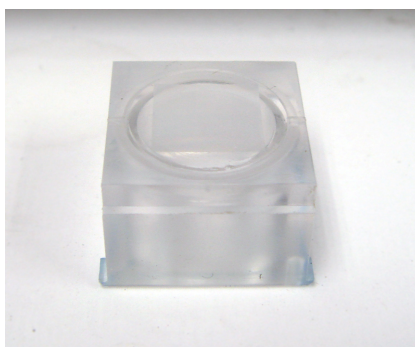


Figure 6-5: A prepared PDMS membrane on a polycarbonate stamp holder.

6.2.5 Mica modification

Mica substrates were cleaned with sulfuric acid and functionalized by immersing in a solution of 2% 3-APTES in dry acetone for 30 min at room temperature. After washing with dry acetone and distilled water, the substrates were oven dried for 1 hour. Modified substrates were always prepared just before carrying out the experiment.

6.2.6 Printing carboxyl terminated quantum dots on modified surface

The stamp was inked by incubating carboxyl terminated QDs 565 diluted in PBS (80 nM) onto the PDMS surface for 45 min in a covered Petri dish at room temperature. Following incubation, the inked stamp was briefly rinsed with PBS and dried under nitrogen gas flow. Contact printing was performed by inverting the QD inked PDMS stamp onto 15×15mm² modified mica surface and held in contact for 15 min while using a weight of 50 g to press gently onto the inverted stamp to make a good contact between both surfaces. Finally, the PDMS stamp was gently removed. The mica substrate was then rinsed with PBS and dried by nitrogen gas. The mica was fixed to a microscope slide with nail polish and the performance of fabricated arrays examined with CLSM.

6.2.7 Microcontact printing of human IgG immunoassay on mica

Indirect immunoassay format was selected for these experiments due to simplicity and comparatively fewer steps. To do indirect immunoassay, the antigen (human IgG) was printed on the modified mica surface. After blocking, a QDs conjugated secondary antibody was added to detect printed antigens on surface. The surface of the PDMS stamp was exposed to solution of 50 µg/ml of the inking antigen for 30 minutes. Excess solution was washed and the stamp dried under a stream of nitrogen gas. Then,

the stamp was brought into contact with the modified mica substrate and a small amount of force applied to make a better contact between surfaces. The stamp was removed after 15 minutes, and the mica surface was washed with PBS and immersed in 0.5% casein in PBS solution as blocking buffer for half hour. After washing the substrate with PBS, it was incubated with a solution of 80 nM of a QDs secondary antibody (Qdot® 605 goat F(ab')₂ anti-human IgG) for one hour. Then the substrate was washed with PBS and dried with nitrogen gas. The mica was fixed to a microscope slide with nail polish and detected with CLSM.

6.2.8 Microcontact printing of multiprotein immunoassays on mica

For printing more than one protein on the surface the sequential inking and printing method has been used. Two stamps with different patterns were used. Stamps of 5 μm wide stripes and 20/20/10 μm donut shape were used to print mouse and human IgG on the modified mica surface sequentially (Figure 6-6). After washing with PBS, the mica substrate was immersed in blocking buffer solution for half hour. After washing and drying, the mica patterned surface was exposed to a mixture solution of both complementary secondary QDs conjugated antibodies (Qdot® 655 goat F(ab')₂ anti-human IgG and Qdot® 565 goat F(ab')₂ anti-mouse IgG) for one hour. After washing with PBS and dried with nitrogen gas, the mica surface was detected with CLSM.

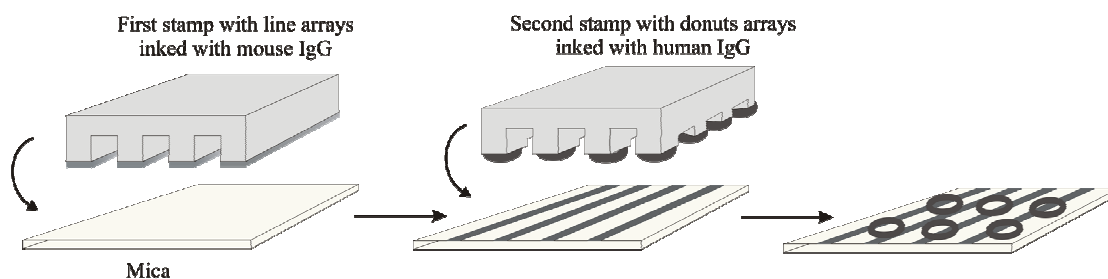


Figure 6-6: Schematic of μCP of two-protein arrays on mica surface.

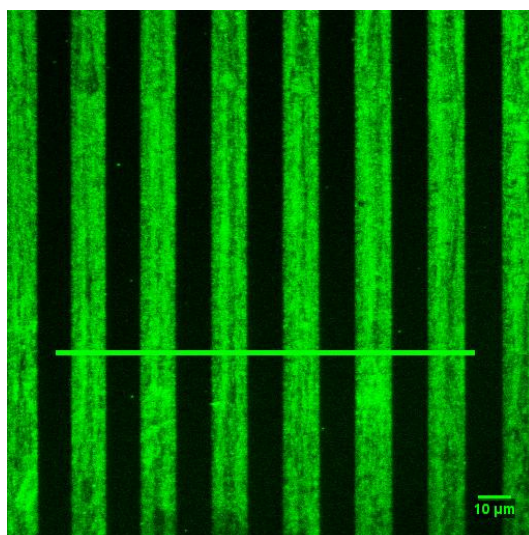
6.2.9 Image analysis

The fluorescent images were acquired with confocal microscopy and analysed using ImageJ software.

6.3 Results and discussion

6.3.1 Microcontact printing of carboxyl terminated quantum dots

The feasibility of fabrication patterned arrays with μ CP method was first tested by μ CP of QDs particles onto the modified mica surface. Carboxyl terminated QDs 565 (80 nM) were inked onto the PDMS stamp with linear patterned arrays of 10 μ m wide stripes. PDMS stamp produced dense and well-defined line patterns of QDs on mica surface (Figure 6-7) demonstrating the good transfer of QD ink from the PDMS stamp to the modified mica surface. The image was taken after washing the printed mica substrate with PBS indicating the good stability of the printed QDs arrays even after washing. The result shows that μ CP can be used as an efficient, simple technique for creating microarrays of QDs onto the mica surface.



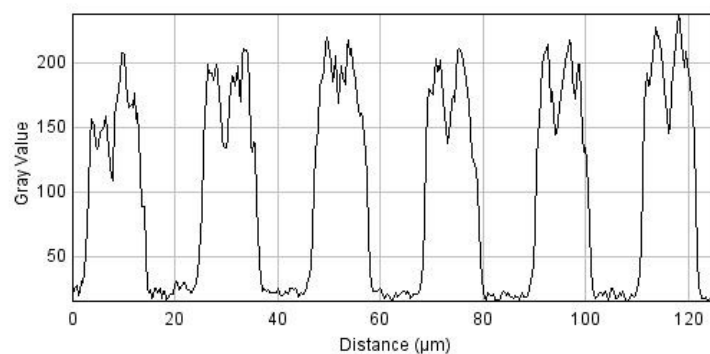


Figure 6-7: Fluorescence image of QDs 565 patterned on a modified mica surface by μ CP accompanied by the intensity profile.

6.3.2 Microcontact printing of an indirect human IgG immunoassay

Microarrays of human IgG immunoassays were printed on modified mica surface by μ CP of antigen on the modified mica surface and detected with complementary QDs-conjugated antibody. PDMS serves as a bulk reservoir from which antigen (human IgG) can be transferred onto the mica surface. Patterns were detected as arrays of 5 μ m wide stripes of human IgG immunoassay on modified mica surface (Figure 6-8). Printed protein arrays must maintain good stability and keep the biological activity on the surface in order to detect the complementary antibodies present in solution. The result confirms that printed antigen molecules remain stable and active on the mica surface in order to capture its specific antibody. Protein molecules appear to be densely packed and the edges of the pattern are well-defined. The protein ink was successfully transferred to the solid surface, and the size of features maintained throughout surface. The result shows that proteins can adhere to the unmodified PDMS stamp. The PDMS stamps used in μ CP experiments were not modified with oxygen plasma or any other modification methods. The antigens transferred from the uncharged stamp to the positively charged APTES-silanized mica substrate in site

specific regions that were in direct contact with each other. The difference between the wettability of two surfaces is the main reason of successful transferring. Previous studies confirmed that any surface modification that increases the wettability of the substrate improved printing in μ CP.³¹²

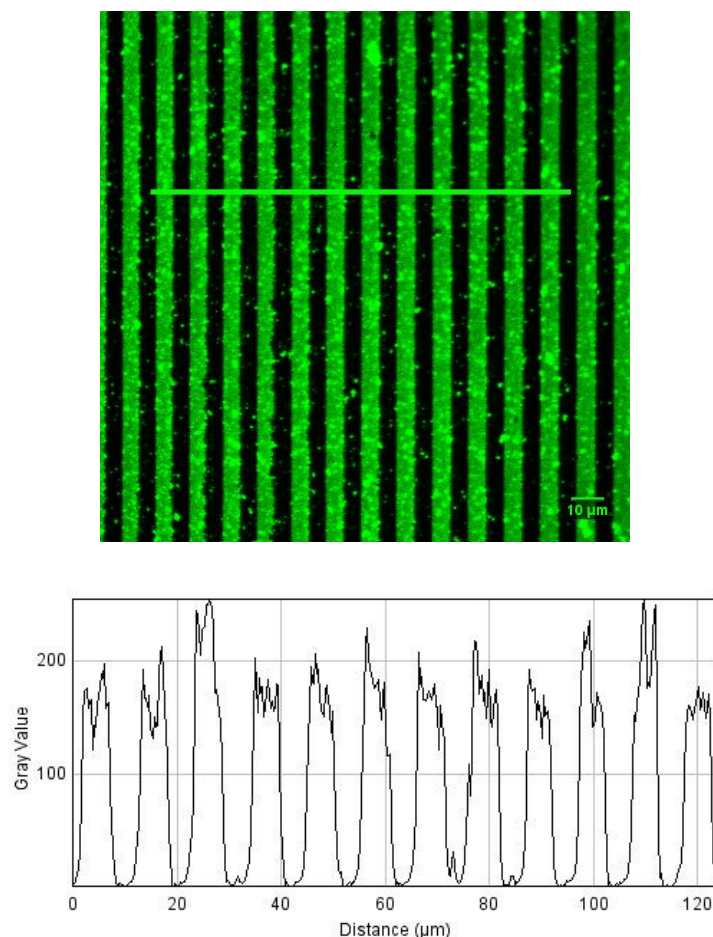


Figure 6-8: Fluorescence image of human IgG QDs 605 patterned on a modified mica surface by μ CP accompanied by the intensity profile.

The intensity profile shows the good agreement with the size of patterns in the used master. The result shows the high degree of immobilization of antigen on the surface in short contact time (10 min) by μ CP compared to the traditional immunoassay which hours of the incubation time in solution is necessary.

6.3.2. Dose response of microarrays of human IgG immunoassays

To evaluate the immunologic competence of μ CP applied immunoassays, it is necessary to investigate the dose dependence of binding the antibody to the patterned antigens on the surface. Four stamps with same patterns of $5\mu\text{m}$ wide stripes were used to print different concentrations of human IgG (0, 25, 50 and $100\ \mu\text{g}/\text{ml}$) on mica substrates. The inking and printing conditions were identical for all samples. The antigens have been detected with $80\ \text{nM}$ concentration of QD605 anti-human IgG. The confocal images of mica surfaces have been shown in Figure 6-9. The results show the dependency of intensity of immunoassays to the concentrations of antigens. No significant signal was observed in the blank sample (no antigen) suggesting that non-specific binding was minimal in μ CP. Higher concentrations of antigens produced dense and well-defined patterns that were packed with intensely bright QD fluorescence. The variation of the human IgG immunoassay response relative to the concentration of the printed antigen on the modified mica surface is shown in Figure 6-10.

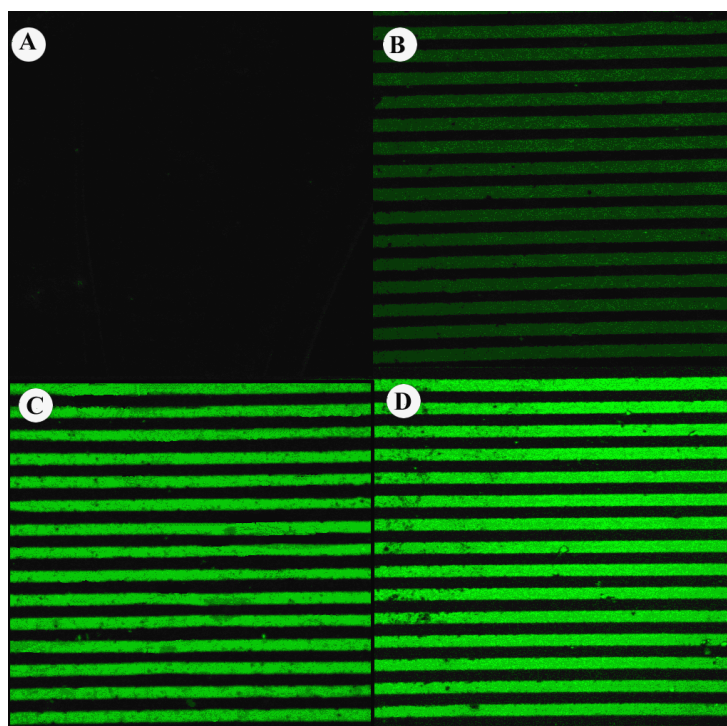


Figure 6-9: Confocal fluorescent images of different concentrations of human IgG in μ CP of human IgG immunoassays. A: 0, B: 25, C: 50 and D: $100\ \mu\text{g}/\text{ml}$.

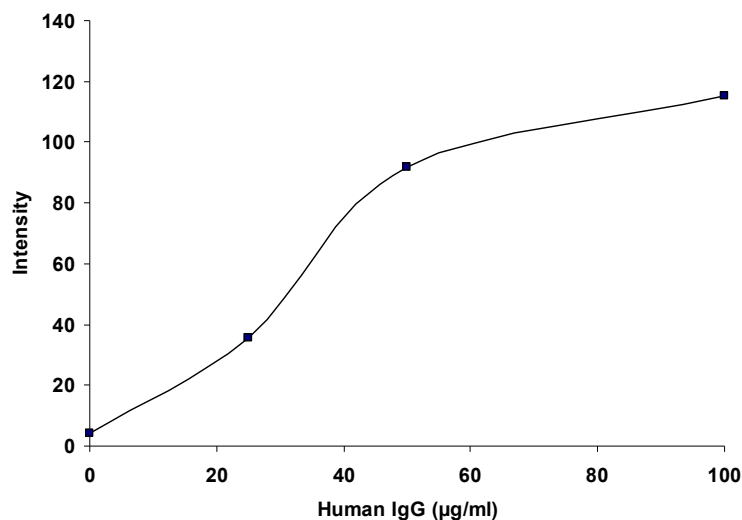


Figure 6-10: Dose response curve of printed human IgG immunoassay with μ CP

6.3.3 Stacked of human IgG immunoassays microarrays

Modified mica substrates with microarrays of 10 μm wide stripes of QDs conjugated human IgG immunoassay on each were prepared. The same concentration of antigen (50 $\mu\text{g/ml}$), and QDs605 conjugated secondary antibody (80 nM) were used for all assays. After conducting the immunoassays with μ CP method, the mica substrates were washed with PBS, dried with nitrogen gas and stacks prepared with distilled water filling the gap between them. The stacks were fixed on a microscope slide with nail polish. Scanning two (Figure 6-11) and three (Figure 6-12) layers produced well defined volume arrays.

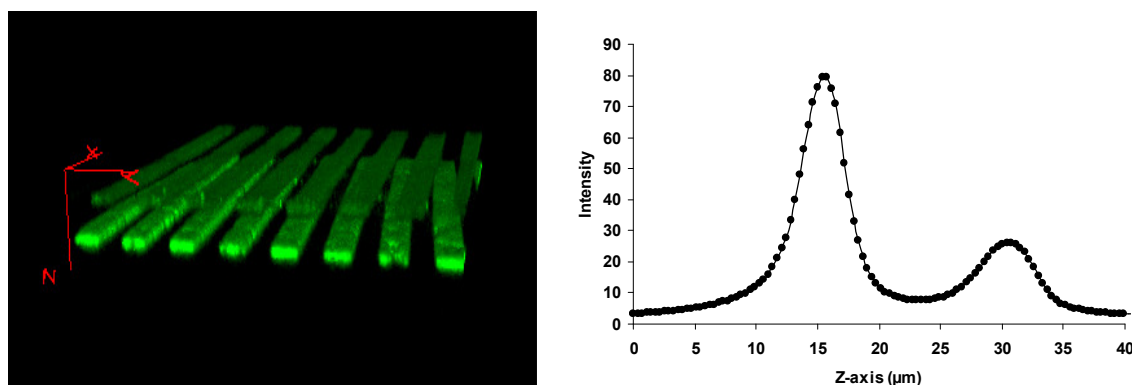


Figure 6-11: The 3D view and z-axis response of stack of two mica layers containing QDs human IgG immunoassays. The orientation of microarray layers in 3D view is based on their

positions in scanning with inverted CLSM (brighter layer is the first scanned layer next to the objective)

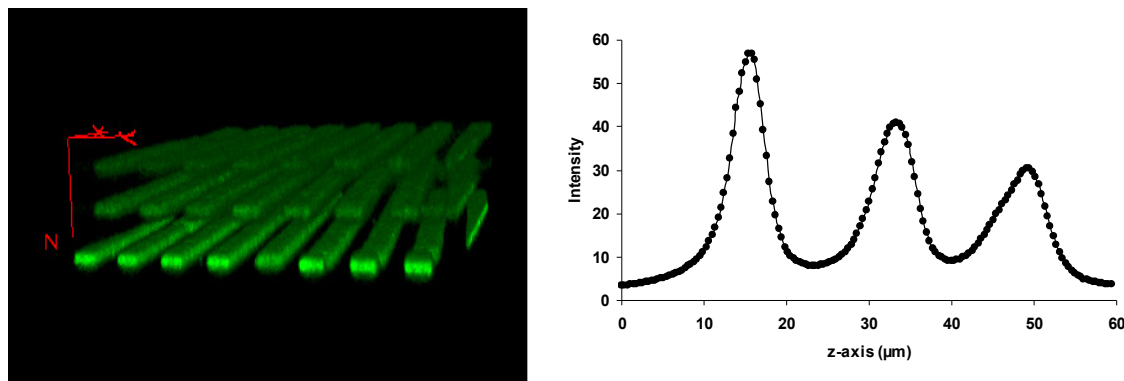


Figure 6-12: The 3D view and z-axis response of stack of three mica layers containing QDs human IgG immunoassays. The orientation of microarray layers in 3D view is based on their positions in scanning with inverted CLSM (brighter layer is the first scanned layer next to the objective).

6.3.4 Microcontact printing of multiprotein immunoassays

Two model immunoassays (human and mouse IgG) have been chosen to show the development of the multiprotein immunoassays in a microarray format. QD565 and QD655 complementary antibodies have been selected to well separate the emission peaks. Figure 6-13 shows the fluorescent images of multiple immunoassays by sequential method printed onto the same mica surface. The images were taken at the same position of a single mica substrate simultaneously by selecting proper filter sets and two PMTs of CLSM. The images show the successful printing of multiprotein patterning on the modified surface which supports the ability of μ CP for multicomponent protein patterning by sequential method.^{286, 329, 333, 348} The result shows that the first stamped protein array retains the most of its line resolution after a successive printing of the secondary protein. The Figure also demonstrates the ability to simultaneously visualize these multiple immunoassays arrays on one mica surface.

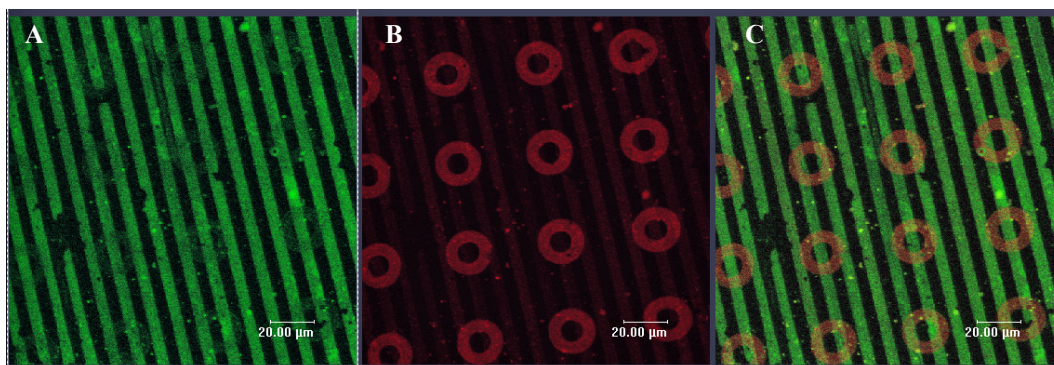


Figure 6-13: Fluorescent images of sequentially stamped multiprotein QD immunoassays; A: line patterns of mouse IgG QD565 immunoassay, B: donuts patterns of human IgG QD656 immunoassay, and C: overlay of both images.

Here, two different colours of fluorophores have been used to separate the patterns in the final image. It is possible to use one colour for printing both patterns and separate the images by transferring the images from the spatial domain to the frequency domain. Use of the frequency domain offers some advantages for image processing. It allows measurements that would be difficult in the spatial domain. Fourier transform is a useful method on images of repetitive structures such as patterns in order to identify a periodic component or lattice in an image. Identifying regular patterns on an image has other advantages like separating the patterns or removing noise from an image. The discrete Fourier transform (DFT) is a useful computational tool that provides an efficient means for detecting directionality or periodicity in the frequency domain.³⁴⁹ The fast Fourier transform (FFT), the fast algorithm for computing the DFT, is used to construct a directional image. In this study, confocal images were subjected to FFT to reveal the characteristic power spectra of each pattern by image J software (Figure 6-14A and B). Image processing by FFT presents distinguishable spectra of line and donut patterns. Fourier spectrum of the linear array shows lines distributed in different directions which is completely different from the FFT spectrum of donut patterns with periodic structures of a circular region around a

central bright center. The Fourier spectrum of the overlayer image (Fig 6-14C) shows the existence of both directional and periodical structures which can be separated.

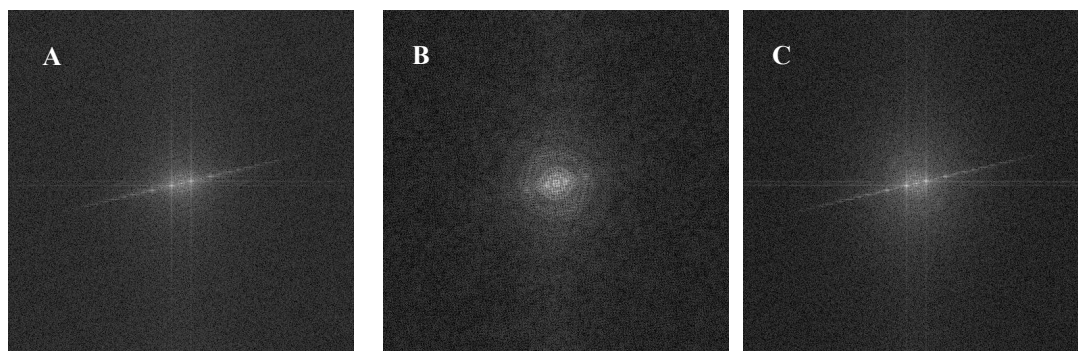


Figure 6-14: The Fourier spectra of confocal images of sequentially stamped multiprotein QD immunoassays; A: line patterns B: donut patterns, and C: overlayer of both patterns.

6.3.5 Stacked of microarrays of multiprotein immunoassays

To demonstrate the spatial expansion of two dimensional microarrays of multiprotein immunoassays into three dimensional, modified mica substrates with microarrays of QDs human and mouse IgG were prepared as described in section 6.3.4. Stacks of two mica layers could be scanned successfully with CLSM. Figure 6-14 shows the 3D views of a stack of two mica layers with two microarray immunoassays on each.

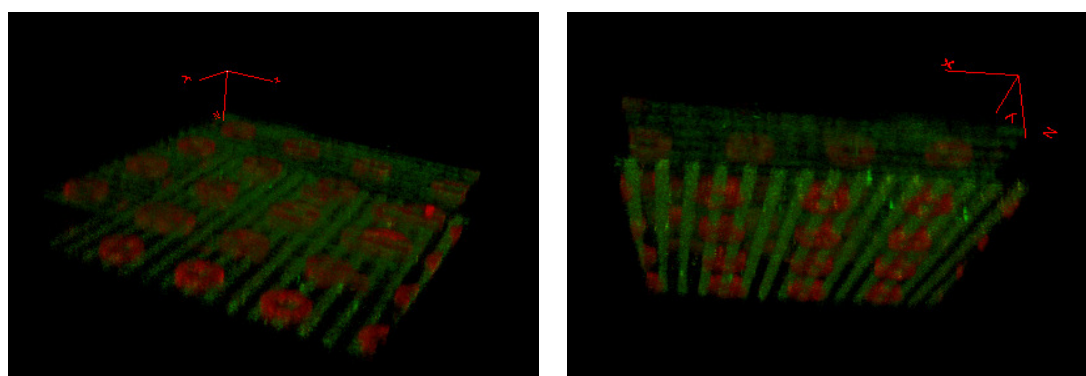


Figure 6-15: Different 3D views of stacking two mica substrates with multiprotein immunoassays on each. Line patterns belong to QD565 mouse IgG immunoassay and donut patterns belong to QD656 human IgG immunoassay.

6.4 Conclusion

The deposition of single and multi-proteins onto modified mica substrates using μ CP without chemical modification of the stamp surface has been explored. Results show that μ CP is a simple, quick and efficient method to produce consistent and well-defined microarrays of immunoassays on the mica surface that remained immobilized even after rinsing with PBS. The results support the use of μ CP as a tool to fabricate microarrays of single and multiple proteins that can be used to study antigen-antibody interactions and bioassays. The dose response study results showed the quantitative application of the μ CP in the measurement of immunoassays. It has been shown before that μ CP allowed concentration-dependent of microarrays of streptavidin conjugated QDs on APTEES-silanized glass surface.³⁵⁰

QDs can be used as suitable labels for detection of microarrayed of immunoassays. Their photostability allows prolonged observation and detection imaging without loss of intensity from photobleaching.

The choice of the substrate and the modification of it are essential for a successful protein patterning due to sensitivity of the protein structure to change upon chemical treatment or the immobilization process. Various substrates like glass, silicon, metals and polymers have been investigated for use in μ CP of proteins. Reports of using mica as substrate for μ CP are limited in the literature at present. Current reviews indicate this is the second report of using mica as a substrate. Wang *et al.* have demonstrated μ CP of multiproteins immunoassays on mica substrates in 2006.²⁸⁶ They used FITC and TRITC labelled antibodies to detect antigens patterns on a modified mica surface with 3-APTES. No dose response study has been shown in their study.

The μ CP technique was extended to the detection of two separate immunoassays on one substrate and then four separate immunoassays on two substrates simultaneously. There is no similar report in the literature to show the extension of microarray immunoassays along the z-axis. It is possible to increase the assay density by printing more microarray multiprotein immunoassays on one surface layer and stack the layers.

Though proteins were used exclusively in these experiments, there is no obstacle for utilizing other biomolecules such as DNA, peptides or drugs. With proper adjustment of the technique, microarrays should be capable of being fabricated from all these substances.

Chapter 7

Conclusions & future work

This chapter summarises the key achievements presented and discussed throughout this thesis and presents suggestions for improvement of the presented confocal method and further studies and future prospects.

7.1 Conclusion

A high demand for separation-free and multiplexed bioassays resulted in development of new bioaffinity assay technologies which have potential for high throughput screening and miniaturization. The current work aimed at the development of the utilization of confocal microscopy as a detection method to readout fluorescent immunosorbent assays on planar surfaces in order to present a non-separation immunoassay detection method. Confocal microscopy has demonstrated its high performance as an optical sectioning imaging technique to obtaining high resolution 3D images. But its key ability to extract information of a thin layer of specimen has not been investigated properly in other fields except imaging. The combination of CLSM with FLISA described in this thesis has been shown to offer novel possibilities for an immunoassay detection method and enhancing the performance of immunoassays due to the separation-free nature of confocal immunosorbent assay method which enables direct measurement of the fluorescent signals in presence of unbound fluorophores. The kinetic measurements and z-axis multiplexing were successfully demonstrated for the first time using a fluorescent immunoassay combined with a confocal detection system.

The main results achieved are summarized below:

- 1) A confocal readout method was demonstrated and the signal decomposition of the thin film of immunoassay and overlaying of the unbound fluorescent solution based on distribution functions showed that it is suitable for signal separation provided the required data for analysing immunoassays. A model of sandwich human IgG fluorescent immunoassay on a conventional solid surface (8 well chamber slide or 96 well plate) was prepared and two different format immunoassays were

developed. Firstly, a heterogeneous approach based on routine protocol of sandwich immunoassays for quantitative determinations of antigen concentrations were obtained by coating the surface with the first antibody, then adding antigen and secondary fluorescent labelled antibody sequentially and following the experiment by measuring the fluorescent response by CLSM. In this format a detection limit of 5.5 nM for human IgG (n=3) were obtained. A second procedure, homogeneous format, was designed with the intention of performing immunoassays in less incubation and washing steps by adding antigen and secondary fluorescent labelled antibody simultaneously. A detection limit of 2.2 nM was calculated confirming better sensitivity of the homogeneous format assay. The comparison of both formats illustrated that homogeneous format assay can preserve the weak interactions which were removed in heterogeneous format assay by the washing step. The total duration of the homogeneous procedure was less than conventional ELISA due to no requirement for enzyme development reaction and fewer washing steps. The HCV experiments were mainly designed to investigate the potential of confocal detection method for a real model of disease. The results with the HCV assays were not comparable with the detection limits in the literature and need more works on assay optimization. The effects of some important parameters affecting the confocal response such as NA and pinhole size were investigated. The results showed the improved resolution in high NA and pinhole size in the range of optimal size resulted in less blurring between film and overlayer and thus improved both sensitivity and limits of detection.

2) In chapter 4 a novel approach for studying binding kinetics on a solid surface using CLSM was demonstrated. The binding reaction of a model of sandwich immunoassay in both homogeneous and heterogeneous format assays using FITC and

QD fluorophores was studied. The results suggest that the confocal immunosorbent assay detection method is a suitable method for real-time investigation of immunoreaction between immobilized antigens on the surface and labelled antibodies in the solution. It is the first report of application of CLSM for real-time kinetic measurements of antigen-antibody interactions. The high photostability of QDs against photobleaching presented a great advantage in the kinetic experiments to fix the scanning point on the solid surface for the whole period of incubation.

3) The first presented report of a confocal readout of a multiplexed assay arrayed along the z-axis in chapter 5 highlighted the advantage of confocal detection method versus conventional immunoassay detection methods. This is the first report of assays arrayed along the z-axis of an optical system, the most extensive study of fluorescence in stratified media, and the most comprehensive treatment of axial distance in layered systems to date. Optically sectioned readout of fluorescent immunoassays allowed detection of more than one signal along the z-axis, potentially increased the analysis speed and array density compared to single layer assay. The results indicated an increased assay density by at least a factor of five by arraying along the z-axis. It was the first report of using mica as non-conventional solid surface material in immunoassay in a sandwich immunoassay and also the first demonstration of a dose response curve on mica, presented it as a suitable solid surface for immunoassay. A novel fluorescence-based optical platform for multiple immunoassay was designed and detected successfully by measuring the intensity of a stack of two mica layers contain two model assay of human and mouse IgG immunoassays.

4) Finally, z-axis multiplexing measurements in 3D were demonstrated for the first time using protein patterning and confocal detection system. After achieving successful detection of multiplexed immunoassay along the z-axis, the possibility of

expanding the assay in 3D to develop a detection method working in 3D was investigated. Antigen arrays were fabricated using PDMS stamp and microcontact printing technique on mica surface and applied in an immunoassay by exposure to QD-conjugated antibody solution. Confocal images indicated the presence of immunoassay arrays on the surface of mica. The quantitative measurements based on dose-response curve of applied immunoassay arrays confirmed the antigen-dependent intensity variation. By the same approach multiplexed immunoassays were developed by sequential stamping of different antigen arrays on the surface and exposure to the mixture of QDs antibodies. The use of the confocal detection system allowed for characterisation of individual layer in a stack of two mica layers each containing two different immunoassays resulted in two fold increasing of immunoassay density.

7.2 Future work

Although the confocal readout method developed in this thesis enable measurements of fluorescent immunosorbent assays in different formats, the following studies could be carried out to improve further performance in bioaffinity assays.

- 1) The confocal detection method has been successful demonstrated in detecting the model of human assay. It would then naturally follow for the detection method to be used with real samples like serum or plasma. It is a suggestion to use real samples for other aspects of confocal detection method which have been investigated in this thesis such as the kinetics analysis, z-axis multiplexing in 2 and 3D.

- 2) Future optimization of the confocal method regarding to the incubation time, alternation of buffer composition and blocking buffers in order to achieve higher

sensitivity immunoassays. The studies on selection the best blocking buffer have been done only on immunoassays using QD-conjugated antibodies (data have not shown). Using covalent binding to attach the antibody on the surface may improve the detection limit.

3) Since the main drawback of confocal microscopy is its slow speed, using high-speed confocal microscopy systems will improve the slow frame rate of currently available confocal systems.

4) The confocal readout method presented in this thesis was applied only for antigen-antibody system. It could be expanded to monitoring other bioaffinity assays such as ligand-receptor or cell-based assays. The feasibility of confocal readout system for an androgen receptor-ligand was studied in our laboratories with successful results.

5) Despite the work carried out within this thesis, further comparative work on kinetics is needed between confocal method and optical biosensors. This will provide further confidence in the kinetic constants published by various authors. The dissociation rate constant determined from the intercept of the confocal response versus conjugated antibodies concentration is poorly defined. A better approach is to directly measure the intensity of the immunoassays after washing the overlayer and fit the dissociation profile.

6) Improved substrate materials and optics should minimize the refractive index mismatches, and yield further improvement. Further work on substrate materials other than mica or glass such as thin plastic films or PDMS may yield more suitable synthetic material.

7) Spatial distortion and blurring in deep layers within a stack arise from aberration leading to intensity attenuation. Partial correction could be done by

adaptive aberration correction and minimization of the refractive index mismatches by careful selection of materials. This attenuation can be overcome by calibration of the intensity response as demonstrated with human IgG immunoassays. Further work on comparing theory with experimental results may lead to precise measurement of FWHM and lowered requirement for calibration each layer.

8) The reported stratified assay in chapter 5 could also be studied with two photon excitation microscopy and other optical sectioning methods. Some advantages may be obtained from the lack of pinholes and the improved depth of penetration. A study on theoretical PSF calculation through a stratified medium showed that in deeper focus (100 μm below the cover glass) the illumination PSF is less blurred in two photon microscopy compared to confocal

9) Heterogeneous format assay was used in all z-axis multiplexing experiments in this thesis. Further work in this area would include working on homogeneous format. Although it is required to careful experiment design due to only one side of the substrate should access to the reagents and contaminating of both sides would cause misleading the results.

10) A qualitative multiplexed immunoassay in microarray format has been demonstrated in chapter 6 (section 6.3.4). Quantitative measurements of the multiplexed microarray fabrication could be assessed by conducting dose-response experiments of each immunoassay to see the possible interfering parameters such as non-specific binding and cross reaction.

7.3 Publications arising from this work

7.3.1 Papers

Stratified media and multiplexed fluorescent immunosorbent assays arrayed along the z-axis. Homanaz Ghafari, Samuel Lawman, Haida Liang, and Quentin S. Hanley, submitted to Biomedical Optics Express 2010.

Confocal detection of planar homogeneous and heterogeneous immunosorbent assays. Homanaz Ghafari, Yanzhou Zhou, Selman Ali, and Quentin S. Hanley
Journal of Biomedical Optics 14(6), 064022 (November/December 2009).

7.3.2 Patent

Improvements relating to Assays including a Labelled Reagent

Homanaz Ghafari, Quentin S. Hanley, patent UK number 0807466.8 24 April 2008

7.3.3 Conference Presentations

Development and optimization of confocal sandwich immunoassays (Talk)

Fluoromag E.U. Consortium symposium: Nanodots and Diagnostics, University of Santiago de Compostela, Spain 27-29 March 2009

Detection of Planar Format Assays with Optical Sectioning Microscopy (poster)

Homanaz Ghafari, Selman Ali and Quentin Hanley

MICROSCIENCE 2008, London, UK

Appendix

Optical model of planar confocal immunosorbent assay

In the confocal microscope, the planar assay format can be thought of as the sum of a thin film and an overlayer. An optical model of this system consists of a 50 nm thin film and a uniformly fluorescent overlayer beginning 50 nm above the glass surface and extending away from the film. The thin film and overlayer differ only in the concentration of fluorophores, designated C_1 and C_2 , respectively. More rigorously, the two fluorescent objects (O) in the microscope can be given as a function of position along the z -axis: $O_1(z) = C_1$ for $0 < z < 50$ nm and is 0 everywhere else and $O_2(z) = C_2$ for $50 \text{ nm} \leq z < \infty$ and is 0 elsewhere. The overall object function is the sum of the two:

$$O(z) = O_1(z) + O_2(z) \quad (\text{A-1})$$

For the purpose of the assay, the key to making accurate measurements of surface bound fluorescence is the ability to selectively determine the concentrations C_1 and C_2 . In the microscope, the object function is not observed directly. Instead, the measured object (M) depends on the object function convolved with \mathbf{h} , the confocal point spread function (PSF):

$$M(z) = \mathbf{h} \otimes O(z) \quad (\text{A-2})$$

Since the diffraction limited resolution along the z -axis in a confocal microscope observed at high numerical aperture is on the order of 500 nm, the surface bound film is thin relative to the resolution of the microscope. This has the consequence that although the object as modelled consists of exclusive zones containing either C_1 or C_2 , the measured z -axis “image” contains signals arising from both the overlayer and the thin film at every position along the z -axis. For large z , the contribution of the film can be made arbitrarily small. A similar condition does not hold for the overlayer; the overlayer will contribute significantly to the signal at all locations along z due to

blurring by the confocal PSF. M can be broken down into the parts corresponding to the two composing objects:

$$M(z) = \mathbf{h} \otimes O_1(z) + \mathbf{h} \otimes O_2(z) \quad (\text{A-3})$$

This equation suggests two ways to obtain information selectively from the thin film. The first approach is to convolve ideal objects (Eq A-1 and A-2) with a computed point spread function. For this study, the PSF as described by van der Woort and Brakenhoff³⁵¹ was applied to idealized objects as in equation A-1. The concentrations are then adjusted until a best fit to the measured data is obtained using least squares minimization. Alternately, a semi-empirical approach may be used in which the axial response of the microscope is measured for a thin film in the absence of an overlayer and for the overlayer in the absence of the thin film. The measured data are then synthesized by making linear combinations of the two measured objects. Best results are obtained by fitting the observed data to simplified functions which mimic much of the behaviour of planar objects modified by PSFs. The Cauchy-Lorentz function and the cumulative Cauchy-Lorentz function are comparatively simple functions that fit the shape of real axial response functions affected by aberrations reasonably well. The semi-empirical fit used the following form:

$$M(z) = C_1 \frac{1}{\pi\gamma \left[1 + \left(\frac{(z-z_0)}{\gamma} \right)^2 \right]} + C_2 \left(\frac{1}{\pi} \arctan \left(\frac{z-z_0}{\gamma} \right) + \frac{1}{2} \right) + B \quad (\text{A-4})$$

where, z is the axial position, z_0 is the center of the thin film, γ is the width of the response, and B is a constant which corrects for electronic offsets and photomultiplier tube background in the confocal microscope.

References

- (1) Warsinke, A.; Nagel, B. Towards separation-free electrochemical affinity sensors by using antibodies, aptamers, and molecularly imprinted polymers - A review. *Anal. Lett.* **2006**, *39*, 2507-2556.
- (2) de Jong, L. A. A.; Uges, D. R. A.; Franke, J. P.; Bischoff, R. Receptor-ligand binding assays: Technologies and applications. *Journal of Chromatography B-Analytical Technologies in the Biomedical and Life Sciences* **2005**, *829*, 1-25.
- (3) Burbaum, J. J.; Sigal, N. H. New technologies for high-throughput screening. *Curr. Opin. Chem. Biol.* **1997**, *1*, 72-78.
- (4) Mulvaney, S. P.; Myers, K. M.; Sheehan, P. E.; Whitman, L. J. Attomolar protein detection in complex sample matrices with semi-homogeneous fluidic force discrimination assays. *Biosens. Bioelectron.* **2009**, *24*, 1109-1115.
- (5) Koskinen, J. O.; Vaarno, J.; Vainionpaa, R.; Meltola, N. J.; Soini, A. E. A novel separation-free assay technique for serum antibodies using antibody bridging assay principle and two-photon excitation fluorometry. *J. Immunol. Methods* **2006**, *309*, 11-24.
- (6) Beasley, J. R.; McCoy, P. M.; Walker, T. L.; Dunn, D. A. Miniaturized, ultra-high throughput screening of tyrosine kinases using homogeneous, competitive fluorescence immunoassays. *Assay Drug Dev. Technol.* **2004**, *2*, 141-151.
- (7) Burns, G.; Kurrle-Weittenhiller, A.; Karl, J.; Engel, W. D.; Gromping, A.; Boos, K. S.; Seidel, D. A simple turbidimetric assay designed for the routine screening well as therapeutic monitoring of native LDL particles. *Clinica Chimica Acta* **2001**, *303*, 155-165.
- (8) Lewellen, L. J.; Mccurdy, H. H. A Novel Procedure for the Analysis of Drugs in Whole-Blood by Homogeneous Enzyme-Immunoassay (Emit). *J. Anal. Toxicol.* **1988**, *12*, 260-264.
- (9) Armbruster, D. A.; Hubster, E. C.; Kaufman, M. S.; Ramon, M. K. Cloned Enzyme Donor Immunoassay (Cedia) For Drugs-Of-Abuse Screening. *Clinical Chemistry* **1995**, *41*, 92-98.
- (10) Wu, Z. S.; Zhang, S. B.; Guo, M. M.; Chen, C. R.; Shen, G. L.; Yu, R. Q. Homogeneous, unmodified gold nanoparticle-based colorimetric assay of hydrogen peroxide. *Analytica Chimica Acta* **2007**, *584*, 122-128.
- (11) Kokko, T.; Kokko, L.; Soukka, T.; Lovgren, T. Homogeneous non-competitive bioaffinity assay based on fluorescence resonance energy transfer. *Anal. Chim. Acta* **2007**, *585*, 120-125.
- (12) Loomans, E.; van Doommalen, A. M.; Wat, J. W. Y.; Zaman, G. J. R. High-throughput screening with immobilized metal ion affinity-based fluorescence

- polarization detection, a homogeneous assay for protein kinases. *Assay Drug Dev. Technol.* **2003**, *1*, 445-453.
- (13) Ullman, E. F.; Kirakossian, H.; Switchenko, A. C.; Ishkanian, J.; Ericson, M.; Wartchow, C. A.; Pirio, M.; Pease, J.; Irvin, B. R.; Singh, S.; Singh, R.; Patel, R.; Dafforn, A.; Davalian, D.; Skold, C.; Kurn, N.; Wagner, D. B. Luminescent oxygen channeling assay (LOCI(TM)): Sensitive, broadly applicable homogeneous immunoassay method. *Clinical Chemistry* **1996**, *42*, 1518-1526.
- (14) Miraglia, S.; Swartzman, E. E.; Mellentin-Michelotti, J.; Evangelista, L.; Smith, C.; Gunawan, I.; Lohman, K.; Goldberg, E. M.; Manian, B.; Yuan, P. M. Homogeneous cell- and bead-based assays for high throughput screening using fluorometric microvolume assay technology. *J. Biomol. Screen.* **1999**, *4*, 193-204.
- (15) Toney, J. H.; Ogawa, A.; Blair, M.; Park, Y. W. A "Mix and read" assay for insulin using fluorometric microvolume assay technology. *Assay Drug Dev. Technol.* **2003**, *1*, 521-525.
- (16) Swartzman, E. E.; Miraglia, S. J.; Mellentin-Michelotti, J.; Evangelista, L.; Yuan, P. M. A homogeneous and multiplexed immunoassay for high-throughput screening using fluorometric microvolume assay technology. *Anal. Biochem.* **1999**, *271*, 143-151.
- (17) Miller, D. K.; Menke, J. D.; Hayes, N. S.; Uzieblo, A.; Tew, D.; Hayashi, Y.; Guan, Y. F.; Zhao, A.; Cummings, R. T.; Park, Y. W.; Yamin, T. T. D. Development of a high-capacity homogeneous fluorescent assay for the measurement of leukotriene B-4. *Anal. Biochem.* **2006**, *349*, 129-135.
- (18) Tanaka, M.; Matsuo, K.; Enomoto, M.; Mizuno, K. A sol particle homogeneous immunoassay for measuring serum cystatin C. *Clin. Biochem.* **2004**, *37*, 27-35.
- (19) Leuvering, J. H. W.; Goverde, B. C.; Thal, P.; Schuurs, A. A Homogeneous Sol Particle Immunoassay For Human Chorionic-Gonadotropin Using Monoclonal-Antibodies. *J. Immunol. Methods* **1983**, *60*, 9-23.
- (20) Aoki, T.; Tsuchida, S.; Yahara, T.; Hamaue, N. Novel assays for proteases using green fluorescent protein-tagged substrate immobilized on a membrane disk. *Anal. Biochem.* **2008**, *378*, 132-137.
- (21) Aoki, T.; Kazama, H.; Satoh, M.; Mizuki, K.; Watabe, H. A homogeneous assay for relative affinity of binding proteins using a green fluorescent protein tag and membrane disk. *Anal. Biochem.* **2005**, *344*, 25-32.
- (22) Datti, A.; Donovan, R. S.; Korczak, B.; Dennis, J. W. A homogeneous cell-based assay to identify N-linked carbohydrate processing inhibitors. *Analytical Biochemistry* **2000**, *280*, 137-142.
- (23) Niles, A. L.; Moravec, R. A.; Hesselberth, P. E.; Scurria, M. A.; Daily, W. J.; Riss, T. L. A homogeneous assay to measure live and dead cells in the same

- sample by detecting different protease markers. *Analytical Biochemistry* **2007**, *366*, 197-206.
- (24) Lee, R.; Tran, M.; Nocerini, M.; Liang, M. A high-throughput hybridoma selection method using fluorometric microvolume assay technology. *Journal Of Biomolecular Screening* **2008**, *13*, 210-217.
- (25) Valanne, A.; Lindroos, H.; Lövgren, T.; Soukka, T. A novel homogeneous assay format utilising proximity dependent fluorescence energy transfer between particulate labels. *Anal. Chim. Acta* **2005**, *539*, 251-256.
- (26) Ratcliff, J. Separation Techniques in Saturation Analysis. *Br. Med. Bull.* **1974**, *30*, 32-37.
- (27) Gooding, J. J. Nanoscale biosensors: Significant advantages over larger devices? *Small* **2006**, *2*, 313-315.
- (28) Ducey, M. W.; Smith, A. M.; Guo, X. A.; Meyerhoff, M. E. Competitive nonseparation electrochemical enzyme binding immunoassay (NEEIA) for small molecule detection. *Anal. Chim. Acta* **1997**, *357*, 5-12.
- (29) Ekins, R. P. Ligand assays: from electrophoresis to miniaturized microarrays. *Clin. Chem.* **1998**, *44*, 2015-2030.
- (30) Meyerhoff, M. E.; Duan, C. M.; Meusel, M. Novel Nonseparation Sandwich-Type Electrochemical Enzyme-Immunoassay System for Detecting Marker Proteins in Undiluted Blood. *Clin. Chem.* **1995**, *41*, 1378-1384.
- (31) Glickman, J. F.; Schmid, A.; Ferrand, S. Scintillation proximity assays in high-throughput screening. *Assay and Drug Development Technologies* **2008**, *6*, 433-455.
- (32) Hart, H. E.; Greenwald, E. B. Scintillation Proximity Assay (Spa) - New Method of Immunoassay - Direct and Inhibition Mode Detection with Human-Albumin and Rabbit Antihuman Albumin. *Mol. Immunol.* **1979**, *16*, 265-267.
- (33) Pallesen, T.; Vangsted, A.; Drivsholm, L.; Clausen, H.; Zeuthen, J.; Wallin, H. Serum Immunoassay of a Small-Cell Lung-Cancer Associated Ganglioside - Development of a Sensitive Scintillation Proximity Assay. *Glycoconj. J.* **1992**, *9*, 331-335.
- (34) Pope, A. J.; Haupts, U. M.; Moore, K. J. Homogeneous fluorescence readouts for miniaturized high-throughput screening: theory and practice. *Drug Discov. Today* **1999**, *4*, 350-362.
- (35) Park, H.; Lee, M.; Seong, G. H.; Choo, J.; Lee, E. K.; Park, J. Y.; Lee, S.; Lee, K. H.; Choi, Y. W. Open sandwich FRET immunoassay of estrogen receptor beta in a PDMS microfluidic channel. *Bulletin of the Korean Chemical Society* **2008**, *29*, 1297-1298.

- (36) Boute, N.; Jockers, R.; Issad, T. The use of resonance energy transfer in high-throughput screening: BRET versus FRET. *Trends Pharmacol. Sci.* **2002**, *23*, 351-354.
- (37) Rouleau, N.; Turcotte, S.; Mondou, M. H.; Roby, P.; Bosse, R. Development of a versatile platform for nuclear receptor screening using AlphaScreen (TM). *Journal of Biomolecular Screening* **2003**, *8*, 191-197.
- (38) Morgan, E.; Varro, R.; Sepulveda, H.; Ember, J. A.; Apgar, J.; Wilson, J.; Lowe, L.; Chen, R.; Shivraj, L.; Agadir, A.; Campos, R.; Ernst, D.; Gaur, A. Cytometric bead array: a multiplexed assay platform with applications in various areas of biology. *Clin. Immunol.* **2004**, *110*, 252-266.
- (39) Saunders, G. C.; Jett, J. H.; Martin, J. C. Amplified Flow-Cytometric Separation-Free Fluorescence Immunoassays. *Clin. Chem.* **1985**, *31*, 2020-2023.
- (40) Gosch, M.; Rigler, R. Fluorescence correlation spectroscopy of molecular motions and kinetics. *Adv. Drug Deliv. Rev.* **2005**, *57*, 169-190.
- (41) Mayboroda, O. A.; van Remoortere, A.; Tanke, H. J.; Hokke, C. H.; Deelder, A. M. A new approach for fluorescence correlation spectroscopy (FCS) based immunoassays. *J. Biotechnol.* **2004**, *107*, 185-192.
- (42) Indyk, H. E.; Filonzi, E. L. Determination of immunoglobulin G in bovine colostrum and milk by direct biosensor SPR-immunoassay. *J. AOAC Int.* **2003**, *86*, 386-393.
- (43) Daly, S. J.; Keating, G. J.; Dillon, P. P.; Manning, B. M.; O'Kennedy, R.; Lee, H. A.; Morgan, M. R. A. Development of surface plasmon resonance-based immunoassay for aflatoxin B-1. *J. Agric. Food Chem.* **2000**, *48*, 5097-5104.
- (44) Matveeva, E.; Gryczynski, Z.; Malicka, J.; Gryczynski, I.; Lakowicz, J. R. Metal-enhanced fluorescence immunoassays using total internal reflection and silver island-coated surfaces. *Anal. Biochem.* **2004**, *334*, 303-311.
- (45) Engstrom, H. A.; Andersson, P. O.; Ohlson, S. A label-free continuous total-internal-reflection-fluorescence-based immunosensor. *Anal. Biochem.* **2006**, *357*, 159-166.
- (46) Lange, J.; Kotitz, R.; Haller, A.; Trahms, L.; Semmler, W.; Weitschies, W. Magnetorelaxometry - a new binding specific detection method based on magnetic nanoparticles. *J Magn Magn Mater* **2002**, *252*, 381-383.
- (47) Chemla, Y. R.; Crossman, H. L.; Poon, Y.; McDermott, R.; Stevens, R.; Alper, M. D.; Clarke, J. Ultrasensitive magnetic biosensor for homogeneous immunoassay. *Proc. Natl. Acad. Sci. U. S. A.* **2000**, *97*, 14268-14272.
- (48) Koskinen JO; Vainionpää R; Meltola NJ; Soukka J; Hänninen PE; AE., S. A rapid method for the detection of influenza A and B virus antigens using TPX

- assay technique and dry-chemistry reagents. *J Clin Microbiol.* **2007**, *45*, 3581-8.
- (49) Waris, M. E.; Meltola, N. J.; Soini, J. T.; Soini, E.; Peltola, O. J.; Hanninen, P. E. Two-photon excitation fluorometric measurement of homogeneous microparticle immunoassay for C-reactive protein. *Anal. Biochem.* **2002**, *309*, 67-74.
- (50) Yang, X.; Janatova, J.; Juenke, J. M.; McMillin, G. A.; Andrade, J. D. An ImmunoChip prototype for simultaneous detection of antiepileptic drugs using an enhanced one-step homogeneous immunoassay. *Anal. Biochem.* **2007**, *365*, 222-229.
- (51) Matsumoto, B. In *Methods in cell biology*; Academic Press: San Diego, Calif. ; London, 2002; .
- (52) Minsky, M. Memoir on Inventing the Confocal Scanning Microscope. *Scanning* **1988**, *10*, 128-138.
- (53) Davidovi.P; Egger, M. D. Scanning Laser Microscope for Biological Investigations. *Appl. Opt.* **1971**, *10*, 1615-&.
- (54) Amos, W. B.; White, J. G.; Fordham, M. Use of Confocal Imaging in the Study of Biological Structures. *Appl. Opt.* **1987**, *26*, 3239-3243.
- (55) Udupa, G.; Singaperumal, M.; Sirohi, R. S.; Kothiyal, M. P. Characterization of surface topography by confocal microscopy: I. Principles and the measurement system. *MEASUREMENT SCIENCE & TECHNOLOGY* **2000**, *11*, 305-314.
- (56) Booth, M. J.; Neil, M. A. A.; Wilson, T. Aberration correction for confocal imaging in refractive-index-mismatched media. *J. Microsc. -Oxf.* **1998**, *192*, 90-98.
- (57) Bansal, V.; Patel, S.; Saggau, P. High-speed addressable confocal microscopy for functional imaging of cellular activity. *J. Biomed. Opt.* **2006**, *11*, 034003.
- (58) Inoue, S.; Inoue, T. Direct-view high-speed confocal scanner: The CSU-10. *Cell Biological Applications of Confocal Microscopy, Second Edition* **2002**, *70*, 87-+.
- (59) Wolleschensky, R.; Zimmermann, B.; Kempe, M. High-speed confocal fluorescence imaging with a novel line scanning microscope. *J. Biomed. Opt.* **2006**, *11*.
- (60) Centonze, V. E.; White, J. G. Multiphoton excitation provides optical sections from deeper within scattering specimens than confocal imaging. *Biophys. J.* **1998**, *75*, 2015-2024.
- (61) Pawley, J. B. (.). In *Handbook of Biological Confocal Microscopy*; Springer: 2006; .

- (62) Conchello, J. A.; Lichtman, J. W. Optical sectioning microscopy. *Nat. Methods* **2005**, *2*, 920-931.
- (63) Kozubek, M. Theoretical versus experimental resolution in optical microscopy. *Microsc. Res. Tech.* **2001**, *53*, 157-166.
- (64) Stelzer, E. H. K. In *Three-dimensional light microscopy*; Handbook of Computer vision and applications; Academic Press: 1999; Vol. 1, pp 541-562.
- (65) Webb, R. H. Confocal optical microscopy. *Reports on Progress in Physics* **1996**, *59*, 427-471.
- (66) McAllister, R. G.; Sisan, D. R.; Urbach, J. S. Design and optimization of a high-speed, high-sensitivity, spinning disk confocal microscopy system. *J. Biomed. Opt.* **2008**, *13*, 054058.
- (67) Verveer, P. J.; Hanley, Q. S.; Verbeek, P. W.; Van Vliet, L. J.; Jovin, T. M. Theory of confocal fluorescence imaging in the programmable array microscope (PAM). *J. Microsc. -Oxf.* **1998**, *189*, 192-198.
- (68) Hanley, Q. S.; Verveer, P. J.; Gemkow, M. J.; Arndt-Jovin, D.; Jovin, T. M. An optical sectioning programmable array microscope implemented with a digital micromirror device. *J. Microsc.* **1999**, *196*, 317-331.
- (69) Hagen, G. M.; Caarls, W.; Thomas, M.; Hill, A.; Lidke, K. A.; Rieger, B.; Fritsch, C.; van Geest, B.; Jovin, T. M.; Arndt-Jovin, D. J. Biological applications of an LCoS-based programmable array microscope (PAM) - art. no. 64410S. *Imaging, Manipulation, and Analysis of Biomolecules, Cells, and Tissues V* **2007**, *6441*, S4410-S4410.
- (70) Verveer, P. J.; Hanley, Q. S.; Verbeek, P. W.; Van Vliet, L. J.; Jovin, T. M. Theory of confocal fluorescence imaging in the programmable array microscope (PAM). *J. Microsc. -Oxf.* **1998**, *189*, 192-198.
- (71) Heintzmann, R.; Hanley, Q. S.; Arndt-Jovin, D.; Jovin, T. M. A dual path programmable array microscope (PAM): simultaneous acquisition of conjugate and non-conjugate images. *J. Microsc. -Oxf.* **2001**, *204*, 119-135.
- (72) Liang, M. H.; Stehr, R. L.; Krause, A. W. Confocal pattern period in multiple-aperture confocal imaging systems with coherent illumination. *Opt. Lett.* **1997**, *22*, 751-753.
- (73) Hanley, Q. S.; Verveer, P. J.; Jovin, T. M. Optical sectioning fluorescence spectroscopy in a programmable array microscope. *Appl. Spectrosc.* **1998**, *52*, 783-789.
- (74) Hanley, Q. S.; Jovin, T. M. Highly multiplexed optically sectioned spectroscopic imaging in a programmable array microscope. *Appl. Spectrosc.* **2001**, *55*, 1115-1123.

- (75) Hanley, Q. S.; Verveer, P. J.; Jovin, T. M. Spectral imaging in a programmable array microscope by hadamard transform fluorescence spectroscopy. *Appl. Spectrosc.* **1999**, *53*, 1-10.
- (76) Hagen, G. M.; Caarls, W.; Lidke, K. A.; De Vries, A. H. B.; Fritsch, C.; Barisas, B. G.; Arndt-Jovin, D. J.; Jovin, T. M. Fluorescence Recovery After Photobleaching and Photoconversion in Multiple Arbitrary Regions of Interest Using a Programmable Array Microscope. *Microsc. Res. Tech.* **2009**, *72*, 431-440.
- (77) Muller, M.; Squier, J.; Wilson, K. R.; Brakenhoff, G. J. 3D microscopy of transparent objects using third-harmonic generation. *J. Microsc. -Oxf.* **1998**, *191*, 266-274.
- (78) Esposito, A.; Federici, F.; Usai, C.; Cannone, F.; Chirico, G.; Collini, M.; Diaspro, A. Notes on theory and experimental conditions behind two-photon excitation microscopy. *Microsc. Res. Tech.* **2004**, *63*, 12-17.
- (79) Diaspro, A.; Bianchini, P.; Vicidomini, G.; Faretta, M.; Ramoino, P.; Usai, C. Multi-photon excitation microscopy. *Biomed. Eng. Online* **2006**, *5*, 36.
- (80) Hell, S. W.; Bahlmann, K.; Schrader, M.; Soini, A.; Malak, H.; Gryczynski, I.; Lakowicz, J. R. Three-photon excitation in fluorescence microscopy. *J. Biomed. Opt.* **1996**, *1*, 71-4.
- (81) Gannaway, J. N.; Sheppard, C. J. R. Second-harmonic imaging in the scanning optical microscope. *Optical and Quantum Electronics* **1978**, *10*, 435-439.
- (82) Campagnola, P. J.; Wei, M. D.; Lewis, A.; Loew, L. M. High-resolution nonlinear optical imaging of live cells by second harmonic generation. *Biophys. J.* **1999**, *77*, 3341-3349.
- (83) Yang, L.; McStay, D.; Quinn, P. J. Surface second harmonic generation (SSHG) - A new scheme for immunoassay. *Biomedical Sensing, Imaging, and Tracking Technologies i* **1996**, *2676*, 290-296.
- (84) Ditcham, W. G. F.; Al-Obaidi, A. H. R.; McStay, D.; Mottram, T. T.; Brownlie, J.; Thompson, I. An immunosensor with potential for the detection of viral antigens in body fluids, based on surface second harmonic generation. *Biosens. Bioelectron.* **2001**, *16*, 221-224.
- (85) Barad, Y.; Eisenberg, H.; Horowitz, M.; Silberberg, Y. Nonlinear scanning laser microscopy by third harmonic generation. *Appl. Phys. Lett.* **1997**, *70*, 922-924.
- (86) Yelin, D.; Silberberg, Y. Laser scanning third-harmonic-generation microscopy in biology. *Optics Express* **1999**, *5*, 169-175.
- (87) Chasles, F.; Dubertret, B.; Boccara, A. C. Optimization and characterization of a structured illumination microscope. *Optics Express* **2007**, *15*, 16130-16140.

- (88) Neil, M. A. A.; Juskaitis, R.; Wilson, T. Method of obtaining optical sectioning by using structured light in a conventional microscope. *Optics Letters* **1997**, *22*, 1905-1907.
- (89) Hell, S.; Stelzer, E. H. K. Properties of a 4pi Confocal Fluorescence Microscope. *Journal of the Optical Society of America A-Optics Image Science and Vision* **1992**, *9*, 2159-2166.
- (90) Gustafsson, M. G. L.; Agard, D. A.; Sedat, J. W. (IM)-M-5: 3D widefield light microscopy with better than 100 nm axial resolution. *J. Microsc. -Oxf.* **1999**, *195*, 10-16.
- (91) Bewersdorf, J.; Schmidt, R.; Hell, S. W. Comparison of (IM)-M-5 and 4Pi-microscopy. *J. Microsc. -Oxf.* **2006**, *222*, 105-117.
- (92) Harke, B.; Keller, J.; Ullal, C. K.; Westphal, V.; Schoenle, A.; Hell, S. W. Resolution scaling in STED microscopy. *Opt. Express* **2008**, *16*, 4154-4162.
- (93) Yalow, R. S.; Berson, S. A. Assay of Plasma Insulin in Human Subjects by Immunological Methods. *Nature* **1959**, *184*, 1648-1649.
- (94) Yalow, R. S.; Berson, S. A. Immunoassay of Endogenous Plasma Insulin in Man. *J. Clin. Invest.* **1960**, *39*, 1157-1175.
- (95) Ekins, R. P. The Estimation of Thyroxine in Human Plasma by an Electrophoretic Technique. *Clinica Chimica Acta* **1960**, *5*, 453-459.
- (96) Price, C. P.; Newman, D. J. In *Principles and practice of immunoassay*; Macmillan Reference: Basingstoke, 1997; .
- (97) Zhao, L.; Sun, L.; Chu, X. Chemiluminescence immunoassay. *TrAC Trends in Analytical Chemistry* **2009**, *28*, 404-415.
- (98) Ronald, A.; Stimson, W. H. The evolution of immunoassay technology. *Parasitology* **1998**, *117*, S13-S27.
- (99) Vanweeme, Bk; Schuurs, A. H. W. Immunoassay using Antigen-Enzyme Conjugates. *FEBS Lett.* **1971**, *15*, 232-&.
- (100) Stimson, W. H.; Sinclair, J. M. Immunoassay for a Pregnancy-Associated Alpha-Macroglobulin using Antibody - Enzyme Conjugates. *FEBS Lett.* **1974**, *47*, 190-192.
- (101) Aalberse, R. C. Quantitative Fluoroimmunoassay. *Clin. Chim. Acta* **1973**, *48*, 109-111.
- (102) Capel, P. J. A. Quantitative Immunofluorescence Method Based on Covalent Coupling of Protein to Sepharose Beads. *J. Immunol. Methods* **1974**, *5*, 165-178.

- (103) Schroeder, H. R.; Vogelhut, P. O.; Carrico, R. J.; Bogulaski, R. C.; Buckler, R. T. Competitive Protein-Binding Assay for Biotin Monitored by Chemiluminescence. *Anal. Chem.* **1976**, *48*, 1933-1937.
- (104) Johnstone, A.; Turner, M. W. In *Immunochemistry : a practical approach*; Practical approach series; IRL at Oxford University Press: Oxford, 1997; Vol. 178.
- (105) Price, C. P.; Newman, D. J. In *Principles and practice of immunoassay*; Macmillan Reference Ltd: London, 1997; .
- (106) Self, C. H.; Cook, D. B. Advances in immunoassay technology. *Curr. Opin. Biotechnol.* **1996**, *7*, 60-65.
- (107) Ekins, R. P. British Patent Patent 8224600, 1983.
- (108) Kusnezow, W.; Syagailo, Y. V.; Goychuk, I.; Hoheisel, J. D.; Wild, D. G. Antibody microarrays: the crucial impact of mass transport on assay kinetics and sensitivity. *Expert Rev. Mol. Diagn.* **2006**, *6*, 111-124.
- (109) Wild, D. In *The immunoassay handbook*; Wild, D., Ed.; London : Elsevier: Amsterdam, 2005; , pp 930.
- (110) Ekins, R. P.; Chu, F. W. Multianalyte Microspot Immunoassay - Microanalytical Compact-Disk of the Future. *Clin. Chem.* **1991**, *37*, 1955-1967.
- (111) Ghafari, H.; Zhou, Y.; Ali, S.; Hanley, Q. S. Confocal detection of planar homogeneous and heterogeneous immunosorbent assays. *J. Biomed. Opt.* **2009**, *14*, 064022.
- (112) Mellentin-Michelotti, J.; Evangelista, L. T.; Swartzman, E. E.; Miraglia, S. J.; Werner, W. E.; Yuan, P. M. Determination of ligand binding affinities for endogenous seven-transmembrane receptors using fluorometric microvolume assay technology. *Anal. Biochem.* **1999**, *272*, 182-190.
- (113) Komatsu, N.; Shichijo, S.; Maeda, Y.; Itoh, K. Measurement of interferon-gamma by high-throughput fluorometric microvolume assay technology system. *Journal Of Immunological Methods* **2002**, *263*, 169-176.
- (114) Zuck, P.; Lao, Z. G.; Skwish, S.; Glickman, J. F.; Yang, K.; Burbaum, J.; Inglese, J. Ligand-receptor binding measured by laser-scanning imaging. *Proc. Natl. Acad. Sci. U. S. A.* **1999**, *96*, 11122-11127.
- (115) Ekins, R.; Chu, F.; Biggart, E. Development of Microspot Multi-Analyte Ratiometric Immunoassay using Dual Fluorescent-Labeled Antibodies. *Anal. Chim. Acta* **1989**, *227*, 73-96.
- (116) Hanninen, P.; Soini, A.; Meltola, N.; Soini, J.; Soukka, J.; Soini, E. A new microvolume technique for bioaffinity assays using two-photon excitation. *Nat. Biotechnol.* **2000**, *18*, 548-550.

- (117) Dietz, L. J.; Dubrow, R. S.; Manian, B. S.; Sizto, N. L. Volumetric capillary cytometry: A new method for absolute cell enumeration. *Cytometry* **1996**, *23*, 177-186.
- (118) Martens, C.; Bakker, A.; Rodriguez, A.; Mortensen, R. B.; Barrett, R. W. A generic particle-based nonradioactive homogeneous multiplex method for high-throughput screening using microvolume fluorimetry. *Anal. Biochem.* **1999**, *273*, 20-31.
- (119) Heinrich, M. Fluorescent cell-based and bead-based assays for high-throughput screening. *Am. Lab.* **2000**, *32*, 22-+.
- (120) Gerritsen, A. F.; Bosch, M.; de Weers, M.; de Winkel, J. G. J. v.; Parren, P. W. H. I. High throughput screening for antibody induced complement-dependent cytotoxicity in early antibody discovery using homogeneous macroconfocal fluorescence imaging. *J. Immunol. Methods* **2010**, *352*, 140-146.
- (121) Corbett, C. R.; Elias, M. D.; Simpson, L. L.; Yuan, X.; Cassan, R. R.; Ballegeer, E.; Kabani, A.; Plummer, F. A.; Berry, J. D. High-throughput homogeneous immunoassay readily identifies monoclonal antibody to serovariant clostridial neurotoxins. *J. Immunol. Methods* **2007**, *328*, 128-138.
- (122) Lee, J. Y.; Miraglia, S.; Yan, X. W.; Swartzman, E.; Cornell-Kennon, S.; Mellentin-Michelotti, J.; Bruseo, C.; France, D. S. Oncology drug discovery applications using the FMAT (TM) 8100 HTS system. *J. Biomol. Screen.* **2003**, *8*, 81-88.
- (123) Matsukuma, E.; Kato, Z.; Omoya, K.; Hashimoto, K.; Li, A.; Yamamoto, Y.; Ohnishi, H.; Hiranuma, H.; Komine, H.; Kondo, N. Development of fluorescence-linked immunosorbent assay for high throughput screening of interferon-gamma. *Allergol. Int.* **2006**, *55*, 49-54.
- (124) Komatsu, N.; Shichijo, S.; Maeda, Y.; Itoh, K. Measurement of interferon- γ by high-throughput fluorometric microvolume assay technology system. *J. Immunol. Methods* **2002**, *263*, 169-176.
- (125) Magistrelli, G.; Gueneau, F.; Muslmani, M.; Ravn, U.; Kosco-Vilbois, M.; Fischer, N. Chemokines derived from soluble fusion proteins expressed in *Escherichia coli* are biologically active. *Biochem. Biophys. Res. Commun.* **2005**, *334*, 370-375.
- (126) Hanninen, P.; Soukka, J.; Soini, J. T. Two-photon excitation fluorescence bioassays. *Ann. NY Acad. Sci.* **2008**, *1130*, 320-326.
- (127) Koskinen, J. O.; Vainionpaa, R.; Meltola, N. J.; Soukka, J.; Hanninen, P. E.; Soini, A. E. Rapid method for detection of influenza A and B virus antigens by use of a two-photon excitation assay technique and dry-chemistry reagents. *J. Clin. Microbiol.* **2007**, *45*, 3581-3588.

- (128) Koskinen, J. O.; Vaarnor, J.; Vainionpaa, R.; Soini, A. E. A novel separation-free assay technique for serum antibodies using antibody bridging assay principle and two-photon excitation fluorometry. *Clinica Chimica Acta* **2005**, *355*, S142-S142.
- (129) Koskinen, J. O.; Vaarno, J.; Meltola, N. J.; Soini, J. T.; Hänninen, P. E.; Luotola, J.; Waris, M. E.; Soini, A. E. Fluorescent nanoparticles as labels for immunometric assay of C-reactive protein using two-photon excitation assay technology. *Anal. Biochem.* **2004**, *328*, 210-218.
- (130) Vaarno, J.; Ylikoski, E.; Meltola, N. J.; Soini, J. T.; Hanninen, P.; Lahesmaa, R.; Soini, A. E. New separation-free assay technique for SNPs using two-photon excitation fluorometry. *Nucleic Acids Res.* **2004**, *32*, e108.
- (131) Bacarese-Hamilton, T.; Mezzasoma, L.; Ardizzoni, A.; Bistoni, F.; Crisanti, A. Serodiagnosis of infectious diseases with antigen microarrays. *Journal Of Applied Microbiology* **2004**, *96*, 10-17.
- (132) Sun, B. Q.; Xie, W. Z.; Yi, G. S.; Chen, D. P.; Zhou, Y. X.; Cheng, J. Microminiaturized immunoassays using quantum dots as fluorescent label by laser confocal scanning fluorescence detection. *Journal Of Immunological Methods* **2001**, *249*, 85-89.
- (133) Aoki, T.; Tsuchida, S.; Yahara, T.; Hamaue, N. Novel assays for proteases using green fluorescent protein-tagged substrate immobilized on a membrane disk. *Analytical Biochemistry* **2008**, *378*, 132-137.
- (134) Ghany, M. G.; Strader, D. B.; Thomas, D. L.; Seeff, L. B. Diagnosis, Management, and Treatment of Hepatitis C: An Update. *Hepatology* **2009**, *49*, 1335-1374.
- (135) Majid, A. M.; Gretch, D. R. Current and future hepatitis C virus diagnostic testing: problems and advancements. *Microb. Infect.* **2002**, *4*, 1227-1236.
- (136) Irshad, M.; Dhar, I. Hepatitis C virus core protein: An update on its molecular biology, cellular functions and clinical implications. *Medical Principles and Practice* **2006**, *15*, 405-416.
- (137) Choo, Q. L.; Kuo, G.; Weiner, A. J.; Overby, L. R.; Bradley, D. W.; Houghton, M. Isolation of a Cdna Clone Derived from a Blood-Borne Non-A, Non-B Viral-Hepatitis Genome. *Science* **1989**, *244*, 359-362.
- (138) Seme, K.; Poljak, M.; Babic, D. Z.; Mocilnik, T.; Vince, A. The role of core antigen detection in management of hepatitis C: a critical review. *Journal of Clinical Virology* **2005**, *32*, 92-101.
- (139) Irving, W. L. The role of the virology laboratory in the management of hepatitis C virus infection. *Journal of Clinical Virology* **2002**, *25*, 3-13.

- (140) Fabrizi, F.; Lunghi, G.; Aucella, F.; Mangano, S.; Barbisoni, F.; Bisegna, S.; Vigilante, D.; Limido, A.; Martin, P. Novel assay using total hepatitis C virus (HCV) core antigen quantification for diagnosis of HCV infection in dialysis patients. *J. Clin. Microbiol.* **2005**, *43*, 414-420.
- (141) Aoyagi, K.; Ohue, C.; Iida, K.; Kimura, T.; Tanaka, E.; Kiyosawa, K.; Yagi, S. Development of a simple and highly sensitive enzyme immunoassay for hepatitis C virus core antigen. *J. Clin. Microbiol.* **1999**, *37*, 1802-1808.
- (142) Lok, A. S. F.; Gunaratnam, N. T. Diagnosis of hepatitis C. *Hepatology* **1997**, *26*, S48-S56.
- (143) Richter, S. S. Laboratory assays for diagnosis and management of hepatitis C virus infection. *J. Clin. Microbiol.* **2002**, *40*, 4407-4412.
- (144) Cunningham, E.; Campbell, C. J. A novel self-assembled nanoparticulate film for covalent attachment of antibodies to plastic. *Langmuir* **2003**, *19*, 4509-4511.
- (145) Wadu-Mesthrige, K.; Amro, N. A.; Garno, J. C.; Xu, S.; Liu, G. Y. Fabrication of nanometer-sized protein patterns using atomic force microscopy and selective immobilization. *Biophysical Journal* **2001**, *80*, 1891-1899.
- (146) Fan, F. R. F.; Bard, A. J. Imaging of biological macromolecules on mica in humid air by scanning electrochemical microscopy. *Proc. Natl. Acad. Sci. U. S. A.* **1999**, *96*, 14222-14227.
- (147) Donnert, G.; Keller, J.; Medda, R.; Andrei, M. A.; Rizzoli, S. O.; Lurmann, R.; Jahn, R.; Eggeling, C.; Hell, S. W. Macromolecular-scale resolution in biological fluorescence microscopy. *Proceedings Of The National Academy Of Sciences Of The United States Of America* **2006**, *103*, 11440-11445.
- (148) Lee, C. S.; Lee, S. H.; Kim, Y. G.; Lee, J. H.; Kim, Y. K.; Kim, B. G. A method of binding kinetics of a ligand to micropatterned proteins on a microfluidic chip. *Biosens. Bioelectron.* **2007**, *22*, 891-898.
- (149) A.W. Adamson, A. P. G. In *Physical Chemistry of Surfaces*; Wiley: New York, 1997; .
- (150) Zucker, R. M. Evaluation of confocal microscopy system performance. *Methods Mol Biol* **2006**, *319*, 77-135.
- (151) Zucker, R. M. Quality assessment of confocal microscopy slide based systems: Performance. *Cytom. Part A* **2006**, *69A*, 659-676.
- (152) Martinez, J. S.; Grace, W. K.; Grace, K. M.; Hartman, N.; Swanson, B. I. Pathogen detection using single mode planar optical waveguides. *Journal Of Materials Chemistry* **2005**, *15*, 4639-4647.

- (153) Pawlak, M.; Schick, E.; Bopp, M. A.; Schneider, M. J.; Oroszlan, P.; Ehrat, M. Zeptosens' protein microarrays: A novel high performance microarray platform for low abundance protein analysis. *Proteomics* **2002**, *2*, 383-393.
- (154) Wilson, T.; Juskaitis, R.; Neil, M. A. A.; Kozubek, M. Confocal microscopy by aperture correlation. *Opt. Lett.* **1996**, *21*, 1879-1881.
- (155) Tanaami, T.; Otsuki, S.; Tomosada, N.; Kosugi, Y.; Shimizu, M.; Ishida, H. High-speed 1-frame/ms scanning confocal microscope with a microlens and Nipkow disks. *Appl. Optics* **2002**, *41*, 4704-4708.
- (156) Neil, M. A. A.; Juskaitis, R.; Wilson, T. Method of obtaining optical sectioning by using structured light in a conventional microscope. *Opt. Lett.* **1997**, *22*, 1905-1907.
- (157) Karadagic, D.; Wilson, T. Image formation in structured illumination wide-field fluorescence microscopy. *Micron* **2008**, *39*, 808-818.
- (158) Seydack, M. Nanoparticle labels in immunosensing using optical detection methods. *Biosens. Bioelectron.* **2005**, *20*, 2454-2469.
- (159) Prix, L.; Uciechowski, P.; Bockmann, B.; Giesing, M.; Schuetz, A. J. Diagnostic biochip array for fast and sensitive detection of K-ras mutations in stool. *Clinical Chemistry* **2002**, *48*, 428-435.
- (160) Souplet, V.; Desmet, R.; Melnyk, O. Imaging of protein layers with an optical microscope for the characterization of peptide microarrays. *Journal Of Peptide Science* **2007**, *13*, 451-457.
- (161) Gu, Q.; Sivanandam, T. M.; Kim, C. A. Signal stability of Cy3 and Cy5 on antibody microarrays. *Proteome Sci* **2006**, *4*, 21.
- (162) Hanninen, P.; Waris, M.; Kettunen, M.; Soini, E. Reaction kinetics of a two-photon excitation microparticle based immunoassay-from modelling to practice. *Biophys. Chem.* **2003**, *105*, 23-28.
- (163) Arndt-Jovin, D. J.; Kantelhardt, S. R.; Caarls, W.; de Vries, A. H. B.; Giese, A.; Jovin, T. M. Tumor-Targeted Quantum Dots Can Help Surgeons Find Tumor Boundaries. *IEEE Trans. Nanobiosci.* **2009**, *8*, 65-71.
- (164) Masalova, O. V.; Atanadze, S. N.; Samokhvalov, E. I.; Petrakova, N. V.; Kalinina, T. I.; Smirnov, V. D.; Khudyakov, Y. E.; Fields, H. A.; Kushch, A. A. Detection of hepatitis C virus core protein circulating within different virus particle populations. *J. Med. Virol.* **1998**, *55*, 1-6.
- (165) Lorenzo, J.; Castro, A.; Aguilera, A.; Prieto, E.; Lopez-Calvo, S.; Regueiro, B.; Pedreira, J. Total HCV core antigen assay - A new marker of HCV viremia and its application during treatment of chronic hepatitis C. *J. Virol. Methods* **2004**, *120*, 173-177.

- (166) Braden, B. C.; Poljak, R. J. Structural Features of the Reactions - between Antibodies and Protein Antigens. *Faseb Journal* **1995**, *9*, 9-16.
- (167) Zhuang, G. Q.; Katakura, Y.; Omasa, T.; Kishimoto, M.; Suga, K. I. Measurement of association rate constant of antibody-antigen interaction in solution based on enzyme-linked immunosorbent assay. *J. Biosci. Bioeng.* **2001**, *92*, 330-336.
- (168) Zuber, E.; Mathis, G.; Flandrois, J. P. Homogeneous two-site immunometric assay kinetics as a theoretical tool for data analysis. *Anal. Biochem.* **1997**, *251*, 79-88.
- (169) Schuck, P. Kinetics of ligand binding to receptor immobilized in a polymer matrix, as detected with an evanescent wave biosensor .1. A computer simulation of the influence of mass transport. *Biophys. J.* **1996**, *70*, 1230-1249.
- (170) Stenberg, M.; Nygren, H. Kinetics of Antigen-Antibody Reactions at Solid-Liquid Interfaces. *J. Immunol. Methods* **1988**, *113*, 3-15.
- (171) Glaser, R. W. Antigen-Antibody Binding and Mass-Transport by Convection and Diffusion to a Surface - a 2-Dimensional Computer-Model of Binding and Dissociation Kinetics. *Anal. Biochem.* **1993**, *213*, 152-161.
- (172) Nygren, H.; Stenberg, M. Kinetics of Antibody-Binding to Surface-Immobilized Antigen - Influence of Mass-Transport on the Enzyme-Linked Immunosorbent-Assay (Elisa). *J. Colloid Interface Sci.* **1985**, *107*, 560-566.
- (173) Nygren, H.; Werthen, M.; Stenberg, M. Kinetics of Antibody-Binding to Solid-Phase-Immobilized Antigen - Effect of Diffusion Rate Limitation and Steric Interaction. *J. Immunol. Methods* **1987**, *101*, 63-71.
- (174) Stenberg, M.; Stibler, L.; Nygren, H. External Diffusion in Solid-Phase Immunoassays. *J. Theor. Biol.* **1986**, *120*, 129-140.
- (175) Stenberg, M.; Werthen, M.; Theander, S.; Nygren, H. A Diffusion Limited Reaction Theory for a Microtiter Plate Assay. *J. Immunol. Methods* **1988**, *112*, 23-29.
- (176) Berg, O. G.; Vonhippel, P. H. Diffusion-Controlled Macromolecular Interactions. *Annu. Rev. Biophys. Biophys. Chem.* **1985**, *14*, 131-160.
- (177) Nygren, H.; Stenberg, M. Immunochemistry at Interfaces. *Immunology* **1989**, *66*, 321-327.
- (178) Northrup, S. H.; Erickson, H. P. Kinetics of Protein Protein Association Explained by Brownian Dynamics Computer-Simulation. *Proc. Natl. Acad. Sci. U. S. A.* **1992**, *89*, 3338-3342.
- (179) Karlsson, R.; Roos, H.; Fagerstam, L.; Persson, B. Kinetic and concentration analysis using BIA technology. *Methods (Orlando)* **1994**, *6*, 99-110.

- (180) Chaiken, I.; Rose, S.; Karlsson, R. Quantitative-Analysis of Protein-Interaction with Ligands .2. Analysis of Macromolecular Interactions using Immobilized Ligands. *Anal. Biochem.* **1992**, *201*, 197-210.
- (181) Green, R. J.; Frazier, R. A.; Shakesheff, K. M.; Davies, M. C.; Roberts, C. J.; Tendler, S. J. B. Surface plasmon resonance analysis of dynamic biological interactions with biomaterials. *Biomaterials* **2000**, *21*, 1823-1835.
- (182) Azimzadeh, A.; Van Regenmortel, M. H. Antibody affinity measurements. *J. Mol. Recognit.* **1990**, *3*, 108-116.
- (183) Wild, D. In *The immunoassay handbook*; Macmillan: Basingstoke, 1994; .
- (184) Wiseman, T.; Williston, S.; Brandts, J. F.; Lin, L. N. Rapid Measurement of Binding Constants and Heats of Binding using a New Titration Calorimeter. *Anal. Biochem.* **1989**, *179*, 131-137.
- (185) Selvi, P. T.; Ashish, B.; Murthy, G. S. Determination of thermodynamic parameters of antigen-antibody interaction from real-time kinetic studies. *Curr. Sci.* **2002**, *82*, 1442-1448.
- (186) Roos, H.; Karlsson, R.; Nilshans, H.; Persson, A. Thermodynamic analysis of protein interactions with biosensor technology. *Journal of Molecular Recognition* **1998**, *11*, 204-210.
- (187) Voss, E. W. J. Kinetic Measurements of Molecular Interactions by Spectrofluorometry. *Journal of Molecular Recognition* **1993**, *6*, 51-58.
- (188) Beatty, J. D.; Beatty, B. G.; Vlahos, W. G. Measurement of Monoclonal-Antibody Affinity by Noncompetitive Enzyme-Immunoassay. *J. Immunol. Methods* **1987**, *100*, 173-179.
- (189) Friguet, B.; Chaffotte, A. F.; Djavadiohanian, L.; Goldberg, M. E. Measurements of the True Affinity Constant in Solution of Antigen-Antibody Complexes by Enzyme-Linked Immunosorbent-Assay. *J. Immunol. Methods* **1985**, *77*, 305-319.
- (190) Stevens, F. J. Modification of an Elisa-Based Procedure for Affinity Determination - Correction Necessary for use with Bivalent Antibody. *Mol. Immunol.* **1987**, *24*, 1055-1060.
- (191) Hardy, F.; DjavadiOhanian, L.; Goldberg, M. E. Measurement of antibody/antigen association rate constants in solution by a method based on the enzyme-linked immunosorbent assay. *J. Immunol. Methods* **1997**, *200*, 155-159.
- (192) Checovich, W. J.; Bolger, R. E.; Burke, T. Fluorescence Polarization - a New Tool for Cell and Molecular-Biology. *Nature* **1995**, *375*, 254-256.

- (193) Tengerdy, R. P. Reaction Kinetic Studies of Antigen Antibody Reaction. *Journal of Immunology* **1967**, *99*, 126-&.
- (194) Haber, E.; Bennett, J. C. Polarization of Fluorescence as a Measure of Antigen-Antibody Interaction. *Proc. Natl. Acad. Sci. U. S. A.* **1962**, *48*, 1935-&.
- (195) Krichevsky, O.; Bonnet, G. Fluorescence correlation spectroscopy: the technique and its applications. *Rep. Prog. Phys.* **2002**, *65*, 251-297.
- (196) Haustein, E.; Schwille, P. Fluorescence correlation spectroscopy: Novel variations of an established technique. *Annu. Rev. Biophys. Biomol. Struct.* **2007**, *36*, 151-169.
- (197) Thompson, N. L.; Lieto, A. M.; Allen, N. W. Recent advances in fluorescence correlation spectroscopy. *Curr. Opin. Struct. Biol.* **2002**, *12*, 634-641.
- (198) Berland, K. M.; So, P. T. C.; Gratton, E. 2-Photon Fluorescence Correlation Spectroscopy - Method and Application to the Intracellular Environment. *Biophys. J.* **1995**, *68*, 694-701.
- (199) Korlach, J.; Schwille, P.; Webb, W. W.; Feigenson, G. W. Characterization of lipid bilayer phases by confocal microscopy and fluorescence correlation spectroscopy. *Proc. Natl. Acad. Sci. U. S. A.* **1999**, *96*, 8461-8466.
- (200) Gell, C.; Brockwell, D. J.; Beddard, G. S.; Radford, S. E.; Kalverda, A. P.; Smith, D. A. Accurate use of single molecule fluorescence correlation spectroscopy to determine molecular diffusion times. *Single Molecules* **2001**, *2*, 177-181.
- (201) Schwille, P.; Bieschke, J.; Oehlenschlager, F. Kinetic investigations by fluorescence correlation spectroscopy: The analytical and diagnostic potential of diffusion studies. *Biophys. Chem.* **1997**, *66*, 211-228.
- (202) Heinze, K. G.; Rarbach, M.; Jahnz, M.; Schwille, P. Two-photon fluorescence coincidence analysis: Rapid measurements of enzyme kinetics. *Biophys. J.* **2002**, *83*, 1671-1681.
- (203) Briddon, S. J.; Hill, S. J. Pharmacology under the microscope: the use of fluorescence correlation spectroscopy to determine the properties of ligand-receptor complexes. *Trends Pharmacol. Sci.* **2007**, *28*, 637-645.
- (204) Xie, C.; Dong, C. Q.; Ren, J. C. Study on homogeneous competitive immune reaction by fluorescence correlation spectroscopy: Using synthetic peptide as antigen. *Talanta* **2009**, *79*, 971-974.
- (205) Widengren, J.; Schwille, P. Characterization of photoinduced isomerization and back-isomerization of the cyanine dye Cy5 by fluorescence correlation spectroscopy. *Journal of Physical Chemistry a* **2000**, *104*, 6416-6428.

- (206) Periasamy, A.; Day, R. N. Visualizing protein interactions in living cells using digitized GFP imaging and FRET microscopy. *Methods in Cell Biology, Vol 58* **1999**, 58, 293-+.
- (207) Hutchinson, A. M. Evanescent-Wave Biosensors - Real-Time Analysis of Biomolecular Interactions. *Mol. Biotechnol.* **1995**, 3, 47-54.
- (208) Bernard, A.; Bosshard, H. R. Real-Time Monitoring of Antigen-Antibody Recognition on a Metal-Oxide Surface by an Optical Grating Coupler Sensor. *European Journal of Biochemistry* **1995**, 230, 416-423.
- (209) Buijs, J.; vandenBerg, P. A. W.; Lichtenbelt, J. W. T.; Norde, W.; Lyklema, J. Adsorption dynamics of IgG and its F(ab')(2) and Fc fragments studied by reflectometry. *J. Colloid Interface Sci.* **1996**, 178, 594-605.
- (210) Valenti, L. E.; Fiorito, P. A.; Garcia, C. D.; Giacomelli, C. E. The adsorption-desorption process of bovine serum albumin on carbon nanotubes. *J. Colloid Interface Sci.* **2007**, 307, 349-356.
- (211) Riquelme, B. D.; Valverde, J. R.; Rasia, R. J. Kinetic study of antibody adhesion on a silicon wafer by laser reflectometry. *Optics and Lasers in Engineering* **2003**, 39, 589-598.
- (212) Bosker, W. T. E.; Iakovlev, P. A.; Norde, W.; Stuart, M. A. C. BSA adsorption on bimodal PEO brushes. *J. Colloid Interface Sci.* **2005**, 286, 496-503.
- (213) Buron, C. C.; Filiatre, C.; Membrey, F.; Perrot, H.; Foissy, A. Mass and charge balance in self-assembled multilayer films on gold. Measurements with optical reflectometry and quartz crystal microbalance. *J. Colloid Interface Sci.* **2006**, 296, 409-418.
- (214) Collings, A. F.; Caruso, F. Biosensors: recent advances. *Rep. Prog. Phys.* **1997**, 60, 1397-1445.
- (215) Cuypers, P. A.; Hermens, W. T.; Hemker, H. C. Ellipsometry as a Tool to Study Protein Films at Liquid-Solid Interfaces. *Anal. Biochem.* **1978**, 84, 56-67.
- (216) Vroman, L.; Adams, A. L. Findings with the recording ellipsometer suggesting rapid exchange of specific plasma proteins at liquid/solid interfaces. *Surf. Sci.* **1969**, 16, 438-446.
- (217) Nygren, H. Kinetics of Antibody-Binding to Surface-Immobilized Antigen - Analysis of Data and an Empiric Model. *Biophys. Chem.* **1994**, 52, 45-50.
- (218) North, J. R. Immunosensors - Antibody-Based Biosensors. *Trends Biotechnol.* **1985**, 3, 180-186.
- (219) Proll, G.; Kumpf, M.; Mehlmann, M.; Tschmelak, J.; Griffith, H.; Abuknesha, R.; Gauglitz, G. Monitoring an antibody affinity chromatography with a label-free optical biosensor technique. *J. Immunol. Methods* **2004**, 292, 35-42.

- (220) Garland, P. B. Optical evanescent wave methods for the study of biomolecular interactions. *Q. Rev. Biophys.* **1996**, *29*, 91-117.
- (221) Bluestein, B. I.; Walczak, I. M.; Chen, S. Y. Fiber Optic Evanescent Wave Immunosensors for Medical Diagnostics. *Trends Biotechnol.* **1990**, *8*, 161-168.
- (222) Schuck, P. Use of surface plasmon resonance to probe the equilibrium and dynamic aspects of interactions between biological macromolecules. *Annu. Rev. Biophys. Biomol. Struct.* **1997**, *26*, 541-566.
- (223) Englebienne, P.; Van Hoonacker, A.; Verhas, M. Surface plasmon resonance: principles, methods and applications in biomedical sciences. *Spectr. -Int. J.* **2003**, *17*, 255-273.
- (224) Mitchell, J. Small Molecule Immunosensing Using Surface Plasmon Resonance. *Sensors* **2010**, *10*, 7323-7346.
- (225) Pattnaik, P. Surface plasmon resonance - Applications in understanding receptor-ligand interaction. *Appl. Biochem. Biotechnol.* **2005**, *126*, 79-92.
- (226) Thillaivinayagalingam, P.; Gommeaux, J.; McLoughlin, M.; Collins, D.; Newcombe, A. R. Biopharmaceutical production: Applications of surface plasmon resonance biosensors. *J. Chromatogr. B* **2010**, *878*, 149-153.
- (227) Schmitt, K.; Oehse, K.; Sulz, G.; Hoffmann, C. Evanescent field sensors based on tantalum pentoxide waveguides - A review. *Sensors* **2008**, *8*, 711-738.
- (228) Cush, R.; Cronin, J. M.; Stewart, W. J.; Maule, C. H.; Molloy, J.; Goddard, N. J. The Resonant Mirror - a Novel Optical Biosensor for Direct Sensing of Biomolecular Interactions .1. Principle of Operation and Associated Instrumentation. *Biosens. Bioelectron.* **1993**, *8*, 347-353.
- (229) Mukundan, H.; Anderson, A. S.; Grace, W. K.; Grace, K. M.; Hartman, N.; Martinez, J. S.; Swanson, B. I. Waveguide-Based Biosensors for Pathogen Detection. *Sensors* **2009**, *9*, 5783-5809.
- (230) Kotitz, R.; Weitschies, W.; Trahms, L.; Brewer, W.; Semmler, W. Determination of the binding reaction between avidin and biotin by relaxation measurements of magnetic nanoparticles. *J Magn Magn Mater* **1999**, *194*, 62-68.
- (231) Eberbeck, D.; Bergemann, C.; Wiekhorst, F.; Steinhoff, U.; Trahms, L. Quantification of specific bindings of biomolecules by magnetorelaxometry. *J Nanobiotechnology* **2008**, *6*, 4.
- (232) Hong, C.; Chen, W. S.; Jian, Z. F.; Yang, S. Y.; Horng, H. E.; Yang, L. C.; Yang, H. C. Wash-free immunomagnetic detection for serum through magnetic susceptibility reduction. *Appl. Phys. Lett.* **2007**, *90*, 074105.

- (233) Eberbeck, D.; Wiekhorst, F.; Steinhoff, U.; Trahms, L. Quantification of biomolecule agglutination by magnetorelaxometry. *Appl. Phys. Lett.* **2009**, *95*, 213701.
- (234) Gill, A.; Leatherbarrow, R. J.; Hoare, M.; PollardKnight, D. V.; Lowe, P. A.; Fortune, D. H. Analysis of kinetic data of antibody-antigen interaction from an optical biosensor by exponential curve fitting. *J. Biotechnol.* **1996**, *48*, 117-127.
- (235) Oshannessy, D. J.; Brighamburke, M.; Soneson, K. K.; Hensley, P.; Brooks, I. Determination of Rate and Equilibrium Binding Constants for Macromolecular Interactions using Surface-Plasmon Resonance - use of Nonlinear Least-Squares Analysis-Methods. *Anal. Biochem.* **1993**, *212*, 457-468.
- (236) Edwards, P. R.; Gill, A.; Pollardknight, D. V.; Hoare, M.; Buckle, P. E.; Lowe, P. A.; Leatherbarrow, R. J. Kinetics of Protein-Protein Interactions at the Surface of an Optical Biosensor. *Anal. Biochem.* **1995**, *231*, 210-217.
- (237) Rodbard, D.; Feldman, Y. Kinetics of 2-Site Immunoradiometric (Sandwich) Assays .1. Mathematical-Models for Simulation, Optimization, and Curve Fitting. *Immunochemistry* **1978**, *15*, 71-76.
- (238) OShannessy, D. J.; Winzor, D. J. Interpretation of deviations from pseudo-first-order kinetic behavior in the characterization of ligand binding by biosensor technology. *Anal. Biochem.* **1996**, *236*, 275-283.
- (239) Bowles, M. R.; Hall, D. R.; Pond, S. M.; Winzor, D. J. Studies of protein interactions by biosensor technology: An alternative approach to the analysis of sensorgrams deviating from pseudo-first-order kinetic behavior. *Anal. Biochem.* **1997**, *244*, 133-143.
- (240) Invitrogen, L. Qdot® Secondary Antibody Conjugates. <http://probes.invitrogen.com/media/pis/mp11001.pdf> (accessed October-2007, 2007).
- (241) Rochira, J. A.; Gudheti, M. V.; Gould, T. J.; Laughlin, R. R.; Nadeau, J. L.; Hess, S. T. Fluorescence intermittency limits brightness in CdSe/ZnS nanoparticles quantified by fluorescence correlation spectroscopy. *Journal of Physical Chemistry C* **2007**, *111*, 1695-1708.
- (242) Taitt, C. R.; Anderson, G. P.; Ligler, F. S. Evanescent wave fluorescence biosensors. *Biosens. Bioelectron.* **2005**, *20*, 2470-2487.
- (243) Butler, J. E. Solid supports in enzyme-linked immunosorbent assay and other solid-phase immunoassays. *Methods* **2000**, *22*, 4-23.
- (244) Cummins, C. M.; Koivunen, M. E.; Stephanian, A.; Gee, S. J.; Hammock, B. D.; Kennedy, I. M. Application of europium(III) chelate-dyed nanoparticle labels in a competitive atrazine fluoroimmunoassay on an ITO waveguide. *Biosens. Bioelectron.* **2006**, *21*, 1077-1085.

- (245) Soukka, T.; Harma, H.; Paukkunen, J.; Lovgren, T. Utilization of kinetically enhanced monovalent binding affinity by immunoassays based on multivalent nanoparticle-antibody bioconjugates. *Anal. Chem.* **2001**, *73*, 2254-2260.
- (246) Park, J. J.; Lacerda, S. H. D. P.; Stanley, S. K.; Vogel, B. M.; Kim, S.; Douglas, J. F.; Raghavan, D.; Karim, A. Langmuir Adsorption Study of the Interaction of CdSe/ZnS Quantum Dots with Model Substrates: Influence of Substrate Surface Chemistry and pH. *Langmuir* **2009**, *25*, 443-450.
- (247) Chan, W. C. W.; Nie, S. M. Quantum dot bioconjugates for ultrasensitive nonisotopic detection. *Science* **1998**, *281*, 2016-2018.
- (248) Hall, M.; Kazakova, I.; Yao, Y. M. High sensitivity immunoassays using particulate fluorescent labels. *Anal. Biochem.* **1999**, *272*, 165-170.
- (249) Soukka, T.; Paukkunen, J.; Harma, H.; Lonnberg, S.; Lindroos, H.; Lovgren, T. Supersensitive time-resolved immunofluorometric assay of free prostate-specific antigen with nanoparticle label technology. *Clin. Chem.* **2001**, *47*, 1269-1278.
- (250) Valanne, A.; Huopalahti, S.; Vainionpaa, R.; Harma, H.; Lovgren, T. Rapid and sensitive HBsAg immunoassay based on fluorescent nanoparticle labels and time-resolved detection. *J. Virol. Methods* **2005**, *129*, 83-90.
- (251) Lin, C. H.; Chen, H. Y.; Yu, C. J.; Lu, P. L.; Hsieh, C. H.; Hsieh, B. Y.; Chang, Y. F.; Chou, C. Quantitative measurement of binding kinetics in sandwich assay using a fluorescence detection fiber-optic biosensor. *Anal. Biochem.* **2009**, *385*, 224-228.
- (252) Chou, C.; Hsu, H. Y.; Wu, H. T.; Tseng, K. Y.; Chiou, A.; Yu, C. J.; Lee, Z. Y.; Chan, T. S. Fiber optic biosensor for the detection of C-reactive protein and the study of protein binding kinetics. *J. Biomed. Opt.* **2007**, *12*.
- (253) Schuck, P.; Minton, A. P. Analysis of mass transport-limited binding kinetics in evanescent wave biosensors. *Anal. Biochem.* **1996**, *240*, 262-272.
- (254) Dmitriev, D. A.; Massino, Y. S.; Segal, O. L. Kinetic analysis of interactions between bispecific monoclonal antibodies and immobilized antigens using a resonant mirror biosensor. *J. Immunol. Methods* **2003**, *280*, 183-202.
- (255) Soman, C.; Giorgio, T. Kinetics of Molecular Recognition Mediated Nanoparticle Self-Assembly. *Nano Research* **2009**, *2*, 78-84.
- (256) Visser, T. D.; Oud, J. L. Volume Measurements in 3-Dimensional Microscopy. *Scanning* **1994**, *16*, 198-200.
- (257) Kuypers, L. C.; Decraemer, W. F.; Dirckx, J. J. J.; Timmermans, J. P. A procedure to determine the correct thickness of an object with confocal microscopy in case of refractive index mismatch. *J. Microsc. -Oxf.* **2005**, *218*, 68-78.

- (258) Visser, T. D.; Oud, J. L.; Brakenhoff, G. J. Refractive-Index and Axial Distance Measurements in 3-D Microscopy. *Optik* **1992**, *90*, 17-19.
- (259) Diaspro, A.; Federici, F.; Robello, M. Influence of refractive-index mismatch in high-resolution three-dimensional confocal microscopy. *Appl. Opt.* **2002**, *41*, 685-690.
- (260) Wan, D. S.; Rajadhyaksha, M.; Webb, R. H. Analysis of spherical aberration of a water immersion objective: application to specimens with refractive indices 1.33-1.40. *J. Microsc. -Oxf.* **2000**, *197*, 274-284.
- (261) Egner, Alexander and Hell, Stefan W. In *Aberrations in confocal and multi-photon fluorescence microscopy induced by refractive index mismatch*; Pawley, J. B. (.), Ed.; Handbook of Biological Confocal Microscopy; Springer: 2006; pp 404-413; 20.
- (262) Flournoy, P. A.; Wyntjes, G.; McClure, R. W. White-Light Interferometric Thickness Gauge. *Appl. Opt.* **1972**, *11*, 1907-&.
- (263) Youngquist, R. C.; Carr, S.; Davies, D. E. N. Optical Coherence-Domain Reflectometry - a New Optical Evaluation Technique. *Opt. Lett.* **1987**, *12*, 158-160.
- (264) Danielson, B. L.; Boisrobert, C. Y. Absolute Optical Ranging using Low Coherence Interferometry. *Appl. Opt.* **1991**, *30*, 2975-2979.
- (265) Cox, G.; Sheppard, C. J. R. Measurement of thin coatings in the confocal microscope. *Micron* **2001**, *32*, 701-705.
- (266) Ilev, I. K.; Waynant, R. W.; Byrnes, K. R.; Anders, J. J. Dual-confocal fiber-optic method for absolute measurement of refractive index and thickness of optically transparent media. *Opt. Lett.* **2002**, *27*, 1693-1695.
- (267) Fukano, T.; Yamaguchi, I. Simultaneous measurement of thicknesses and refractive indices of multiple layers by a low-coherence confocal interference microscope. *Opt. Lett.* **1996**, *21*, 1942-1944.
- (268) Kim, S.; Na, J.; Kim, M. J.; Lee, B. H. Simultaneous measurement of refractive index and thickness by combining low-coherence interferometry and confocal optics. *Opt. Express* **2008**, *16*, 5516-5526.
- (269) Sheppard, C. J. R.; Connolly, T. J.; Lee, J.; Cogswell, C. J. CONFOCAL IMAGING OF A STRATIFIED MEDIUM. *Appl. Optics* **1994**, *33*, 631-640.
- (270) Rajadhyaksha, M.; Gonzalez, S.; Zavislan, J. M.; Anderson, R. R.; Webb, R. H. In vivo confocal scanning laser microscopy of human skin II: Advances in instrumentation and comparison with histology. *J. Invest. Dermatol.* **1999**, *113*, 293-303.

- (271) Rajadhyaksha, M.; Grossman, M.; Esterowitz, D.; Webb, R. H. In-Vivo Confocal Scanning Laser Microscopy of Human Skin - Melanin Provides Strong Contrast. *J. Invest. Dermatol.* **1995**, *104*, 946-952.
- (272) Lucas, L. J.; Chesler, J. N.; Yoon, J. Y. Lab-on-a-chip immunoassay for multiple antibodies using microsphere light scattering and quantum dot emission. *Biosensors & Bioelectronics* **2007**, *23*, 675-681.
- (273) Peng, C. F.; Li, Z. K.; Zhu, Y. Y.; Chen, W.; Yuan, Y.; Liu, L. Q.; Li, Q. S.; Xu, D. H.; Qiao, R. R.; Wang, L. B.; Zhu, S. F.; Jin, Z. Y.; Xu, C. L. Simultaneous and sensitive determination of multiplex chemical residues based on multicolor quantum dot probes. *Biosensors & Bioelectronics* **2009**, *24*, 3657-3662.
- (274) Goldman, E. R.; Clapp, A. R.; Anderson, G. P.; Uyeda, H. T.; Mauro, J. M.; Medintz, I. L.; Mattoussi, H. Multiplexed toxin analysis using four colors of quantum dot fluororeagents. *Anal. Chem.* **2004**, *76*, 684-688.
- (275) Berggren, W. T.; Takova, T.; Olson, M. C.; Eis, P. S.; Kwiatkowski, R. W.; Smith, L. M. Multiplexed gene expression analysis using the invader RNA assay with MALDI-TOF mass spectrometry detection. *Anal. Chem.* **2002**, *74*, 1745-1750.
- (276) Zhang, X. K.; Elbin, C. S.; Chuang, W. L.; Cooper, S. K.; Marashio, C. A.; Beauregard, C.; Keutzer, J. M. Multiplex enzyme assay screening of dried blood spots for lysosomal storage disorders by using tandem mass spectrometry. *Clin. Chem.* **2008**, *54*, 1725-1728.
- (277) Marshall, D. J.; Reisdorf, E.; Harms, G.; Beaty, E.; Moser, M. J.; Lee, W. M.; Gern, J. E.; Nolte, F. S.; Shult, P.; Prudents, J. R. Evaluation of a multiplexed PCR assay for detection of respiratory viral pathogens in a public health laboratory setting. *J. Clin. Microbiol.* **2007**, *45*, 3875-3882.
- (278) Balboni, I.; Chan, S. M.; Kattah, M.; Tenenbaum, J. D.; Butte, A. J.; Utz, P. J. Multiplexed protein array platforms for analysis of autoimmune diseases. *Annu. Rev. Immunol.* **2006**, *24*, 391-418.
- (279) Park, K. H.; Park, H. G.; Kim, J. H.; Seong, K. H. Poly(dimethyl siloxane)-based protein chip for simultaneous detection of multiple samples: Use of glycidyl methacrylate photopolymer for site-specific protein immobilization. *Biosens. Bioelectron.* **2006**, *22*, 613-620.
- (280) Kellar, K. L.; Kalwar, R. R.; Dubois, K. A.; Crouse, D.; Chafin, W. D.; Kane, B. E. Multiplexed fluorescent bead-based immunoassays for quantitation of human cytokines in serum and culture supernatants. *Cytometry* **2001**, *45*, 27-36.
- (281) Khalifeh, K.; Ranjbar, B. Application of quantum dots in quantitative proteomics for multiplex colour system assay. *Med. Hypotheses* **2006**, *67*, 203-204.

- (282) Sarno, D. M.; Murphy, A. V.; DiVirgilio, E. S.; Jones, W. E.; Ben, R. N. Direct observation of antifreeze glycoprotein-fraction 8 on hydrophobic and hydrophilic interfaces using atomic force microscopy. *Langmuir* **2003**, *19*, 4740-4744.
- (283) Lindsay, S. M.; Lyubchenko, Y. L.; Gall, A. A.; Shlyakhtenko, L. S.; Harrington, R. E. In *IMAGING DNA-MOLECULES CHEMICALLY BOUND TO A MICA SURFACE*; Manne, S., Ed.; Scanning Probe Microscopies; Spie - Int Soc Optical Engineering: Bellingham, 1992; Vol. 1639, pp 84-90.
- (284) Liu, Z. G.; Zu, Y. G.; Fu, Y. J.; Zhang, Z. H.; Meng, R. H. Assembling and Imaging of His-Tag Green Fluorescent Protein on Mica Surfaces Studied by Atomic Force Microscopy and Fluorescence Microscopy. *Microsc. Res. Tech.* **2008**, *71*, 802-809.
- (285) Bezanilla, M.; Manne, S.; Laney, D. E.; Lyubchenko, Y. L.; Hansma, H. G. ADSORPTION OF DNA TO MICA, SILYLATED MICE, AND MINERALS - CHARACTERIZATION BY ATOMIC-FORCE MICROSCOPY. *Langmuir* **1995**, *11*, 655-659.
- (286) Wang, L. K.; Feng, X. Z.; Hou, S.; Chan, Q. L.; Qin, M. Microcontact printing of multiproteins on the modified mica substrate and study of immunoassays. *Surf. Interface Anal.* **2006**, *38*, 44-50.
- (287) Hou, S.; Li, X. X.; Li, X. Y.; Feng, X. Z.; Wang, R.; Wang, C.; Yu, L.; Qiao, M. Q. Surface modification using a novel type I hydrophobin HGFI. *Anal. Bioanal. Chem.* **2009**, *394*, 783-789.
- (288) Qin, M.; Wang, L. K.; Feng, X. Z.; Yang, Y. L.; Wang, R.; Wang, C.; Yu, L.; Shao, B.; Qiao, M. Q. Bioactive surface modification of mica and poly(dimethylsiloxane) with hydrophobins for protein immobilization. *Langmuir* **2007**, *23*, 4465-4471.
- (289) Visser, T. D.; Oud, J. L.; Brakenhoff, G. J. REFRACTIVE-INDEX AND AXIAL DISTANCE MEASUREMENTS IN 3-D MICROSCOPY. *Optik* **1992**, *90*, 17-19.
- (290) Anonymous In *Handbook of mineralogy*; Anthony, J. W., Ed.; Mineral Data: Tucson, 1995; , pp 904.
- (291) Lyubchenko, Y. L.; Gall, A. A.; Shlyakhtenko, L. S. Atomic force microscopy of DNA and protein-DNA complexes using functionalized mica substrates. *Methods Mol Biol* **2001**, *148*, 569-78.
- (292) Li, J. R.; Henry, G. C.; Garno, J. C. Fabrication of nanopatterned films of bovine serum albumin and staphylococcal protein A using latex particle lithography. *Analyst* **2006**, *131*, 244-250.
- (293) Potyrailo, R. A.; Cawse, J. N. USA Patent US 2003/0162179, 2003.

- (294) You, H. X.; Lowe, C. R. AFM studies of protein adsorption .2. Characterization of immunoglobulin G adsorption by detergent washing. *J. Colloid Interface Sci.* **1996**, *182*, 586-601.
- (295) Ouerghi, O.; Touhami, A.; Othmane, A.; Ben Ouada, H.; Martelet, C.; Fretigny, C.; Jaffrezic-Renault, N. Investigating specific antigen/antibody binding with the atomic force microscope. *Biomol. Eng.* **2002**, *19*, 183-188.
- (296) Hell, S.; Reiner, G.; Cremer, C.; Stelzer, E. H. K. Aberrations in Confocal Fluorescence Microscopy Induced by Mismatches in Refractive-Index. *Journal of Microscopy-Oxford* **1993**, *169*, 391-405.
- (297) Haeberle, O. Focusing of light through a stratified medium: a practical approach for computing microscope point spread functions - Part II: confocal and multiphoton microscopy. *Opt. Commun.* **2004**, *235*, 1-10.
- (298) Voldman, J.; Gray, M. L.; Schmidt, M. A. Microfabrication in biology and medicine. *Annu. Rev. Biomed. Eng.* **1999**, *1*, 401-425.
- (299) Li, H. W.; Muir, B. V. O.; Fichet, G.; Huck, W. T. S. Nanocontact printing: A route to sub-50-nm-scale chemical and biological patterning. *Langmuir* **2003**, *19*, 1963-1965.
- (300) Perl, A.; Reinhoudt, D. N.; Huskens, J. Microcontact Printing: Limitations and Achievements. *Adv Mater* **2009**, *21*, 2257-2268.
- (301) Wallraff, G. M.; Hinsberg, W. D. Lithographic imaging techniques for the formation of nanoscopic features. *Chem. Rev.* **1999**, *99*, 1801-1821.
- (302) Schreiber, F. Structure and growth of self-assembling monolayers. *Prog Surf Sci* **2000**, *65*, 151-256.
- (303) Xia, Y. N.; Whitesides, G. M. Soft lithography. *Annual Review of Materials Science* **1998**, *28*, 153-184.
- (304) Kane, R. S.; Takayama, S.; Ostuni, E.; Ingber, D. E.; Whitesides, G. M. Patterning proteins and cells using soft lithography. *Biomaterials* **1999**, *20*, 2363-2376.
- (305) Ganesan, R.; Kratz, K.; Lendlein, A. Multicomponent protein patterning of material surfaces. *J. Mater. Chem.* **2010**, *20*, 7322-7331.
- (306) Kumar, A.; Whitesides, G. M. Features of Gold having Micrometer to Centimeter Dimensions can be Formed through a Combination of Stamping with an Elastomeric Stamp and an Alkanethiol Ink Followed by Chemical Etching. *Appl. Phys. Lett.* **1993**, *63*, 2002-2004.
- (307) Sinclair, J.; Salem, A. K. Rapid localized cell trapping on biodegradable polymers using cell surface derivatization and microfluidic networking. *Biomaterials* **2006**, *27*, 2090-2094.

- (308) Xia, Y. N.; McClelland, J. J.; Gupta, R.; Qin, D.; Zhao, X. M.; Sohn, L. L.; Celotta, R. J.; Whitesides, G. M. Replica molding using polymeric materials: A practical step toward nanomanufacturing. *Adv Mater* **1997**, *9*, 147-149.
- (309) Zhao, X. M.; Xia, Y. N.; Whitesides, G. M. Fabrication of three-dimensional micro-structures: Microtransfer molding. *Adv Mater* **1996**, *8*, 837-&.
- (310) Kim, E.; Xia, Y. N.; Whitesides, G. M. Polymer Microstructures Formed by Molding in Capillaries. *Nature* **1995**, *376*, 581-584.
- (311) Kim, E.; Xia, Y. N.; Zhao, X. M.; Whitesides, G. M. Solvent-assisted microcontact molding: A convenient method for fabricating three-dimensional structures on surfaces of polymers. *Adv Mater* **1997**, *9*, 651-654.
- (312) Tan, J. L.; Tien, J.; Chen, C. S. Microcontact printing of proteins on mixed self-assembled monolayers. *Langmuir* **2002**, *18*, 519-523.
- (313) Biebuyck, H. A.; Whitesides, G. M. Self-Organization of Organic Liquids on Patterned Self-Assembled Monolayers of Alkanethiolates on Gold. *Langmuir* **1994**, *10*, 2790-2793.
- (314) Wilbur, J. L.; Kumar, A.; Kim, E.; Whitesides, G. M. Microfabrication by Microcontact Printing of Self-Assembled Monolayers. *Adv Mater* **1994**, *6*, 600-604.
- (315) Arrington, D.; Curry, M.; Street, S. C. Patterned thin films of polyamidoamine dendrimers formed using microcontact printing. *Langmuir* **2002**, *18*, 7788-7791.
- (316) Lange, S. A.; Benes, V.; Kern, D. P.; Horber, J. K. H.; Bernard, A. Microcontact printing of DNA molecules. *Anal. Chem.* **2004**, *76*, 1641-1647.
- (317) Bernard, A.; Delamarche, E.; Schmid, H.; Michel, B.; Bosshard, H. R.; Biebuyck, H. Printing patterns of proteins. *Langmuir* **1998**, *14*, 2225-2229.
- (318) Singhvi, R.; Kumar, A.; Lopez, G. P.; Stephanopoulos, G. N.; Wang, D. I. C.; Whitesides, G. M.; Ingber, D. E. Engineering Cell-Shape and Function. *Science* **1994**, *264*, 696-698.
- (319) Abbott, N. L.; Kumar, A.; Whitesides, G. M. Using Micromachining, Molecular Self-Assembly, and Wet Etching to Fabricate 0.1-1-Mu-M-Scale Structures of Gold and Silicon. *Chem. Mat.* **1994**, *6*, 596-602.
- (320) Xia, Y. N.; Tien, J.; Qin, D.; Whitesides, G. M. Non-photolithographic methods for fabrication of elastomeric stamps for use in microcontact printing. *Langmuir* **1996**, *12*, 4033-4038.
- (321) Xia, Y. N.; Whitesides, G. M. Extending microcontact printing as a microlithographic technique. *Langmuir* **1997**, *13*, 2059-2067.

- (322) Campbell, D. J.; Beckman, K. J.; Calderon, C. E.; Doolan, P. W.; Ottosen, R. M.; Ellis, A. B.; Lisensky, G. C. Replication and compression of bulk and surface structures with polydimethylsiloxane elastomer. *J. Chem. Educ.* **1999**, *76*, 537-541.
- (323) Choi, J. W.; Oh, B. K.; Kim, Y. K.; Min, J. H. Nanotechnology in biodevices. *Journal of Microbiology and Biotechnology* **2007**, *17*, 5-14.
- (324) Owen, M. J.; Smith, P. J. Plasma Treatment of Polydimethylsiloxane. *J. Adhes. Sci. Technol.* **1994**, *8*, 1063-1075.
- (325) Wang, D.; Huang, Y.; Chiang, H.; Wo, A. M.; Huang, Y. Microcontact printing of laminin on oxygen plasma activated substrates for the alignment and growth of Schwann cells. *J. Biomed. Mater. Res. Part B* **2007**, *80B*, 447-453.
- (326) Delamarche, E.; Geissler, M.; Bernard, A.; Wolf, H.; Michel, B.; Hilborn, J.; Donzel, C. Hydrophilic poly (dimethylsiloxane) stamps for microcontact printing. *Adv Mater* **2001**, *13*, 1164-+.
- (327) Chen, C. S.; Mrksich, M.; Huang, S.; Whitesides, G. M.; Ingber, D. E. Micropatterned surfaces for control of cell shape, position, and function. *Biotechnol. Prog.* **1998**, *14*, 356-363.
- (328) Thiebaud, P.; Lauer, L.; Knoll, W.; Offenhausser, A. PDMS device for patterned application of microfluids to neuronal cells arranged by microcontact printing. *Biosens. Bioelectron.* **2002**, *17*, 87-93.
- (329) Bernard, A.; Renault, J. P.; Michel, B.; Bosshard, H. R.; Delamarche, E. Microcontact printing of proteins. *Adv Mater* **2000**, *12*, 1067-1070.
- (330) Schena, M.; Shalon, D.; Davis, R. W.; Brown, P. O. Quantitative Monitoring of Gene-Expression Patterns with a Complementary-Dna Microarray. *Science* **1995**, *270*, 467-470.
- (331) Ressine, A.; Ekstrom, S.; Marko-Varga, G.; Laurell, T. Macro-/nanoporous silicon as a support for high-performance protein microarrays. *Anal. Chem.* **2003**, *75*, 6968-6974.
- (332) Kannan, B.; Castelino, K.; Chen, F. F.; Majumdar, A. Lithographic techniques and surface chemistries for the fabrication of PEG-passivated protein microarrays. *Biosens. Bioelectron.* **2006**, *21*, 1960-1967.
- (333) Inerowicz, H. D.; Howell, S.; Regnier, F. E.; Reifenger, R. Multiprotein immunoassay arrays fabricated by microcontact printing. *Langmuir* **2002**, *18*, 5263-5268.
- (334) Prime, K. L.; Whitesides, G. M. Self-Assembled Organic Monolayers - Model Systems for Studying Adsorption of Proteins at Surfaces. *Science* **1991**, *252*, 1164-1167.

- (335) Graber, D. J.; Zieziulewicz, T. J.; Lawrence, D. A.; Shain, W.; Turner, J. N. Antigen binding specificity of antibodies patterned by microcontact printing. *Langmuir* **2003**, *19*, 5431-5434.
- (336) LaGraff, J. R.; Chu-LaGraff, Q. Scanning force microscopy and fluorescence microscopy of microcontact printed antibodies and antibody fragments. *Langmuir* **2006**, *22*, 4685-4693.
- (337) Delamarche, E.; Bernard, A.; Schmid, H.; Bietsch, A.; Michel, B.; Biebuyck, H. Microfluidic networks for chemical patterning of substrate: Design and application to bioassays. *J. Am. Chem. Soc.* **1998**, *120*, 500-508.
- (338) Delamarche, E.; Bernard, A.; Schmid, H.; Michel, B.; Biebuyck, H. Patterned delivery of immunoglobulins to surfaces using microfluidic networks. *Science* **1997**, *276*, 779-781.
- (339) Hergenrother, P. J.; Depew, K. M.; Schreiber, S. L. Small-molecule microarrays: Covalent attachment and screening of alcohol-containing small molecules on glass slides. *J. Am. Chem. Soc.* **2000**, *122*, 7849-7850.
- (340) Foley, J. O.; Fu, E.; Gamble, L. J.; Yager, P. Microcontact printed antibodies on gold surfaces: Function, uniformity, and silicone contamination. *Langmuir* **2008**, *24*, 3628-3635.
- (341) Mrksich, M.; Dike, L. E.; Tien, J.; Ingber, D. E.; Whitesides, G. M. Using microcontact printing to pattern the attachment of mammalian cells to self-assembled monolayers of alkanethiolates on transparent films of gold and silver. *Exp. Cell Res.* **1997**, *235*, 305-313.
- (342) Lee, J. P.; Jang, Y. J.; Sung, M. M. Atomic layer deposition of TiO₂ thin films on mixed self-assembled monolayers studied as a function of surface free energy. *Adv. Funct. Mater.* **2003**, *13*, 873-876.
- (343) Nanci, A.; Wuest, J. D.; Peru, L.; Brunet, P.; Sharma, V.; Zalzal, S.; McKee, M. D. Chemical modification of titanium surfaces for covalent attachment of biological molecules. *J. Biomed. Mater. Res.* **1998**, *40*, 324-335.
- (344) Tao, Y. T. Structural Comparison of Self-Assembled Monolayers of N-Alkanoic Acids on the Surfaces of Silver, Copper, and Aluminum. *J. Am. Chem. Soc.* **1993**, *115*, 4350-4358.
- (345) Fixe, F.; Dufva, M.; Telleman, P.; Christensen, C. B. V. Functionalization of poly(methyl methacrylate) (PMMA) as a substrate for DNA microarrays. *Nucleic Acids Res.* **2004**, *32*, e9.
- (346) Henry, A. C.; Tutt, T. J.; Galloway, M.; Davidson, Y. Y.; McWhorter, C. S.; Soper, S. A.; McCarley, R. L. Surface modification of poly(methyl methacrylate) used in the fabrication of microanalytical devices. *Anal. Chem.* **2000**, *72*, 5331-5337.

- (347) Renault, J. P.; Bernard, A.; Bietsch, A.; Michel, B.; Bosshard, H. R.; Delamarche, E.; Kreiter, M.; Hecht, B.; Wild, U. P. Fabricating arrays of single protein molecules on glass using microcontact printing. *J Phys Chem B* **2003**, *107*, 703-711.
- (348) Chalmeau, J.; Thibault, C.; Carcenac, F.; Vieu, C. Self-aligned patterns of multiple biomolecules printed in one step. *Appl. Phys. Lett.* **2008**, *93*.
- (349) Park, C. H.; Park, H. Fingerprint classification using fast Fourier transform and nonlinear discriminant analysis. *Pattern Recognit* **2005**, *38*, 495-503.
- (350) Pattani, V. P.; Li, C. F.; Desai, T. A.; Vu, T. Q. Microcontact printing of quantum dot bioconjugate arrays for localized capture and detection of biomolecules. *Biomed. Microdevices* **2008**, *10*, 367-374.
- (351) Vandervoort, H. T. M.; Brakenhoff, G. J. 3-D Image-Formation In High-Aperture Fluorescence Confocal Microscopy - A Numerical-Analysis. *Journal Of Microscopy-Oxford* **1990**, *158*, 43-54.